

UC San Diego

UC San Diego Electronic Theses and Dissertations

Title

Cardiac Cell Engineering, Preservation and Phenotyping

Permalink

<https://escholarship.org/uc/item/58x6z371>

Author

Firouzi, Fareheh

Publication Date

2022

Peer reviewed|Thesis/dissertation

UNIVERSITY OF CALIFORNIA SAN DIEGO
SAN DIEGO STATE UNIVERSITY

Cardiac Cell Engineering, Preservation and Phenotyping

A Dissertation submitted in partial satisfaction of the requirements
for the degree Doctor of Philosophy

in

Biology

by

Fareheh Firouzi

Committee in charge:

University of California San Diego

Professor Asa B. Gustafsson
Professor Xin Sun

San Diego State University

Professor Mark A. Sussman, Chair
Professor Sanford I. Bernstein
Professor Christopher C. Glembotski

2022

Copyright
Fareheh Firouzi, 2022
All rights reserved

The dissertation of Fareheh Firouzi is approved, and it is acceptable in quality and form for publication on microfilm and electronically.

Chair

University of California San Diego
San Diego State University

2022

DEDICATION

First and foremost, I'd like to dedicate this work to my love, Alireza. Thank you for being a true companion and comforter. You have been my rock throughout this difficult journey. From discussing scientific ideas to listening to my concerns and anxieties, you have always been there for me, and I can't thank you enough. I love you.

Next, I'd like to dedicate this to my parents, Vajiheh and Ali. Thank you for teaching me the meaning of hard work and determination. To my sister, Firoozeh and my brothers, Farjad and Farhad, as the youngest child in the family I have always looked up to you and learned so much from you. Thank you.

EPIGRAPH

"I cannot think of a single field in biology or medicine in which we can claim genuine understanding."

-Lewis Thomas

TABLE OF CONTENTS

| | |
|--|-------|
| DISSERTATION APPROVAL PAGE | iii |
| DEDICATION | iv |
| EPIGRAPH | v |
| TABLE OF CONTENTS | vi |
| LIST OF FIGURES | xi |
| LIST OF TABLES | xiii |
| LIST OF ABBREVIATIONS..... | xiv |
| ACKNOWLEDGEMENTS | xviii |
| VITA | xx |
| ABSTRACT OF THE DISSERTATION | xxiii |
| CHAPTER 1..... | 1 |
| Introduction of the Dissertation..... | 1 |
| Cardiovascular disease | 2 |
| Cell-based therapies | 3 |
| Cell fusion to generate “Next generation” cardiac cell therapeutic | 3 |
| Cardiomyocyte-based therapies | 4 |
| Fibroblast-based therapies | 5 |
| References | 7 |
| CHAPTER 2 | 10 |
| Human CardioChimeras: Creation of a Novel ‘Next Generation’ Cardiac Cell | 10 |
| INTRODUCTION | 11 |
| METHODS | 14 |
| cCIC and MSC isolation | 14 |

| | |
|---|----|
| Lentiviral constructs and stem cell infection | 14 |
| Cell fusion and creation of hCCs | 15 |
| Light microscopy and measurement of cell morphology..... | 15 |
| Proliferation and doubling time | 15 |
| Immunocytochemistry | 16 |
| Immunoblot analysis | 16 |
| Real-Time PCR | 16 |
| Ploidy and cytogenic analysis | 17 |
| Cell death assay | 17 |
| NRCM co-culture with stem cells | 18 |
| Statistical analysis | 19 |
| RESULTS | 20 |
| hCCs creation from c-kit CIC and MSC cell fusion | 20 |
| hCCs possess diploid DNA content | 20 |
| hCCs phenotypic and proliferative characteristics resemble parent cells . | 21 |
| Profiling for commitment and secretory gene expression reveals hCC variability | 22 |
| Survival in response to environmental stress is enhanced in hCC | 23 |
| Cardiomyocyte survival is enhanced by hCC co-culture | 24 |
| DISCUSSION | 26 |
| TABLES | 31 |
| FIGURES | 35 |
| REFERENCES | 48 |
| CHAPTER 3 | 54 |
| PIM1 Promotes Survival of Cardiomyocytes by Upregulating c-Kit Protein Expression.. | 54 |
| INTRODUCTION | 55 |

| | |
|--|----|
| METHODS | 57 |
| Animal Experiments | 57 |
| Isolation and Culture of Adult Mouse Cardiomyocytes | 57 |
| Viral Infections | 58 |
| Pharmacological Treatments | 58 |
| Immunoblot | 58 |
| Quantitative RT-PCR | 59 |
| Co-Immunoprecipitation | 59 |
| Proximity Ligation Assay | 60 |
| Cell Death Assay | 61 |
| Statistical Analyses | 61 |
| RESULTS | 63 |
| PIM1 upregulates c-Kit protein expression | 63 |
| PIM1 interacts with c-Kit | 63 |
| Cardioprotective signaling downstream of c-Kit is elevated in PIM1 cardiomyocytes | 64 |
| Elevated c-Kit expression enhances resistance against oxidative stress in cardiomyocytes | 65 |
| PIM1 and c-Kit act independently to confer cardioprotection | 65 |
| DISCUSSION | 67 |
| TABLES | 69 |
| FIGURES | 70 |
| REFERENCES | 80 |
| CHAPTER 4 | 86 |
| ‘Youthful’ Phenotype of c-Kit ⁺ Cardiac Fibroblasts | 86 |
| INTRODUCTION | 87 |

| | |
|--|-----|
| METHODS | 89 |
| Mouse models | 89 |
| Myocardial infarction | 89 |
| CIC isolation and expansion | 90 |
| Flow cytometry and cell sorting | 90 |
| Immunohistochemistry and confocal microscopy | 91 |
| Immunoblotting | 91 |
| Immunocytochemistry and confocal microscopy | 92 |
| Senescence-associated beta-galactosidase (SA- β -Gal) staining | 92 |
| Morphology measurement | 93 |
| Proliferation assay and doubling time..... | 93 |
| Cell motility measurement | 93 |
| scRNA-Seq | 94 |
| Statistical analysis | 96 |
| RESULTS | 97 |
| c-Kit promoter is active in cardiac fibroblasts <i>in vitro</i> | 97 |
| c-Kit promoter is active in cardiac fibroblasts <i>in vivo</i> | 97 |
| c-Kit protein is expressed in a subset of cardiac fibroblast population and diminishes with physiological aging | 98 |
| c-Kit and DDR2 expression as well as coincidence upregulate following pathological damage | 98 |
| Transcriptomic phenotype of c-Kit expressing CFs | 99 |
| c-Kit expressing CFs transcriptionally associate with higher cell cycle progression and lower senescence-associated secretory phenotype | 101 |
| c-Kit expressing CFs are morphologically distinct | 102 |
| Cellular senescence is attenuated in c-Kit expressing CFs | 102 |

| | |
|--|-----|
| Self-renewal and cellular motility are enhanced in c-Kit expressing CFs.. | 103 |
| c-Kit expressing CFs are enriched for signaling genes implicated in proliferation and cell migration | 103 |
| DISCUSSION | 105 |
| TABLES | 111 |
| FIGURES | 114 |
| REFERENCES | 136 |

LIST OF FIGURES

| | |
|--|----|
| Figure 2.1. hCCs are created from cCIC and MSC cell fusion | 35 |
| Figure 2.2. Flow cytometry plots of one representative fusion experiment | 36 |
| Figure 2.3. Live native fluorescent images of hCCs illustrating double positivity of the fused cells | 37 |
| Figure 2.4. Immunocytochemistry images parent cells validating antibody specificity for their respective fluorophores | 38 |
| Figure 2.5. hCCs reveal ploidy status and DNA content corresponding to the parent cells | 39 |
| Figure 2.6. Morphometric and proliferative characteristics of hCCs | 40 |
| Figure 2.7. hCCs exhibit variable expression level of cardiomyogenic commitment markers | 41 |
| Figure 2.8. hCCs exhibit variable secretory gene profiles | 42 |
| Figure 2.9. hCCs demonstrate enhanced survival in response to stress..... | 43 |
| Figure 2.10. Percentage of survival (live cells) of D2 clones in cCIC media, cCICs in cCIC media, D2 clones in MSC media and MSCs in MSC media (from left to right) after treatment with hydrogen peroxide (350 μ mol/L) | 44 |
| Figure 2.11. Percentage of apoptotic, necrotic and live cells | 45 |
| Figure 2.12. hCCs promote cardiomyocytes survival in response to serum deprivation .. | 46 |
| Figure 2.13. Cell doubling time of hCCs up to and after passage 10 in culture represented in hours | 47 |
| Figure 3.1. PIM1 upregulates c-Kit protein expression | 70 |
| Figure 3.2. Full blot of cropped image presented in Figure 3.1A., Figure 3.1B, and Figure 3.1C of the manuscript | 71 |
| Figure 3.3. PIM1 interacts with c-Kit | 72 |
| Figure 3.4. Full blot of cropped image presented in Figure 3.3A of the manuscript | 73 |
| Figure 3.5. Negative controls for the Proximity Ligation Assay | 74 |
| Figure 3.6. Cardioprotective signaling downstream of c-Kit is elevated in PIM1 cardiomyocytes | 75 |

| | |
|--|-----|
| Figure 3.7. Full blot of cropped image presented in Figure 3.6A and Figure 3.6B of the manuscript | 76 |
| Figure 3.8. Cardiomyocytes with elevated c-Kit expression demonstrate enhanced resistance against oxidative stress | 77 |
| Figure 3.9. Full blot of cropped image presented in Figure 3.8B of the manuscript | 78 |
| Figure 3.10. PIM1 and c-Kit act independently to confer cardioprotection | 79 |
| Figure 4.1. Transgenic cardiac fibroblasts express EGFP upon Doxy treatment in vitro | 114 |
| Figure 4.2. DDR2 expression and coincidence with EGFP adapt to culture media | 116 |
| Figure 4.3. Transgenic cardiac fibroblasts express EGFP upon Doxy treatment in vivo | 117 |
| Figure 4.4. c-Kit protein colocalization with EGFP and DDR2 | 118 |
| Figure 4.5. c-Kit protein is present in a subset of cardiac fibroblast population. | 119 |
| Figure 4.6. Expression as well as coincidence of c-Kit and DDR2 increase in response to myocardial infarction | 120 |
| Figure 4.7. Quality control for scRNA-seq experiment | 122 |
| Figure 4.8. CD45 expression in freshly isolated CICs | 124 |
| Figure 4.9. Unsupervised clustering reveals 16 clusters | 125 |
| Figure 4.10. c-Kit ⁺ cardiac fibroblasts are transitional in the transcriptional trajectory . | 126 |
| Figure 4.11. c-Kit ⁺ cardiac fibroblasts are transcriptionally associated with higher cell cycle progression and lower SASP | 128 |
| Figure 4.12. c-Kit expressing cardiac fibroblasts are morphologically distinct | 130 |
| Figure 4.13. c-Kit expressing cardiac fibroblasts exhibit lower level of cellular senescence | 131 |
| Figure 4.14. Self-renewal and cellular motility are enhanced in c-Kit expressing cardiac fibroblasts | 133 |
| Figure 4.15. c-Kit protein is present in a subset of CFs | 135 |

LIST OF TABLES

| | |
|---|-----|
| Table 2.1. List of Media | 31 |
| Table 2.2. List of Antibodies | 32 |
| Table 2.3. List of Primers | 33 |
| Table 2.4. List of Fusions | 34 |
| Table 3.1. Antibody list | 69 |
| Table 4.1. List of Antibodies | 111 |
| Table 4.2. List of SASPs and Growth Factors | 113 |

LIST OF ABBREVIATIONS

| | |
|----------|---|
| BDM | 2,3-Butanedione 2-monoxime |
| BSA | bovine serum albumin |
| CC | CardioChimera |
| cCICs | c-Kit ⁺ cardiac interstitial cells |
| Ccl3 | C-C motif ligand 3 |
| CCN2 | cellular communication network factor 2 |
| cDNA | complementary DNA |
| CF | cardiac fibroblast |
| CICs | cardiac interstitial cells |
| CND | CD45-non-depleted |
| Ctsb | cathepsin B |
| Cxcl | C-X-C motif chemokine |
| DAPI | 4',6-diamidino-2-phenylindole |
| DDR2 | discoidin domain-containing receptor 2 |
| DEGs | differentially expressed genes |
| DMEM | dulbecco's modified eagle medium |
| DMEM/F12 | dulbecco's modified eagle medium: nutrient mixture F-12 |
| ECM | extracellular matrix |

| | |
|--------|--|
| EGFP | enhanced green fluorescent protein |
| EMT | epithelial–mesenchymal transition |
| EPDCs | epicardial-derived cells |
| ERK | extracellular signal–regulated kinase |
| ES FBS | embryonic stem cell FBS qualified |
| FACS | fluorescence-activated cell sorting |
| FBS | fetal bovine serum |
| FGF2 | basic fibroblast growth factor |
| GAPDH | glyceraldehyde 3-phosphate dehydrogenase |
| GATA4 | GATA binding protein 4 |
| GEO | gene expression omnibus |
| GFP | green fluorescent protein |
| GM | growth medium |
| GO | gene ontology |
| H2B | histone H2B |
| H2O2 | hydrogen peroxide |
| HB-EGF | heparin binding EGF like growth factor |
| HBSS | hank's balanced salt solution |
| hCC | human CardioChimera |

| | |
|--------|--|
| hcCICs | human c-kit+ cardiac interstitial cells |
| HEPES | 4-(2-hydroxyethyl)-1-piperazineethanesulfonic acid |
| HGF | hepatocyte growth factor |
| hMSC | human mesenchymal stem cell |
| HS | horse serum |
| Icam1 | intercellular adhesion molecule 1 |
| ICC | immunocytochemistry |
| Igfbp | insulin-like growth factor (IGF) binding protein |
| IHC | immunohistochemistry |
| Il1B | interleukin 1 Beta |
| IL-6 | interlukin-6 |
| Il6st | interleukin 6 cytokine family signal transducer |
| I/R | Ischemia-reperfusion |
| Kitl | kit ligand |
| LAD | left anterior descending artery |
| LIF | leukemia inhibitory factor |
| MACs | magnetic-activated cell sorting |
| MEFs | mouse embryonic fibroblasts |
| MI | myocardial infarction |

| | |
|------------------|---|
| Ngf | nerve growth factor |
| NRCM | neonatal rat cardiomyocyte |
| PBS | phosphate buffered saline |
| PDGFR | platelet-derived growth factor receptor |
| PECAM1 | platelet endothelial cell adhesion molecule or CD31 |
| PI | propidium iodide |
| rtTA | reverse tetracycline controlled transactivator |
| SA- β -Gal | senescence-associated beta-galactosidase |
| SCF | stem cell factor |
| scRNA-Seq | single cell RNA sequencing |
| SDF | stromal derived factor |
| SMA | smooth muscle actin |
| TCF21 | transcription factor 21 |
| TGF-B | transforming growth factor beta |
| TNNT2 | troponin T2, cardiac type |
| TRE | tet-responsive element |
| WB | western blot |
| WT | wild type |

ACKNOWLEDGMENTS

First, I would like to acknowledge my mentor, Dr. Mark Sussman for his leadership and support throughout my academic journey. Under his supervision, I have had the great opportunity to develop my skills and knowledge as a scientist. The environment he created in the lab has allowed me to grow both personally and professionally.

I would also like to thank my committee members Dr. Sanford Bernstein, Dr. Christopher Glembotski, Dr. Asa Gustafsson and Dr. Xin Sun for their guidance and valuable feedback. It was my honor to have their support and expertise throughout my PhD endeavor.

I would like to acknowledge the American Heart Association, San Diego state University Graduate program and Grace Hoover Sciences foundation for supporting my research. I would like to extend my thanks to the SDSU Flow Cytometry Core and the vivarium staff. I would also like to extend my thanks to the present and past members of the Sussman lab.

Chapter 2, with slight modifications, is a reprint of the material as it appears in Journal of the American Heart Association, 2020. Human CardioChimeras: Creation of a Novel “Next-Generation” Cardiac Cell. Fareheh Firouzi, Sarmistha Sinha Choudhury, Kathleen Broughton, Adriana Salazar, Barbara Bailey, Mark A. Sussman. The dissertation author was the primary author and investigator on this manuscript.

Chapter 3, with slight modifications, is a reprint of the material as it appears in Cells, 2020. PIM1 Promotes Survival of Cardiomyocytes by Upregulating c-Kit Protein Expression. David E Ebeid, Fareheh Firouzi, Carolina Y Esquer, Julian M Navarrete,

Bingyan J Wang, Natalie A Gude, Mark A Sussman. The dissertation author was the co-first author and investigator on this manuscript.

Chapter 4, with slight modifications, has been submitted for publication. 'Youthful' Phenotype of c-Kit⁺ Cardiac Fibroblasts. Fareheh Firouzi, Oscar Echeagaray, Carolina Esquer, Natalie A. Gude, Mark A. Sussman. The dissertation author was the primary author and investigator on this manuscript.

VITA

EDUCATION

- 2017-2022 PhD, Biology, University of California San Diego, San Diego State University Joint Doctoral Program, San Diego, CA
- 2015-2017 MSc, Molecular Biology, San Diego State University, San Diego, CA
- 2010-2012 MSc, Cell and Developmental Biology, University of Guilan, Iran
- 2006-2010 BSc, Marine Biology, University of Guilan, Iran

PUBLICATIONS

Firouzi F, Echeagaray O, Esquer C, Gude NA, Sussman MA. “Youthful” Phenotype of c-Kit+ Cardiac Fibroblasts. *Journal of Cellular and Molecular Life Sciences* 2022, in press.

Broughton K, Esquer C, Echeagaray O, **Firouzi F**, Ebeid D, Monsanto M, Yaareb D, Golgolab L, Gude NA, Sussman MA. Surface Lin28A Expression Consistent With Cellular Stress Parallels Indicators of Senescence. *Cardiovasc Res* 2022, in press.

Gude NA, **Firouzi F**, Sussman MA. Transient reprogramming primes the heart for repair. *J Cardiovasc Aging* 2022.

Esquer C, Echeagaray O, **Firouzi F**, Savko C, Shain G, Bose P, Rieder A, Rokaw S, Witon-Paulo A, Gude N, Sussman MA Fundamentals of vaping-associated pulmonary injury leading to severe respiratory distress. *Life Sci Alliance* 2022.

Monsanto MM, **Firouzi F**, Sussman MA Hiding in plain sight: an encapsulated approach to cardiac cell therapy. *Cardiovasc Res* 2021.

Ebeid DE, **Firouzi F**, Esquer CY, Navarrete JM, Wang BJ, Gude NA, Sussman MA PIM1 Promotes Survival of Cardiomyocytes by Upregulating c-Kit Protein Expression. *Cells* 2020.

Firouzi F, Sussman MA Blood speaks: Personalised medicine profiling for heart failure patients. *EBioMedicine* 2020.

Ebeid DE, Khalafalla FG, Broughton KM, Monsanto MM, Esquer CY, Sacchi V, Hariharan N, Korski KI, Moshref M, Emathingier J, Cottage CT, Quijada PJ, Nguyen JH, Alvarez R, Völkens M, Konstandin MH, Wang BJ, **Firouzi F**, Navarrete JM, Gude NA, Goumans MJ, Sussman MA Pim1 maintains telomere length in mouse cardiomyocytes by inhibiting TGF β signalling. *Cardiovasc Res* 2021.

Firouzi F, Sinha Choudhury S, Broughton K, Salazar A, Bailey B, Sussman MA Human CardioChimeras: Creation of a Novel "Next-Generation" Cardiac Cell. *J Am Heart Assoc* 2020.

Gude NA, **Firouzi F**, Broughton KM, Ilves K, Nguyen KP, Payne CR, Sacchi V, Monsanto MM, Casillas AR, Khalafalla FG, Wang BJ, Ebeid DE, Alvarez R, Dembitsky WP, Bailey BA, van Berlo J, Sussman MA Cardiac c-Kit Biology Revealed by Inducible Transgenesis. *Circ Res* 2018.

Alvarez R, Wang BJ, Quijada PJ, Avitabile D, Ho T, Shaitrit M, Chavarria M, **Firouzi F**, Ebeid D, Monsanto MM, Navarrete N, Moshref M, Siddiqi S, Broughton KM, Bailey BA, Gude NA, Sussman MA Cardiomyocyte cell cycle dynamics and proliferation revealed through cardiac-specific transgenesis of fluorescent ubiquitinated cell cycle indicator (FUCCI). *J Mol Cell Cardiol* 2019.

Korski KI, Kubli DA, Wang BJ, Khalafalla FG, Monsanto MM, **Firouzi F**, Echeagaray OH, Kim T, Adamson RM, Dembitsky WP, Gustafsson ÅB, Sussman MA Hypoxia Prevents Mitochondrial Dysfunction and Senescence in Human c-Kit Cardiac Progenitor Cells. *Stem Cells* 2019 04 37(4):555-567. Epub 2019.

Broughton KM, Khieu T, Nguyen N, Rosa M, Mohsin S, Quijada P, Wang BJ, Echeagaray OH, Kubli DA, Kim T, **Firouzi F**, Monsanto MM, Gude NA, Adamson RM, Dembitsky WP, Davis ME, Sussman MA Cardiac interstitial tetraploid cells can escape replicative senescence in rodents but not large mammals. *Commun Biol* 2019.

Broughton KM, Wang BJ, **Firouzi F**, Khalafalla F, Dimmeler S, Fernandez-Aviles F, Sussman MA Mechanisms of Cardiac Repair and Regeneration. *Circ Res* 2018.

Gude NA, Broughton KM, **Firouzi F**, Sussman MA Cardiac ageing: extrinsic and intrinsic factors in cellular renewal and senescence. *Nat Rev Cardiol* 2018.

Hemmati M, Mashayekhi F, **Firouzi F**, Ashori M, Mashayekhi H. Effects of electromagnetic fields on reelin and Dab1 expression in the developing cerebral cortex. *Neurological Sciences* 2014.

PRESENTATIONS

Firouzi F, Echeagaray O, Esquer C, Gude NA, Sussman MA. “Youthful” Phenotype of c-Kit+ Cardiac Fibroblasts. AHA Scientific Sessions, Nov. 2021 (poster presentation).

Firouzi F, Echeagaray O, Esquer C, Gude NA, Sussman MA. “Youthful” Phenotype of c-Kit+ Cardiac Fibroblasts. BCVS Scientific Sessions Conference, Aug. 2021 (poster presentation).

Firouzi F, Mashayekhi F. Effect of electromagnetic fields on cell migration in cerebral cortex during early postnatal period, The 17th National & 5th International Iranian Biology Conference, Kerman, Iran, Sep. 2012.

Firouzi F, Mashayekhi F. Effect of electromagnetic fields on cell proliferation in cerebral cortex during early postnatal period, 10th Iranian Anatomical Science Congress, Guilan University of Medical Sciences, Rasht, Iran, May 2012.

AWARDS

San Diego state University Graduate Fellowship (2021-2022)

American Heart Association Fellowship (2019-2021)

Grace Hoover Sciences Scholarship (2018)

ABSTRACT OF THE DISSERTATION

c-Kit in Cardiac Cell Engineering, Preservation and Phenotyping

by

Fareheh Firouzi

Doctor of Philosophy in Biology

University of California San Diego, 2022

San Diego State University, 2022

Professor Mark A. Sussman, Chair

Tangible returns from cell and molecular therapeutic interventions to promote cardiac repair have been predominantly underwhelming at both basic research and clinical levels. The field of cardiovascular research would benefit tremendously from identification of optimal protein(s), signaling pathways and/or an optimal cell population to enhance cardiac repair. Cell fusion has been used to create novel therapeutic cellular effectors by incorporating beneficial characteristics of two different cardiac derived cells. Human CardioChimeras (hCCs) produced by fusion of c-kit⁺ cardiac interstitial cells with

mesenchymal stem cells exhibited enhanced survival relative to the parent cells and promoted cardiomyocyte survival in response to serum deprivation. Feasibility of creating human hybrid cells prompts consideration of multiple possibilities to create novel chimeric cells derived from cells with desirable traits to promote healing in pathologically damaged myocardium.

Enhancing cardiomyocyte survival is crucial to blunt deterioration of myocardial structure and function following pathological damage. PIM1 is a cardioprotective serine threonine kinase that promotes cardiomyocyte survival and antagonizes senescence through multiple concurrent molecular signaling cascades. In hematopoietic stem cells, PIM1 interacts with the receptor tyrosine kinase c-Kit to promote cell proliferation and survival. The relationship between PIM1 and c-Kit activity has not been explored in the myocardial context. The study presented in this dissertation delineated the interaction between PIM1 and c-Kit leading to enhanced protection of cardiomyocytes from stress. The mechanistic relationship between PIM1 and c-Kit in cardiomyocytes identifies a novel facet of cardioprotection regulated by PIM1 kinase.

Cardiac fibroblast (CF) population heterogeneity and plasticity present a challenge for categorization of biological and functional properties. Distinct molecular markers and associated signaling pathways provide valuable insight for CF biology and interventional strategies to influence injury response and aging-associated remodeling. Receptor tyrosine kinase c-Kit mediates cell survival, proliferation, migration, and is activated by pathological injury. However, the biological significance of c-Kit within CF population has not been addressed. The work presented in this dissertation demonstrated the phenotype of c-kit⁺ on CFs correlated with multiple characteristics of 'youthful' cells. This study

provides a fundamental basis for future studies to influence myocardial biology, response to pathological injury and physiological aging.

CHAPTER 1

Introduction of the Dissertation

Cardiovascular disease

Cardiovascular disease (CVD) is the leading cause of death in the United States and worldwide¹. By 2030, more than 43% of American adults are anticipated to have a form of CVD and the annual CVD mortality rate is expected to grow from approximately 17.8 million deaths globally reported in 2017 to more than 22.2 million^{1,2}. Different types of CVD including congenital heart disease, coronary artery disease, cardiomyopathy and myocardial infarction are the major drivers to heart failure. The main hallmark of the progressive heart failure is a substantial cardiomyocyte loss followed by replacement of the lost cells with scar tissue through the pathological cardiac remodeling process also known as fibrosis³. There are two forms of cardiac fibrosis differentially characterized: compensatory and maladaptive. Initially, activation of cardiac fibroblasts followed by ECM production maintains cardiac tissue integrity upon pathological damage. However, excessive ECM deposition impairs cardiac structure and function leading to heart failure⁴.

Despite the advancement of the field in detection of CVD and attenuation of symptoms related to heart disease, lack of therapeutic interventions to effectively reverse the cardiac remodeling process including cardiomyocyte replacement and prevention of collagen deposition still exist. Adult heart is a post-mitotic organ with a limited regenerative potential. The inherently limited cardiac regenerative capacity coupled with insufficient exogenous reparative tools have rendered regenerative medicine incompetent to repair damaged myocardium. Cardiac therapeutics exploiting a combination of key mechanisms including 1) preservation of tissue and cell function, 2) reducing inflammation and pathological remodeling, and 3) increasing cell-cell

communication, angiogenesis and cardiomyogenesis are highly sought after to replenish the damaged myocardium and induce cardiovascular repair⁵.

Cell-based therapies

Endogenous deficiency of the heart to restore structural and functional integrity following myocardial damage prompted researchers to look for an optimal cell population to promote repair and regeneration. Attempts to differentiate embryonic stem cells (ESCs) and induced pluripotent stem (IPS) cells into cardiomyocytes failed to generate mature cells with the ability to electronically couple with preexisting myocardium^{6,7}. In addition, preclinical studies and clinical trials using bone marrow-derived cells and mesenchymal stem cells (MSCs) demonstrated modest beneficial effects to treat myocardial damage⁸. Similarly, investigations using cardiac-derived cells including (but not limited to) c-Kit⁺ cardiac interstitial cells (cCICs), sca-1⁺ cells, side population cells and MSCs revealed little improvement in myocardial structure and function due in part to limited cell survival and engraftment along with poor reparative potential of delivered cells⁹. Improvement of cellular biological properties to enhance reparative potential has been attempted using interventional strategies such as injection of cells with biomaterials, cytokines, and growth factors as well as genetic engineering approaches to overexpress pro-survival and anti-apoptotic factors¹⁰⁻¹². Despite decades of research, the field of cardiovascular research continues to struggle with identification of optimal protein(s), signaling pathways and/or an optimal cell population to mediate cardiac repair.

Cell fusion to generate “Next generation” cardiac cell therapeutic

Cell fusion is a validated reprogramming approach to create cells with youthful and pre-committed biological phenotypes^{13,14}. MSCs and cCICs demonstrate cell-specific

characteristics that make them favorable cells for cell fusion. MSCs are multipotent cells with capacity to differentiate into bone, cartilage, and adipose tissues. Upon transplantation, MSCs secrete paracrine and anti-inflammatory factors and activate endogenous cardiac cells, induce angiogenesis, preserve cardiomyocytes, and reduce scar formation. On the other hand, cCICs differentiate into multiple cardiac lineages such as smooth muscle cells, endothelial cells, and cardiomyocytes^{15,16}. In the myocardial context, fusion of murine cCICs and MSCs resulted in creation of hybrid cells named CardioChimeras (CCs) that harnessed the beneficial properties of the parent cells and bestowed enhanced functional and structural recovery in a mouse model of myocardial infarction¹⁴. However, therapeutic relevance of CCs to human cells remains unknown. Therefore, as the next step in translational development of this *ex vivo* cell engineering approach, human CardioChimeras (hCCs) are created and characterized. Findings of the study are presented in the chapter 2 of the dissertation.

Cardiomyocyte-based therapies

Loss of cardiomyocytes upon pathological damage or aging coupled with the failure of the heart to generate additional cardiomyocyte to replace damaged or lost cells is the main contributor to heart failure. Adult mammalian cardiomyocytes are post-mitotic with a very limited proliferative capacity both in healthy myocardium and upon pathological damage. During the past decade, cumulative studies intended to enhance cardiomyocyte cell cycle progression using interventional strategies such as overexpression of cell cycle proteins or pluripotency factors, induction of systemic hypoxaemia as well as transcriptional and hormonal manipulations¹⁷. Collectively, these studies failed to force cardiomyocytes to complete mitosis and underscored a further

critical facet of cardiomyocyte-based therapy to identify novel signaling pathways to enhance cardiomyocyte survival.

PIM1 (Proviral Insertion site in Murine leukemia virus kinase 1) is the main isoform of PIM family of kinases expressed in the heart. The serine threonine kinase PIM1 promotes cardiomyocyte survival and antagonizes senescence. Similarly, receptor tyrosine kinase c-Kit is expressed in different cell types including cardiomyocytes as well as multiple populations of CICs and is functionally implicated in biological activities such as transcriptional activation, cell proliferation and survival¹⁸⁻²¹. In hematopoietic stem cells, c-Kit mediates PIM1-induced cell proliferation and survival²². However, the relationship between c-Kit and PIM1 in the myocardial context remains to be demonstrated. Our assessment presented in chapter 3 of the dissertation, validated that PIM1 enhances survival of cardiomyocytes by upregulating c-Kit expression.

Fibroblast-based therapies

Cardiac fibroblast (CF) is a heterogeneous population of cells in terms of origin or source, tissue location, function, and gene expression profile²³. The multifaceted role of CFs including (but not limited to) cardiac development, tissue homeostasis and pathological remodeling makes them critical for cardiovascular therapies. However, heterogeneity of CF population remains as a challenge for fundamental understanding of fibroblast biology and development of therapeutics targeting CFs. Identifying molecular signatures characteristics of CF subpopulations in healthy myocardium and upon injury-induced remodeling would distinguish subpopulations with superior functional capacity requisite of proper adaptation to pathological stimuli and reversing maladaptive remodeling.

c-Kit is a type III receptor tyrosine kinase expressed in different cardiac cells involved in tissue homeostasis and repair^{24,25}. Presence of c-Kit has been detected in fibroblast population in different tissue and organs such as lung, liver, and aorta²⁶⁻²⁸. However, limited is known about the functional contribution of c-Kit signaling within fibroblast population in different tissues. In addition, expression, and functional implication of c-Kit in CF population has not been addressed. Therefore, we aimed to determine functional significance of c-Kit signaling within CICs of fibroblast lineage. Findings of the study are presented in the chapter 4 of the dissertation.

REFERENCES

1. Virani SS, Alonso A, Benjamin EJ, Bittencourt MS, Callaway CW, Carson AP, Chamberlain AM, Chang AR, Cheng S, Delling FN, Djousse L, Elkind MSV, Ferguson JF, Fornage M, Khan SS, Kissela BM, Knutson KL, Kwan TW, Lackland DT, Lewis TT, Lichtman JH, Longenecker CT, Loop MS, Lutsey PL, Martin SS, Matsushita K, Moran AE, Mussolino ME, Perak AM, Rosamond WD, Roth GA, Sampson UKA, Satou GM, Schroeder EB, Shah SH, Shay CM, Spartano NL, Stokes A, Tirschwell DL, VanWagner LB, Tsao CW. Heart Disease and Stroke Statistics-2020 Update: A Report From the American Heart Association. *Circulation*. 2020;141:e139–e596.
2. Benjamin EJ, Blaha MJ, Chiuve SE, Cushman M, Das SR, Deo R, de Ferranti SD, Floyd J, Fornage M, Gillespie C, Isasi CR, Jiménez MC, Chaffin Jordan L, Judd SE, Lackland D, Lichtman JH, Lisabeth L, Liu S, Longenecker CT, Mackey RH, Matsushita K, Mozaffarian D, Mussolino ME, Nasir K, Neumar RW, Palaniappan L, Pandey DK, Thiagarajan RR, Reeves MJ, Ritchey M, Rodriguez CJ, Roth GA, Rosamond WD, Sasson C, Towfighi A, Tsao CW, Turner MB, Virani SS, Voeks JH, Willey JZ, Wilkins JT, Wu JH, Alger HM, Wong SS, Muntner P. Heart Disease and Stroke Statistics-2017 Update: A Report From the American Heart Association WRITING GROUP MEMBERS. *Circulation*. 2017;135:e146–e603.
3. az ar EL, Sadek HA, Bergmann O. Cardiomyocyte renewal in the human heart: insights from the fall-out. *Eur Hear J*. 2017;38:2333–2342.
4. Krenning G, Zeisberg EM, Kalluri R. The Origin of Fibroblasts and Mechanism of Cardiac Fibrosis. *J Cell Physiol*. 2010;225:631–637.
5. Broughton KM, Wang BJ, Firouzi F, Khalafalla F, Dimmeler S, Fernandez-Aviles F, Sussman MA. Mechanisms of Cardiac Repair and Regeneration. *Circ Res*. 2018;122:1151.
6. Anderson ME, Goldhaber J, Houser SR, Puceat M, Sussman MA. Embryonic stem cell-derived cardiac myocytes are not ready for human trials. *Circ Res*. 2014;115:335–338.
7. Shiba Y, Filice D, Fernandes S, Minami E, Dupras SK, Van Biber B, Trinh P, Hirota Y, Gold JD, Viswanathan M, Laflamme MA. Electrical Integration of Human Embryonic Stem Cell-Derived Cardiomyocytes in a Guinea Pig Chronic Infarct Model. *J Cardiovasc Pharmacol Ther*. 2014;19:368–381.
8. Nowbar AN, Mielewczik M, Karavassilis M, Dehbi HM, Shun-Shin MJ, Jones S, Howard JP, Cole GD, Francis DP. Discrepancies in autologous bone marrow stem cell trials and enhancement of ejection fraction (DAMASCENE): weighted regression and meta-analysis. *BMJ*. 2014;348.
9. Li Q-H, Cao P, Vajravelu BN, Guo Y, Du J, Bolli R, Hong KU, Zhu X, Bhatnagar A, Book MJ, Nong Y, Al-Maqtari T. c-kit+ Cardiac Stem Cells Alleviate Post-Myocardial Infarction Left Ventricular Dysfunction Despite Poor Engraftment and Negligible Retention

in the Recipient Heart. *PLoS One*. 2014;9:e96725.

10. Cheng K, Blusztajn A, Shen D, Li TS, Sun B, Galang G, Zarembinski TI, Prestwich GD, Marbán E, Smith RR, Marbán L. Functional performance of human cardiosphere-derived cells delivered in an in situ polymerizable hyaluronan-gelatin hydrogel. *Biomaterials*. 2012;33:5317–5324.

11. Beohar N, Rapp J, Pandya S, Losordo DW. Rebuilding the damaged heart: The potential of cytokines and growth factors in the treatment of ischemic heart disease. *J Am Coll Cardiol*. 2010;56:1287–1297.

12. Mohsin S, Khan M, Toko H, Bailey B, Cottage CT, Wallach K, Nag D, Lee A, Siddiqi S, Lan F, Fischer KM, Gude N, Quijada P, Avitabile D, Truffa S, Collins B, Dembitsky W, Wu JC, Sussman MA. Human cardiac progenitor cells engineered with Pim-I kinase enhance myocardial repair. *J Am Coll Cardiol*. 2012;60:1278–1287.

13. Acquistapace A, Bru T, Lesault PF, Figeac F, Coudert AE, Le Coz O, Christov C, Baudin X, Auber F, Ylou R, Dubois-Randé JL, Anne-Marie R. Human mesenchymal stem cells reprogram adult cardiomyocytes toward a progenitor-like state through partial cell fusion and mitochondria transfer. *Stem Cells*. 2011;29:812–824.

14. Quijada P, Salunga HT, Hariharan N, Cubillo JD, El-Sayed FG, Moshref M, Bala KM, Emathingier JM, De La Torre A, Ormachea L, Alvarez R, Gude NA, Sussman MA. Cardiac stem cell hybrids enhance myocardial repair. *Circ Res*. 2015;117:695–706.

15. Leri A, Kajstura J, Anversa P. Cardiac stem cells and mechanisms of myocardial regeneration. *Physiol Rev*. 2005;85:1373–1416.

16. Wang Y, Chen X, Cao W, Shi Y. Plasticity of mesenchymal stem cells in immunomodulation: pathological and therapeutic implications. *Nat Immunol*. 2014;15:1009–1016.

17. Gude NA, Sussman MA. Cardiac regenerative therapy: Many paths to repair. *Trends Cardiovasc Med*. 2020;30:338–343.

18. Muraski JA, Rota M, Misao Y, Fransioli J, Cottage C, Gude N, Esposito G, Delucchi F, Arcarese M, Alvarez R, Siddiqi S, Emmanuel GN, Wu W, Fischer K, Martindale JJ, Glembotski CC, Leri A, Kajstura J, Magnuson N, Berns A, Beretta RM, Houser SR, Schaefer EM, Anversa P, Sussman MA. Pim-1 regulates cardiomyocyte survival downstream of Akt. *Nat Med*. 2007;13:1467–1475.

19. Zhu HH, Wang XT, Sun YH, He WK, Liang JB, Mo BH, Li L. Pim1 Overexpression Prevents Apoptosis in Cardiomyocytes after Exposure to Hypoxia and Oxidative Stress via Upregulating Cell Autophagy. *Cell Physiol Biochem*. 2018;49:2138–2150.

20. Wang Z, Bhattacharya N, Weaver M, Petersen K, Meyer M, Gapter L, Magnuson NS. Pim-1: A serine/threonine kinase with a role in cell survival, proliferation, differentiation and tumorigenesis. *J Vet Sci*. 2001;2:167.

21. Borillo GA, Mason M, Quijada P, Völkers M, Cottage C, McGregor M, Din S, Fischer K, Gude N, Avitabile D, Barlow S, Alvarez R, Truffa S, Whittaker R, Glassy MS, Gustafsson AB, Miyamoto S, Glembotski CC, Gottlieb RA, Brown JH, Sussman MA. Pim-1 kinase protects mitochondrial integrity in cardiomyocytes. *Circ Res*. 2010;106:1265–1274.
22. An N, Cen B, Cai H, Song JH, Kraft A, Kang Y. Pim1 kinase regulates c-Kit gene translation. *Exp Hematol Oncol*. 2016;5:1–8.
23. Tallquist MD. Cardiac Fibroblast Diversity. *Annu Rev Physiol*. 2020;82:63–78.
24. Lennartsson J, Rönstrand L. Stem Cell Factor Receptor/c-Kit: From Basic Science to Clinical Implications. *Physiol Rev*. 2012;92:1619–1649.
25. Rönstrand L. Signal transduction via the stem cell factor receptor/c-Kit. *Cell Mol Life Sci*. 2004;61:2535–2548.
26. Ding L, Dolgachev V, Wu Z, Liu T, Nakashima T, Wu Z, Ullenbruch M, Lukacs NW, Chen Z, Phan SH. Essential role of stem cell factor-c-Kit signalling pathway in bleomycin-induced pulmonary fibrosis. *J Pathol*. 2013;230:205–214.
27. Ni Z, Deng J, Potter CMF, Nowak WN, Gu W, Zhang Z, Chen T, Chen Q, Hu Y, Zhou B, Xu Q, Zhang L. Recipient c-Kit Lineage Cells Repopulate Smooth Muscle Cells of Transplant Arteriosclerosis in Mouse Models. *Circ Res*. 2019;125:223–241.
28. Zani BC, Sanches BDA, Maldarine JS, Biancardi MF, Santos FCA, Barquilha CN, Zucão MI, Baraldi CMB, Felisbino SL, Góes RM, Vilamaior PSL, Taboga SR. Telocytes role during the postnatal development of the Mongolian gerbil jejunum. *Exp Mol Pathol*. 2018;105:130–138.

CHAPTER 2

Human CardioChimeras: Creation of a Novel 'Next Generation' Cardiac Cell

INTRODUCTION

Beneficial, albeit modest, effects of cell therapy for treatment of myocardial damage have been established in extensive preclinical studies^{1,2} as well as early clinical trial testing³⁻⁵. Improvement of efficacy remains a primary focus of the cell therapy field with ongoing studies attempting to define whether there is an optimal cell type or even a combination of cell types delivered simultaneously to promote reparative remodeling^{6,7}. The concept of creating an 'enhanced' cell with augmented biological properties to promote healing remains a longstanding interest of our group. Simply stated, we have sought to create 'unnatural solutions' to the natural limitations of myocardial repair by ex vivo modification resulting in engineered cell products derived from c-kit⁺ cardiac interstitial cells (cCICs) possessing enhanced survival, persistence, proliferation, and many other desirable characteristics that deliver greater recovery from myocardial injury than corresponding originating parental cells⁸⁻¹¹. One example of this philosophy is the CardioChimera, named for the fusion of cCICs and mesenchymal stem cells (MSCs) together into a single hybrid cell that can be expanded in culture and used for adoptive transfer therapy to mitigate myocardial infarction injury⁸. The seminal study of CardioChimeras was performed using a homotypic murine model system with delivery murine CardioChimeras and results demonstrated superiority of the CardioChimeras over either cCICs alone, MSCs alone, or the combination of cCICs and MSCs delivered together as a single cell suspension. These promising findings prompted subsequent studies to translate the murine findings into the human context but, working with myocardial-derived human cells presents a new set of challenges to be overcome.

As opposed to murine cCICs and MSCs obtained from 2-3-month-old hearts with high yield quantities⁸, human cardiac cells are derived from small ventricular biopsy specimens¹². Limited source material results in lower yield of human myocardial-derived cells, and the relatively slow proliferation of myocardial-derived human cells relative to mouse counterparts^{12,13} further hampers therapeutic manipulations. Furthermore, replicative senescence occurs much earlier in culture passaging of human cells, whereas murine cardiac cells demonstrate significantly extended passaging capability^{8,14,15}. Another technical challenge posed by inherent species-specific biology are differences between murine and human cells in response to experimental interventions¹⁶. Murine cells readily fuse and form polyploid hybrid cells⁸ whereas human cells are much less tolerant of polyploidy leading to genomic instability^{17,18} that necessitates rigorous optimization of culture conditions to overcome impaired expansion following fusion. Efficient and reproducible creation of CardioChimeras is facilitated by use of murine cardiac cell populations from syngeneic healthy young donors⁸ unlike the individual patient-specific nature of human myocardial derived cells with unavoidable sample characteristic variability¹⁴. Collectively, these challenges prompted this study to demonstrate feasibility and reproducibility of human CardioChimera (hCC) generation.

Concurrent isolation of three distinct CIC types comprised of cCIC, MSC, and endothelial progenitor cells (EPC) from a single human myocardial tissue sample with optimized culture condition was developed by our group¹². Therefore, this protocol was employed to obtain human cCIC and MSC for subsequent fusion proof of concept using low passage neonatal human myocardial-derived cells. The rationale for using neonatal cells for feasibility testing is based upon their more youthful biological phenotype of

enhanced proliferation and survival, preservation of telomere length, and decreased level of senescence relative to cells derived from heart failure patients^{14,15,19}.

hCCs created in the present study represent novel hybrid cells with phenotypic properties consistent with our previous observations of murine CCs. Having overcome the multiple aforementioned challenges of human myocardial-derived cell utilization, cell fusion is a feasible promising engineering approach to enhance functional properties of human cardiac cells and pave the way for 'designer' hCC exhibiting enhanced reparative properties.

METHODS

cCIC and MSC isolation

The study was designed in accordance with and approved by the institutional review committees at San Diego State University along with the IRB (#120686) and no informed consent was required. Neonatal cells were derived from non-surgically obtained post-mortem cardiac tissue. Cells were isolated as previously published¹². Briefly, heart samples were mechanically minced into 1mm³ pieces and digested in collagenase II (150 U mg/mL, Worthington, LS004174) followed by brief low speed (850 rpm, for 2 minutes) centrifugation to remove cardiomyocytes and tissue debris. The supernatant was subjected to magnetic activated cell sorting (MACS) using c-kit conjugated microbeads (Miltenyi Biotec, #130-091-332) and c-kit enriched cells were plated in human c-kit CIC media. The c-Kit negative population was further purified by MACS for MSC surface markers CD90 and CD105. c-kit CICs and MSCs were incubated at 37°C in 5% CO₂ and used for cellular fusion between passages 5 and 10. Media used in the study are listed in Table 2.1.

Lentiviral constructs and stem cell infection

Lentiviral plasmids and viral particles were created as previously described⁸. c-kit CICs and MSCs were stably transduced at passage 6 with PGK-EGFP-Puro and PGK-mCherry-Bleo respectively at a multiplicity of infection (MOI) of 40. Expression of EGFP and mCherry fluorescent proteins in c-kit CICs and MSCs was confirmed by fluorescent microscopy as well as flow cytometry. Lentivirally-modified cells were stabilized through multiple rounds of passaging and freeze/thaw cycles before fusion experiments.

Cell fusion and creation of hCCs

Cell fusion was performed with GenomeONETM-CF EX Sendai Virus (Hemagglutinating Virus of Japan-Envelope or HVJ-E) Envelope Cell Fusion Kit (Cosmo Bio, USA) using the suspension method according to the manufacturer's protocol. Briefly, cCIC-EGFP and MSC-mCherry populations were combined in 25 μ L of 1X cell fusion buffer at a ratio of 2:1 (total cell number of 100,000). The 2:1 ratio yielded the maximum number of double positive fused cells (hCCs) and therefore was chosen for the study. Inactivated Sendai virus was added to the cell mixture and incubated on ice for 5 minutes. Cell suspension was transferred to the 37°C incubator for 30 minutes with intermittent shaking every 5 minutes. Next, cells were plated in 2 ml fusion media on a well of a 6-well dish. Media was changed after 24 hours and cells were then cultured in fusion media for 4 days. Hybrid cells were identified and isolated by FACS sorting using parent cells in pure as well as mixed (but not fused) as controls. hCCs were plated on a 96-well microplate (1 cell per well) for clonal expansion. Clone nomenclature was based on well number in the plate. All hCCs were used between passages 4 to 6 for experiments.

Light microscopy and measurement of cell morphology

Bright field images of hCCs and the parent cells were obtained using a LEICA DMIL microscope and cell boundaries were outlined by image analysis using ImageJ software. Cell surface area and length to width ratio were determined as previously described²⁰.

Proliferation and doubling time

c-kit CICs, MSCs and hCCs were plated on a 6-well dish at a density of 20,000 cells per well. At three time points (days 1,3, and 5) cells were trypsinized and counted

manually using a hemocytometer. Cell proliferation rate was determined for each group as fold change over day 1. Cell doubling times were calculated using online population doubling time software (http://www.doubling-time.com/compute_more.php).

Immunocytochemistry

c-kit CICs, MSCs and hCCs were plated on a two-well chamber slide (15,000 per well). Staining was performed following the protocol previously described²⁰. Nuclei were stained with DAPI diluted in 1X PBS at room temperature for 15 minutes. Cells were imaged using a Leica TCS SP8 confocal microscope. Antibodies and dilutions are listed in Table 2.2.

Immunoblot analysis

c-kit CICs, MSCs and hCCs were plated on 100-mm plates. Protein cell lysates were collected using 200 μ l of SDS-PAGE protein sample buffer. Proteins were separated on a 4-12% NuPage Novex Bis Tris gel (Invitrogen) and transferred onto a polyvinylidene fluoride (PVDF) membrane. Non-specific binding sites were blocked using Odyssey blocking buffer (LI-COR) and proteins were labeled with primary antibodies in 0.2% Tween in Odyssey blocking buffer overnight. After washing, blots were incubated with secondary antibodies in 0.2% Tween 20 in Odyssey blocking buffer for 1.5 hours at room temperature and scanned using the LICOR Odyssey CLx scanner. Quantification was performed using ImageJ software. Antibodies and their dilutions are listed in Table 2.2.

Real-Time PCR

c-kit CICs, MSCs and hCCs were plated on 100-mm plates. RNA lysate was collected from the culture and purified using Quick-RNA MiniPrep (Zymo Research). cDNA synthesis was conducted using iScript cDNA Synthesis Kit (Bio Rad). qPCR was performed on a Bio-Rad CFX real time cycler using iQ SYBR Green (Bio Rad) and gene specific primers. Signals were normalized to 18S for analysis. Data were calculated using the $\Delta\Delta C(t)$ method. Primers are listed in Table 2.3.

Ploidy and cytogenic analysis

c-kit CICs, MSCs and hCCs were plated on a 6- well plate at a density of 50,000 cells per well. Cells were collected the following day and centrifuged at 1200 rpm for 5 minutes, the pellet was re-suspended in 70% ethanol, and stored at -20°C for at least 24 hours prior to use. After centrifugation at 1300 rpm for 5 minutes, cell pellet was re-suspended in 300 ul of Propidium Iodide incubated at 37°C for 15 minutes prior to flow cytometry analysis. Cytogenetic analysis of c-kit CICs, MSCs, and hCCs (G4) plated at a density of 300,000 cells on 2500 mm² flasks was performed by KaryoLogic, Inc (North Carolina; www.karyologic.com).

Cell death assay

For reactive oxygen injury, c-kit CICs, MSCs and hCCs were plated on a 6- well plate at a density of 60,000 cells per well. Cells were subjected to low serum media for 24 hours (depleted to 25% of growth media serum level) followed by 4 hours of hydrogen peroxide (350 μ mol/L) treatment. Annexin V and Sytox Blue staining was performed to label apoptotic and necrotic cells and cell death was measured using FACS Aria (BD Biosciences).

For ischemia-reperfusion injury, cCICs, MSCs and hCCs were seeded on 6-well plates at a density of 60,000 cells per well. The following day, media was replaced with Kreb's Heinsleit buffer (KH buffer) to induce glucose starvation, and cells were transferred to a hypoxic incubator with 1% oxygen tension for 3 hours to simulate ischemia. Cells were re-exposed to regular growth media and incubated in a standard cell culture incubator with ambient (21%) oxygen for 24 hours to simulate reperfusion. Annexin V and Sytox Blue staining was performed to label apoptotic and necrotic cells and cell death was measured using FACS Aria (BD Biosciences). Cells cultured in growth media in normoxic conditions and cells subjected to Kreb's Heinsleit buffer (KH buffer) in hypoxic condition were used as the controls of the experiment to measure basal and hypoxia-induced cell death, respectively. KH buffer and the respective media used inside the hypoxic glove box were equilibrated in hypoxia overnight before starting the experiment.

NRCM co-culture with stem cells

NRCMs were isolated as previously described^{21,22} and seeded in a 6-well dish at a density of 200,000 per well in M199 media with 15% fetal bovine serum (FBS). The following day, cells were incubated in media with 10% FBS for 8 hours followed by 24-hour serum depletion in serum free media. Stem cells (cCICs, MSCs, combination of cCICs and MSCs, hCCs) were added to the culture at a 1:5 ratio. The slow growing clone B3 was excluded from this experiment due to a low expansion rate. After 24 hours in co-culture, cells were stained with Annexin V and Sytox Blue. Unlike CardioChimeras or their parent cells, the NRCMs were non-transduced allowing for separation by fluorescent activated cell sorting (FACS) of negative cells (NRCMs) versus GFP+, mCherry+ or GFP+/mcherry+ cells. Thus, parental and CardioChimera cells were removed from the

population for survival analysis of NRCMs, which was completed by flow cytometry using the FACS Aria. Controls for the NRCMs included 1) culture in serum free media alone (SF), 2) “rescue” by replenishment with M199 media + 10% serum, or 3) constant culture in M199 media + 10% serum for the duration of the experiment.

Statistical analysis

All data are expressed as mean \pm SEM. Statistical significance was assessed using one-way ANOVA or two-way ANOVA for multiple comparisons, with the Dunnett and Tukey tests as post hoc tests to compare groups to a control group in Graph Pad Prism v5.0. or Microsoft excel. $P < 0.05$ was considered statistically significant.

RESULTS

hCCs creation from c-kit CIC and MSC cell fusion

Human c-kit CICs expressing GFP and human MSCs expressing mCherry, incubated in the presence of inactivated RNA Sendai virus, underwent cellular fusion to form mononuclear hybrid cells^{23,24} (Figure 2.1A). A group of mixed c-kit CICs and MSCs without the viral treatment was used as the negative control for the fusion experiment (Figure 2.2E). Readily detectable uniform fluorescence labeling of parental c-kit CICs and MSCs is required for optimal yield of double fluorescent hybrids. Flow cytometry analysis shows 96.6% of c-kit CICs and 92% of MSCs expressed EGFP and mCherry, respectively (Figure 2.2A-D). Double fluorescent hybrids were sorted into 96-well microplates for clonal expansion to derive hybrid clones called hCCs. Five unique hCCs named D6, F1, G4, D2 and B3 were derived from five independent fusion experiments with 1-4% efficiency (Table 2.4). Dual fluorescent positivity of hCCs was validated by fluorescence microscopy (Figure 2.3). Immunocytochemistry with respective EGFP and mCherry antibodies confirmed integration of genomic content from both parent cells into hCC that was maintained after clonal expansion and passaging in culture (Figure 2.1B). Parent cells immunolabeled for EGFP and mCherry exhibited appropriate single wavelength fluorescence signal, validating antibody specificity for their respective fluorophores (Figure 2.4). Immunoblotting results corroborate flow cytometry and microscopy observations for expression of both fluorescent marker proteins (Figure 2.1C). Collectively, these findings indicate successful cellular fusion and stability of the chimeric state after clonal expansion.

hCCs possess diploid DNA content

Fusion of two parental lines resulted in elevated ploidy in murine CCs DNA content⁸. In comparison, hCCs possess diploid (2n) DNA content comparable to the parent cells as assessed using flow cytometry analysis (Figure 2.5A). Since all hCCs exhibited 2n ploidy status, a representative line (hCC G4) was chosen for karyotypic analysis that confirmed normal male karyotype with 46 chromosomes including XY as observed in G-banded spreads (Figure 2.5B). Therefore, hCCs maintain normal 2n ploidy content relative to the parent cells, in contrast to increased ploidy of murine CCs⁸.

hCCs phenotypic and proliferative characteristics resemble parent cells

Murine CCs characteristics of survival and proliferation were comparable to parental lines albeit with increased DNA content⁸. Cellular properties of select hCCs were assessed for phenotypic traits of morphology and growth rate relative to parental lines, chosen to represent typical examples for variability of hCC characteristics. Cellular morphology measured using bright field images of the hCCs and parent cells reveals a range of cell surface area, length to width ratio (Figure 2.6). hCCs D6, F1, and G4 exhibited cell surface area similar to cCICs that was significantly lower than MSCs (Figure 2.6A). Length to width ratio of these clones was significantly greater compared to MSCs and was comparable to that of cCICs (Figure 2.6B). Proliferation rate of these hCCs was increased relative to parental cells with a doubling time of approximately 24 hours and were therefore characterized as fast growth (Figure 2.6C,D). Cell surface area of hCC D2 was significantly greater than the cCICs and similar to the MSCs (Figure 2.6A). Length to width ratio for hCC D2 was significantly decreased relative to cCICs, instead resembling that of MSCs (Figure 2.6B). Proliferation rate of hCC D2 was intermediate compared to parent cells with a doubling time of 32 hours and was identified as a medium growth

(Figure 2.6C,D). Lastly, hCC B3 cell surface area was increased, length to width ratio was reduced, and proliferation rate was slow compared to either of the parent cells, resulting in designation of slow growth (Figure 2.6A-D). Collectively, these data profile phenotypic properties of hCCs with cell surface areas and length to width ratios that correspond to their proliferative rates, consistent with previous findings for murine CCs⁸.

Profiling for commitment and secretory gene expression reveals hCC variability

Gene expression profiling revealed significant heterogeneity between various murine CCs⁸, so commitment and secretory gene profiles for hCCs were assessed to find if similar diversity was present. Cardiac lineage markers including cardiac type troponin T2 (TNNT2), GATA Binding Protein 4 (GATA4), Platelet and Endothelial Cell Adhesion Molecule 1 (PECAM1), and smooth muscle actin (SMA) were investigated by measuring mRNA expression level by qPCR analysis. Early cardiac transcription factor GATA4 was significantly upregulated in all hCCs except B3 in which GATA4 expression was not detected when compared to MSCs. When measured relative to cCICs, GATA4 was approximately one-fold higher in F1, unchanged in D6 and G4, and downregulated in D2 (Figure 2.7A). Cardiomyocyte marker TNNT2 level was reduced in fast growing hCCs D6, F1 and G4 as opposed to medium and slow growing clones D2 and B3 (Figure 2.7B). PECAM1 level was higher in F1, G4 and D2 clones than in MSCs, but lower than cCICs. PECAM1 was not detected in B3 (Figure 2.7C). All hCCs significantly downregulated SMA relative to MSCs resembling closely to cCICs (Figure 2.7D). Collectively, these data demonstrate that fast-growing hCCs upregulate expression of early cardiac transcription factor GATA4 and downregulate expression of maturational cardiac marker TNNT2, reflective of their cardiac progenitor-like phenotype. In contrast, medium and slow growing

hCCs exhibit a more committed mRNA profile from this cursory assessment with select transcripts.

hCCs were also analyzed for expression of pro-survival paracrine factors that mediate protective effects. HB-EGF, a secreted glycoprotein involved in wound healing and cardiac development^{25,26}, was significantly upregulated in hCC F1. In comparison, hCCs D6, G4 and D2 expressed HB-EGF at levels intermediate between the two parent cell ranges. HB-EGF expression was undetectable in hCC B3 clone (Figure 2.8A). HGF, a paracrine growth, motility and morphogenic factor^{27,28} was expressed at low levels in hCC D6, F1, G4 and D2, but at a comparable level to MSCs in B3 (Figure 2.8B). hCCs F1 and D2 expressed high levels of chemotactic factor SDF relative to cCICs but lower than in MSCs. SDF expression was downregulated in D6 and G4 and undetectable in B3 (Figure 2.8C). FGF2, an important growth factor for wound healing, angiogenesis and cellular proliferation²⁹ was highly upregulated in B3. hCC F1 and D2 increased FGF2 expression relative to cCICs and were more reminiscent of MSCs, while hCC D6 and G4 expressed lower levels of FGF2 compared to both parent cells (Figure 2.8D). In summary, similar to what was previously observed with murine CC⁸, profiling of hCC reveals distinct transcriptome profiling signatures between the clones.

Survival in response to environmental stress is enhanced in hCC

hCCs response to stress was assessed by serum deprivation with cell death quantitation by flow cytometric measurement of necrosis and apoptosis. Cell death rates were similar between hCCs and MSCs but lower than in cCICs (Figure 2.9A). Response to oxidative stress induced by hydrogen peroxide treatment (350 $\mu\text{mol/L}$) in serum free conditions reveals significantly lower rates of apoptosis and necrosis compared to either

parental line with correspondingly higher rate of survival (Figure 2.9B), consistently present even when media formulations for parental lines (cCIC or MSC) are used for hCC culture (Figure 2.10; D2 line). Simulated ischemia-reperfusion injury was also used as an environmental stress with cells subjected to KH buffer in hypoxia, and growth media in normoxia as experimental controls. Lower necrotic cell death was found for all hCCs compared to parent cells. Similar apoptosis rates were observed comparing hCCs to the parental lines with the exception of D2, which exhibited higher apoptotic cell death (Figure 2.9C). Correspondingly, survival of all the hCCs except D2 was not significantly different from either parental cell. Similar percentages of apoptotic, necrotic and live cells were observed in experimental controls (Figure 2.11). In conclusion, unlike susceptibility to environmental stress in murine CCs similar to parent lines⁸, hCCs exhibit enhanced resistance to oxidative stress.

Cardiomyocyte survival is enhanced by hCC co-culture

Protective effects in response to serum deprivation challenge of NRCMs in vitro is similar between murine CCs or their corresponding parental cells⁸. The protective effect of hCCs was similarly assessed, with serum deprivation challenge of NRCMs that prompted significantly increased cell death which was partially mitigated by addition of serum for 24 hours (Figure 2.12). Clone B3 was excluded from further experiments due to slow expansion rate, undergoing replicative senescence after passage 10 in culture. In comparison, lines D6, F1 and G4 expansion rate slowed after passage 10, yet had not reached replicative senescence. Line D2 maintained consistent proliferation rate for more than 10 passages, currently expanded more than 27 passages without arrest (Figure 2.13). NRCMs showed improved

survival mediated by each hCC in response to serum deprivation, co-culture with hCC D2 yielding the highest rate of survival (Figure 2.12). NRCMs co-cultured with cCICs exhibited high level of survival in response to serum deprivation. Co-culture of MSCs and hCCs G4 partially rescued NRCMs resembling the effect of serum addition for 24 hours. hCCs D6 and F1 exerted intermediate protective effect on NRCMs compared to parental cells while hCCs D2 provided the highest protective effect on NRCMs, exceeding even that of NRCMs in high serum. Except for hCC G4 which exhibited protective effect similar to MSCs, most hCCs resembled cCICs in co-culture effect upon NRCMs. Therefore, in contrast to murine CCs with protective effect similar to their corresponding parent cells, hCCs exhibit individually distinct variability in protective action.

DISCUSSION

Myocardial repair and regeneration research continues to progress on multiple fronts supported by over a decade of cumulative studies despite a recent “whipsaw” movement of controversies related to the terminology and biology of “cardiac stem cells”^{30,31}. Although cardiogenic potential of “cardiac stem cells” remains debatable^{32,33}, cardioprotective effects have been repeatedly demonstrated by our group and others^{13,34-36} with “cardiac stem cells”, now referred to as cCIC in this report to avoid being misconstrued as cardiogenic cells. Furthermore, cardioprotective effects of cCICs are enhanced by combinatorial delivery with MSCs⁶. These findings are encouraging, but efficacy of such adoptive transfer cell therapies is inherently limited by multiple factors including poor cell survival, engraftment, and persistence that can be overcome to some extent by *ex vivo* cell engineering. Our group has focused upon potentiation of myocardial repair through use of modified cells created by genetic engineering^{9,10,14,37}, fusion⁸, and combinatorial culture / delivery³⁸ (Megan Monsanto, unpublished data, [2019]). Implementation of these ‘unnatural’ approaches to create engineered cell types and combinations is deliberately intended and rationally designed to overcome inherent limitations of normal mammalian myocardial that lacks endogenous cellular reservoirs to repair and restore myocardial structure and function following pathological damage. The rationale for CC in our initial study was to avoid issues related to variable survival, engraftment, persistence, and proliferation rates of cCIC versus MSC when mixing these two distinct populations together for cell therapy administration. We posited that creating a novel fused hybrid CC would deliver significantly enhanced reparative activity compared to each parental cell type used either alone or in mixed single cell suspensions; a

postulate that was validated in a syngeneic murine infarction model⁸. The next logical advance of this patented technology (US Patent #20160346330A1) was to apply a comparable approach in the context of human cCIC and MSC. Species-specific characteristics between murine versus human biology result in differences in the creation and phenotypic properties of CC, as reinforced by results in this report.

Comparison between human versus murine CC reveal both similarities as well as important distinctions. Specifically with respect to similarities between mouse CC and hCC, there were a few notable parallels including 1) variable proliferative characteristics (slow, medium, fast), 2) variable CC size, 3) comparable PECAM 1 expression (intermediate level in both mouse and human CCs compared to the parent cells), and 4) cardiac troponin T expression at high level relative to parental lines in hCC D2 and B3 (medium and slow grower lines, respectively) similar to mouse CC versus parental lines. In comparison, differences between mouse CC and hCC were numerous and significant as demonstrated by 1) higher survival level compared to parental cells in response to oxidative stress by hCCs, whereas murine CC survival was either similar or lower than parental cells, 2) normal diploid DNA content of hCC compared to tetraploidy in murine CC, 3) SMA expression was lower in hCC than either parental cell, but higher in mouse CCs than the cCIC parental cell, 4) cardiac troponin T expression level in hCC similar to fast growing parental lines versus higher level expression in mouse CC, and 5) variable protective effects in NRCM co-culture studies of hCC relative to parental cells versus similar protective effects between murine CC and parental cells. Even with an admittedly small sampling size of two murine CCs and 5 hCCs there are demonstrable biological

and phenotypic differences between species-specific CC warranting further characterization.

Polyploidy observed in mouse CC was notably absent from human CC lines. The diploid (2n) DNA content of hCC (Figure 2.5) contrasts with that of murine CCs which had increased DNA content⁸. Cytogenic analysis of hCC G4 further confirmed a normal karyotype with 46 chromosomes. The most straightforward interpretation of this finding is that human cell fusions do not tolerate polyploidy as a permissive state for mitotic growth, unlike their murine counterparts. hCCs may acquire one copy of each chromosome complement from either of the parent cells leading to no change in ploidy content, despite being successfully fused. This cytogenetic state eliminates concerns regarding fusion-induced increased DNA content and aneuploidy which can lead to genomic instability and cellular senescence³⁹. All hCCs retained cellular properties corresponding to cCIC and MSCs consistent with chromosomal mosaicism in somatic cells without significantly altering stem cell behavior⁴⁰.

MSCs mediate cell survival through secretion of pro-survival chemokines and cytokines including SDF-1 and IGF-1^{41,42}. hCCs expressed growth factors and cardioprotective cytokines including EGF and SDF and were resistant against starvation-induced cell death (Figure 2.8A,C and Figure 2.9A). Similarly, hCCs demonstrated enhanced survival in response to oxidative stress (Figure 2.9B) and attenuated necrotic cell death in response to I/R injury (Figure 2.9B,C). When co-cultured with NRCMs, hCC G4 exhibited cardioprotective effect similar to MSCs whereas hCCs F1, D6 and D2 exhibited cardioprotective effect similar to cCIC with hCC D2 exhibiting the highest cardioprotective activity (Figure 2.12). Cellular cross talk survival signals might be

facilitated in CC, since exosome contents such as MSC-secreted micro-RNA 21 protects c-Kit⁺ stem cells from oxidative injury through the PTEN/PI3K/Akt signaling pathway⁴³. Paracrine signaling activity has been suggested as the mechanistic basis for cardioprotection using cell therapy⁴⁴⁻⁴⁶, so the relevance of the secretome from hCCs deserves further detailed analyses to establish a putative role in enhancing survival signaling. The potential contribution of cell fusion to heart regeneration is essentially unexplored despite the established role of cell fusion as a reprogramming mechanism leading to enhanced proliferation and growth rate in differentiated cells⁴⁷. The findings presented here suggest cell fusion as a reliable and stable technique to generate human hybrid cells. cCICs and MSCs are ideal cellular candidates for cell fusion. They can be consistently isolated and expanded in laboratory settings and they are well established cell candidates for cellular therapy based on the results of basic biological studies and clinical trials^{4,48}. In the present study, cCICs and MSCs were used at a ratio of 2:1 but cell ratios used for fusion can influence the fate and functional potential of resultant hybrids. Therefore, modifying the cell number ratio prior to fusion could be a promising future direction leading to the design of hybrids with individualized phenotypic characteristics. Moreover, adapting cell fusion ratios for future studies may promote creation of hCCs with more consistent biological profiles.

Cell fusion is a tractable engineering approach to generate a novel cell population incorporating characteristics of two different human cardiac derived interstitial cell populations into a single cell. Hybrid CCs possess molecular and phenotypic characteristics similar to previously established murine CCs with enhanced myocardial repair potential⁸. However, cell engraftment, cardiomyogenic and reparative potential of

hCCs need to be determined and are the subject of the future investigation that could support next steps toward translational application of hCCs.

TABLES

Table 2.1. List of Media

| Media | Components |
|------------------------|--|
| Human cCIC Media | 10% ES FBS, 1% Penicillin-Streptomycin-Glutamine (100X), 5 mU/mL human erythropoietin, 10 ng/mL human recombinant basic FGF, 0.2 mmol/L L-Glutathione in F12 HAM's (1x) |
| Human MSC Media | 20% FBS, 1% Penicillin-Streptomycin-Glutamine (100X) in 10.1 g/L Minimum Essential Medium Eagle, Alpha Modification |
| Human Fusin Media | 15% ES-FBS, 1% Penicillin-Streptomycin-Glutamine (100X), 5 mU/mL human erythropoietin, 10 ng/mL human recombinant basic FGF, 0.2 mmol/L L-Glutathione, 0.2 mg/ml human IL-6, 0.25 mg/ml human LIF in F12 HAM's (1x) |
| KH Buffer | 125 mmol/L NaCl, 8 mmol/L KCl, 1.2 mmol/L KH_2PO_4 , 1.25 mmol/L MgSO_4 , 1.2 mmol/L CaCl_2 , 6.25 mmol/L NaHCO_3 , 20 mmol/L deoxy-glucose, 5 mmol/L Na-lactate, 20 mmol/L HEPES |
| NRCM Plating Media | 15% FBS, 1% Penicillin-Streptomycin-Glutamine (100X) in medium 199 |
| NRCM Maintenance Media | 10% FBS, 1% Penicillin-Streptomycin-Glutamine (100X) in medium 199 |

Table 2.2. List of Antibodies

| Antibody | Manufacturer | # Catalog | Dilution | Application |
|--------------------|---------------------|------------------|-----------------|---------------------|
| GFP anti rabbit | Thermofisher | A11122 | 1:80 | Immunocytochemistry |
| mCherry anti Rat | Thermofisher | M11217 | 1:80 | Immunocytochemistry |
| DAPI | Sigma | D9542 | 1:5000 | Immunocytochemistry |
| GFP anti Goat | Rockland | 35059 | 1:500 | Immunoblotting |
| mCherry anti mouse | Abcam | Ab125096 | 1:500 | Immunoblotting |
| GAPDH anti Goat | Sicgen | AB0067 | 1:3000 | Immunoblotting |
| Annexin V-APC | Biosciences | 550475 | 1:175 | Cell death assay |
| Sytox Blue | Life Technologies | S11348 | 1:2000 | Cell death assay |
| Propidium Iodide | Invitrogen | P3566 | 1:75 | Ploidy analysis |

Table 2.3. List of Primers

| mRNA Primers | Forward | Reverse |
|---------------------|----------------------------|--------------------------|
| GATA 4 | CTCAGAAGGCAGAGAGTGTGTCAA | CACAGATAGTGACCCGTCCCAT |
| TNNT2 | GGAGAGAGAGTGGACTTTATG | CCTCCTCTTTCTTCCTGTTTC |
| PECAM1 | CCAAGCCCGAACTGGAATCT | CACTGTCCGACTTTGAGGCT |
| SMA | CCCAGCCAAGCACTGTCAGGAATCCT | TCACACACCAAGGCAGTGCTGTCC |
| HB-EGF | ACAAGGAGGAGCACGGGAAAAG | CGATGACCAGCAGACAGACAGATG |
| HGF | GGCTGGGGCTACACTGGATTG | CCACCATAATCCCCCTCACAT |
| SDF | CAGTCAACCTGGGCAAAGCC | AGCTTTGGTCCTGAGAGTCC |
| FGF2 | CTGGCTATGAAGGAAGATGGA | TGCCCAGTTCGTTTCAGTG |
| 18s | CGAGCCGCCTGGATACC | CATGGCCTCAGTTCCGAAAA |

Table 2.4. List of Fusions

| Fusions | % Yield | hCC analyzed |
|----------------|----------------|---------------------|
| 1 | % 4 | G4 |
| 2 | % 3.1 | D6 |
| 3 | % 1.5 | F1 |
| 4 | % 1.3 | B3 |
| 5 | % 1.2 | D2 |

FIGURES

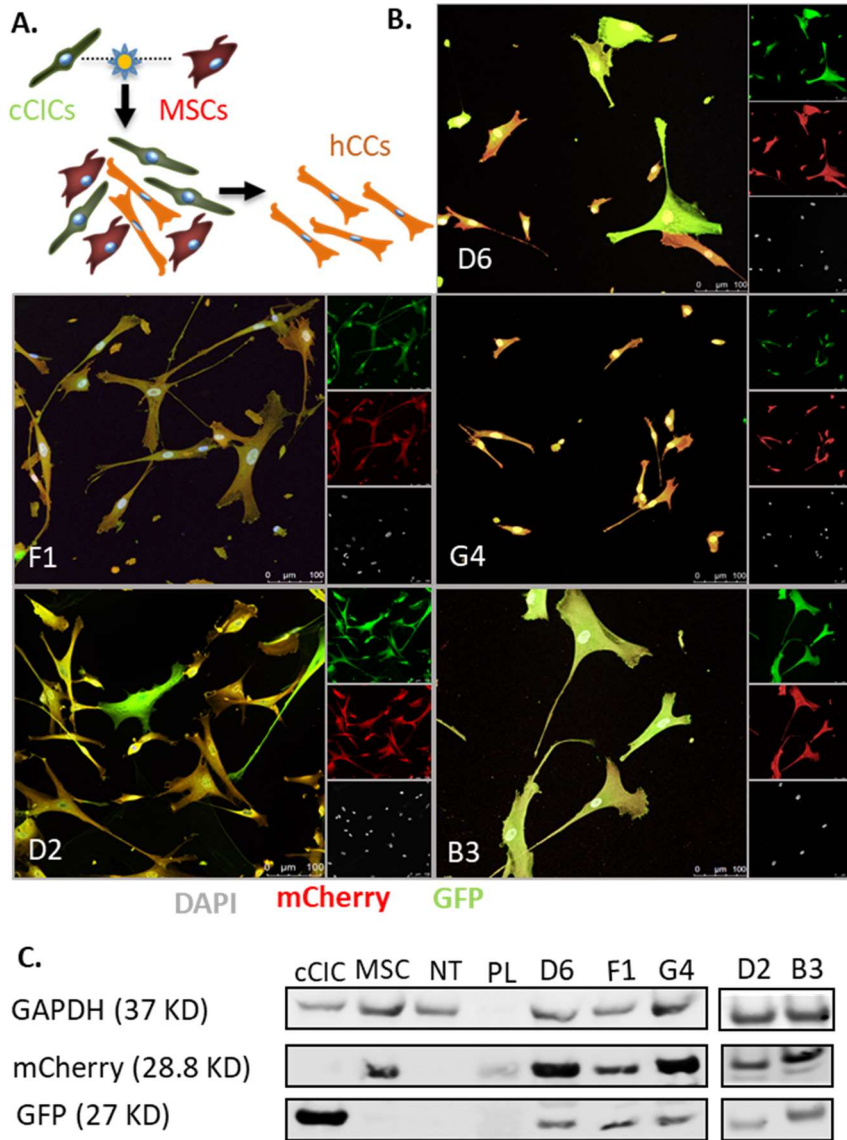


Figure 2.1. hCCs are created from cCIC and MSC cell fusion. A. Schematic of the cell fusion. Phase A: fusion-suspension of cCICs and MSCs. Phase B: initial fused cells undergo mitotic event to combine chromatin content. Phase C: Sorting of successfully fused cell. B. ICC of the hCCs for GFP and mCherry. C. Immunoblot analysis of cCIC-GFP, MSC-mCherry, Non-Transduced (NT) MSC, and hCCs. PL: protein ladder. GAPDH is used as the loading control.

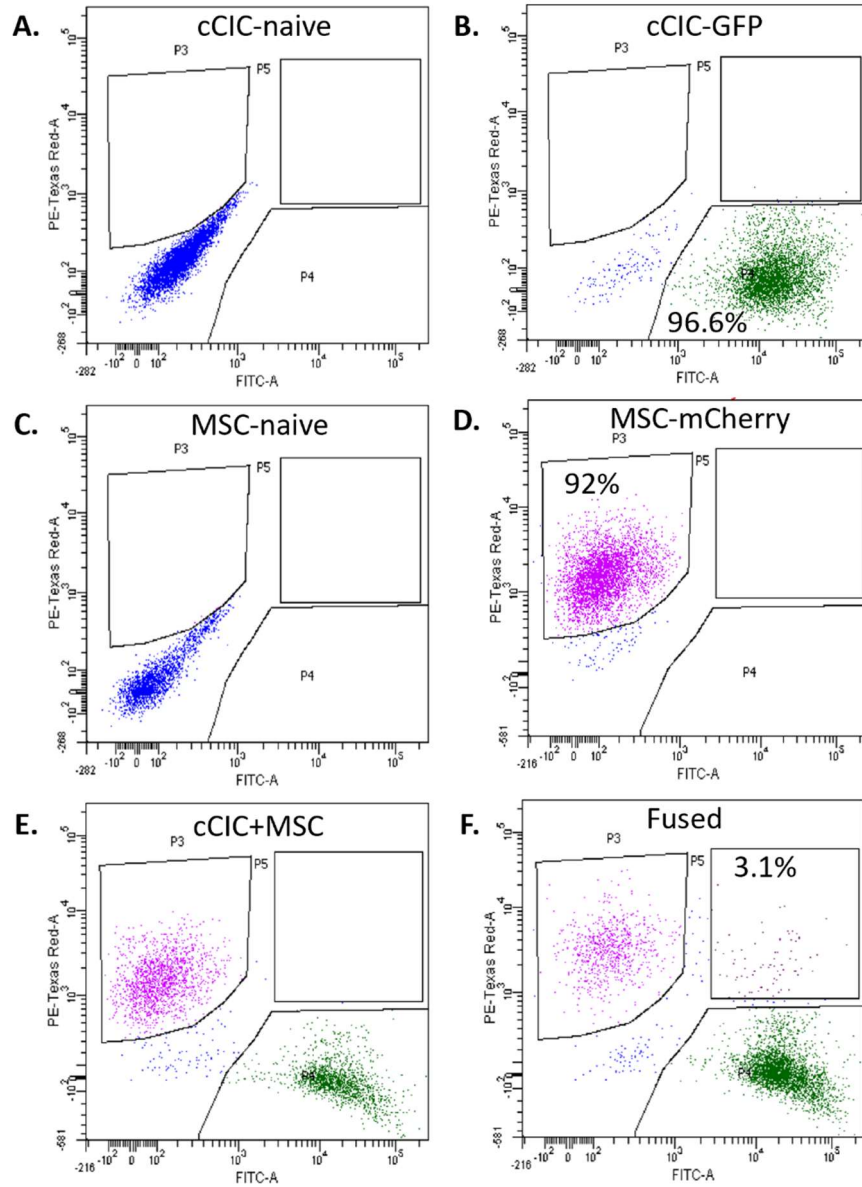


Figure 2.2. Flow cytometry plots of one representative fusion experiment. A. naive cCICs, B. cCIC-GFP, C. naive MSCs, D. MSC-mCherry, E. the combinatorial cCIC and MSC group as the negative control and F. Sendai virus-induced fused cells.

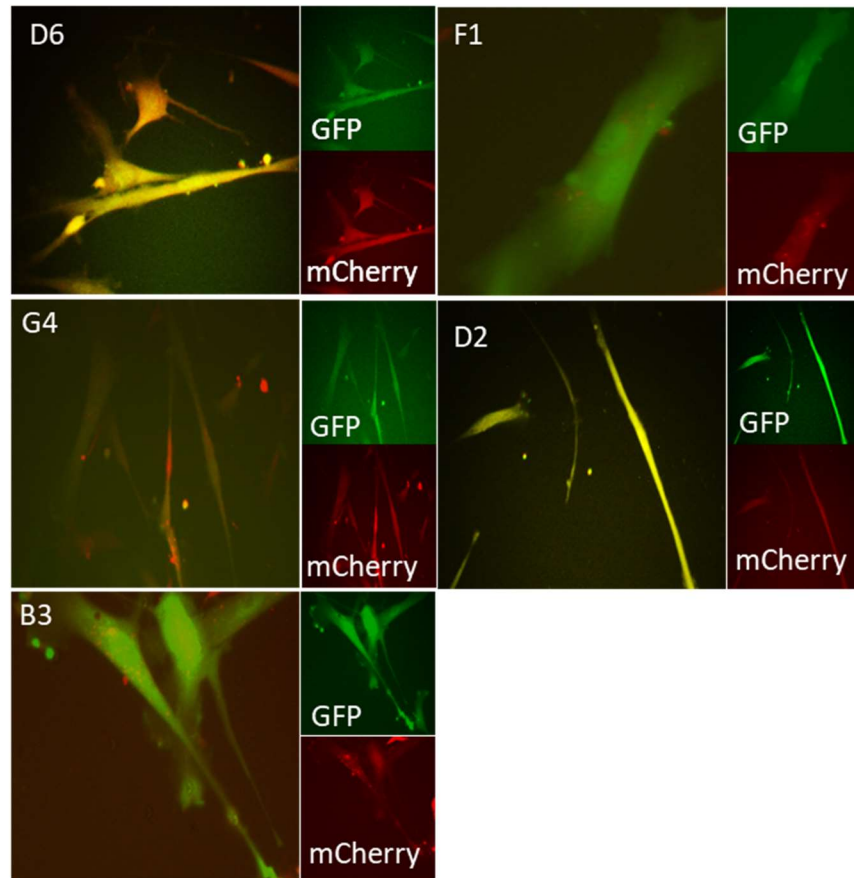


Figure 2.3. Live native fluorescent images of hCCs illustrating double positivity of the fused cells.

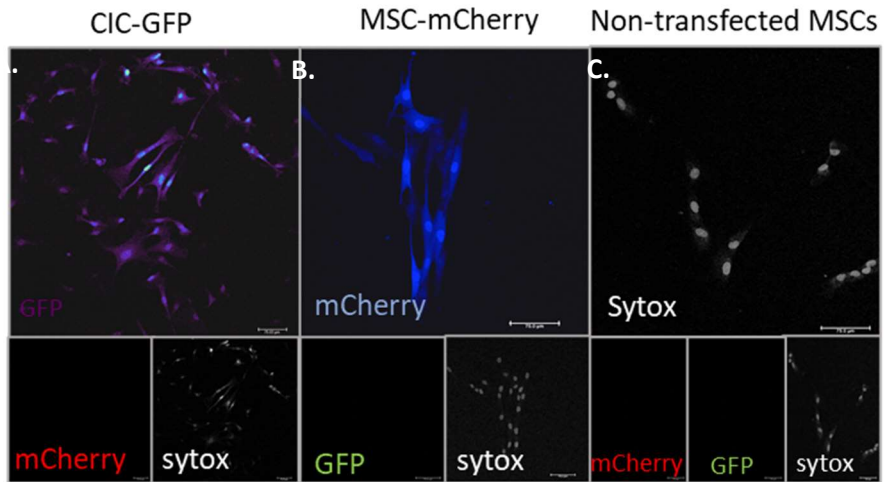


Figure 2.4. Immunocytochemistry images parent cells validating antibody specificity for their respective fluorophores. A. cCIC-GFP, B. MSC-mCherry, and C. Non-transduced MSCs stained for GFP and mCherry. Sytox green was used as the nuclear stain.

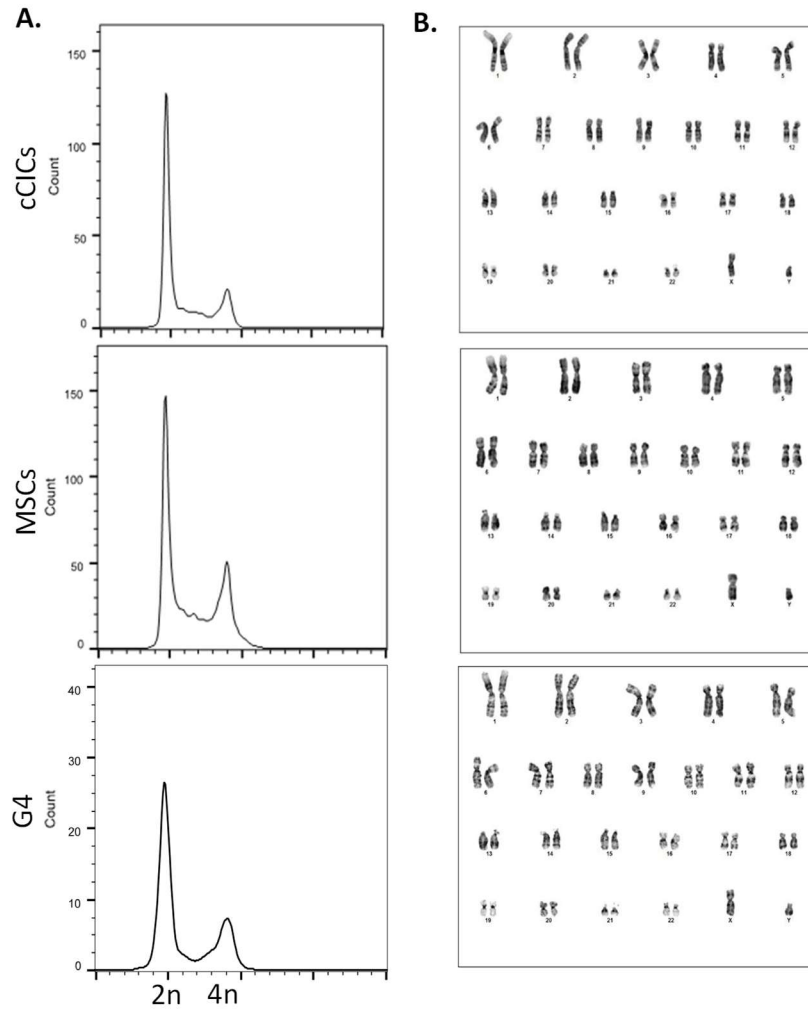


Figure 2.5. hCCs reveal ploidy status and DNA content corresponding to the parent cells. A. Flow Cytometry plots for PI/RNase staining of parent cells and hCCs, G4. N=3 independent experiments. B. Cytogenetic analysis of parent cells and hCC, G4.

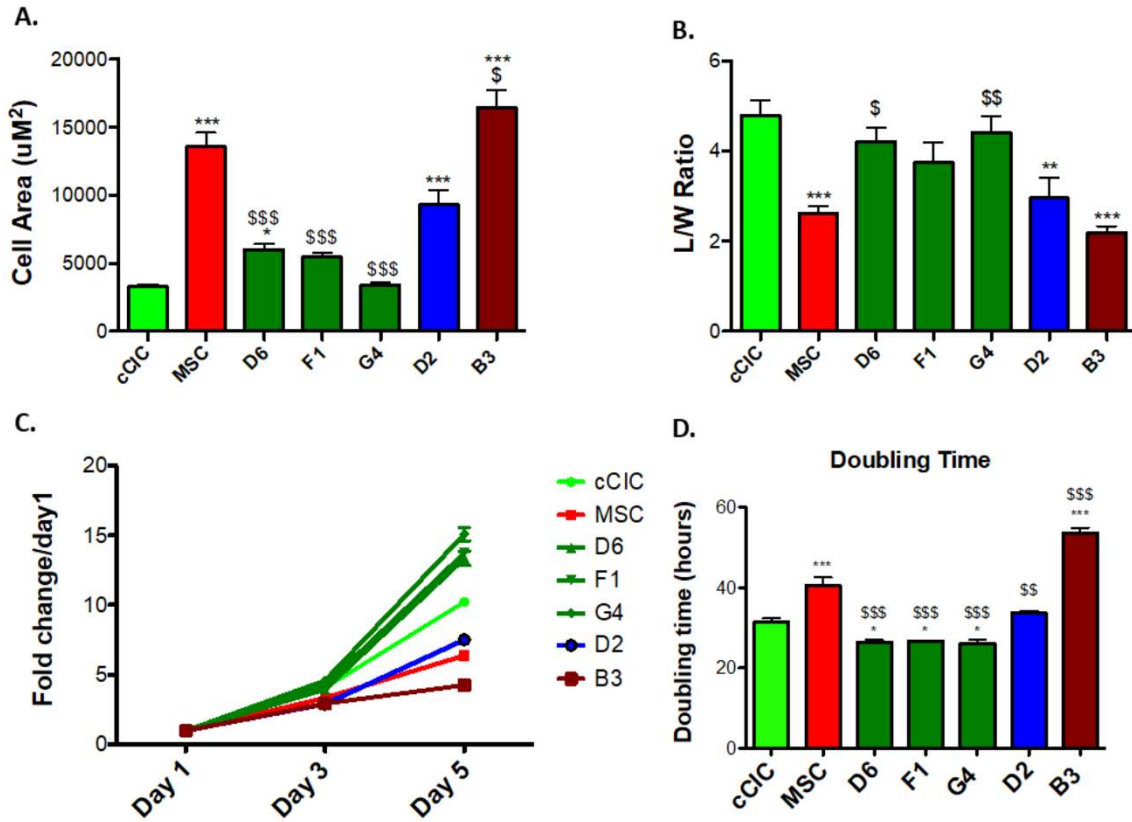


Figure 2.6. Morphometric and proliferative characteristics of hCCs. A. Cell surface area and B. length to width ratio of the parent cells and hCCs. C. Proliferation rate of parent cells and hCCs represented as fold change over day 1, and D. cell doubling time represented in hours. N=3 independent experiments. Statistical analysis was performed by One-Way ANOVA multiple comparison with Dunnett. *P<0.05 Vs cCIC, **P<0.001 Vs cCIC, ***P< 0.0001 Vs cCIC, \$P<0.05 Vs MSC, \$\$P<0.001 Vs MSC, \$\$\$P<0.0001 Vs MSC. Error bars are \pm SEM.

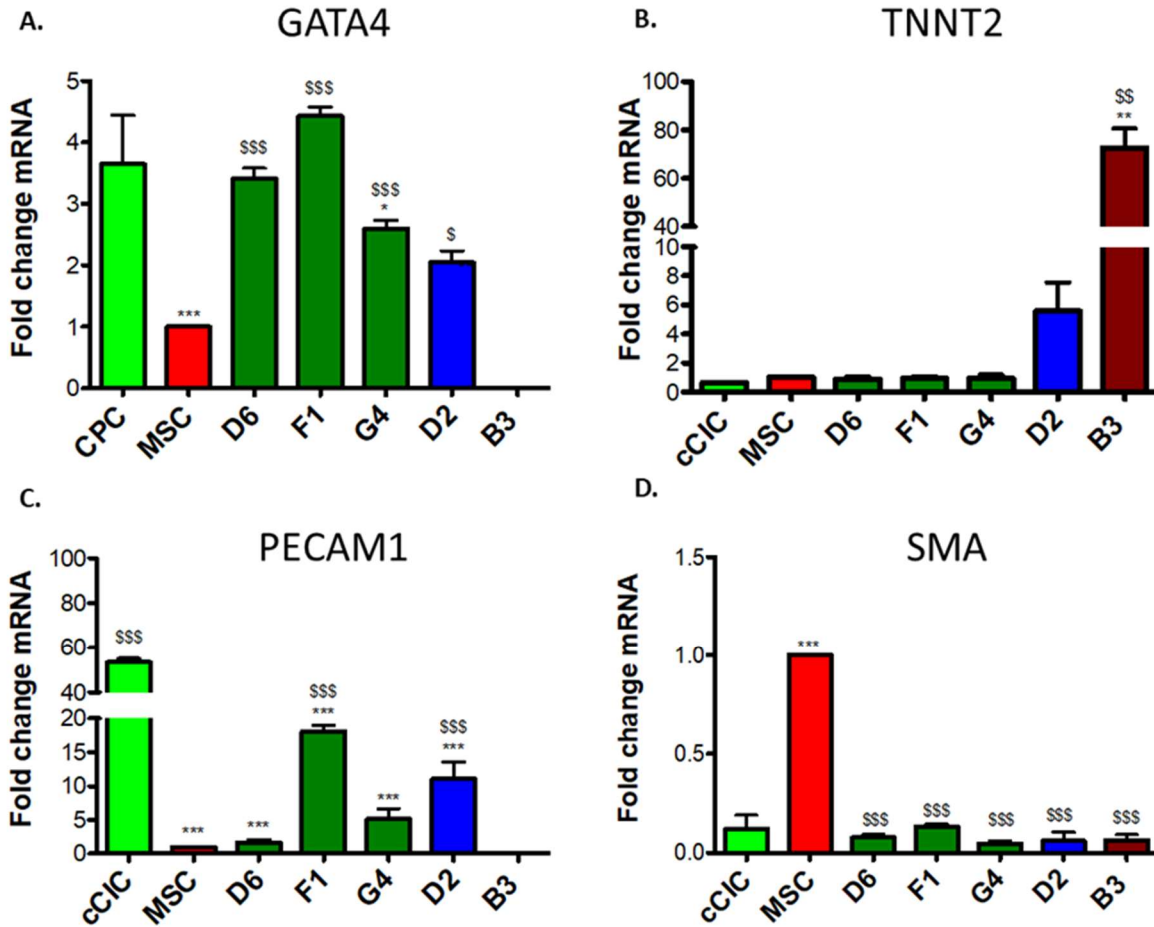


Figure 2.7. hCCs exhibit variable expression level of cardiomyogenic commitment markers. mRNA expression level of A. GATA4, B. TNNT2, C. PECAM1, and D. SMA for parent cells and hCCs. N=3 independent experiments, 3 replicates (wells) per group per experiment. All genes expression is normalized to ribosomal 18s and represented as a fold change relative to MSCs. Statistical analysis was performed by One-Way ANOVA multiple comparison with Dunnett. *P<0.05 Vs cCIC, **P<0.001 Vs cCIC, ***P< 0.0001 Vs cCIC, \$P<0.05 Vs MSC, \$\$P<0.001 Vs MSC, \$\$\$P<0.0001 Vs MSC. Error bars are \pm SEM.

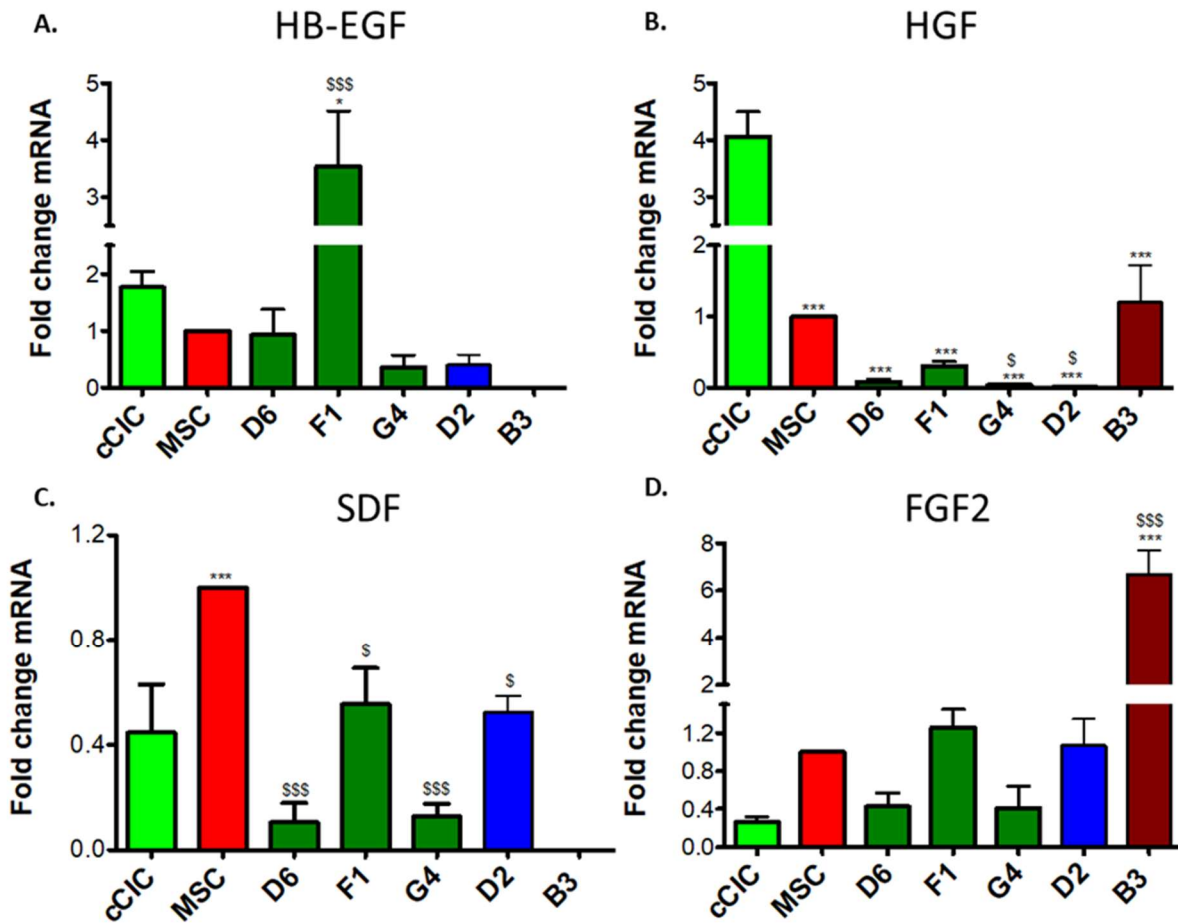


Figure 2.8. hCCs exhibit variable secretory gene profiles. mRNA expression level of A. HB-EGF, B. HGF, C. SDF, and D. FGF2. N=3 independent experiments, 3 replicates (wells) per group per experiment. All genes expression is normalized to ribosomal 18s and represented as a fold change relative to MSCs. Statistical analysis was performed by One-Way ANOVA multiple comparison with Dunnett. *P<0.05 Vs cCIC, **P<0.001 Vs cCIC, ***P< 0.0001 Vs cCIC, \$P<0.05 Vs MSC, \$\$P<0.001 Vs MSC, \$\$\$P<0.0001 Vs MSC. Error bars are \pm SEM.

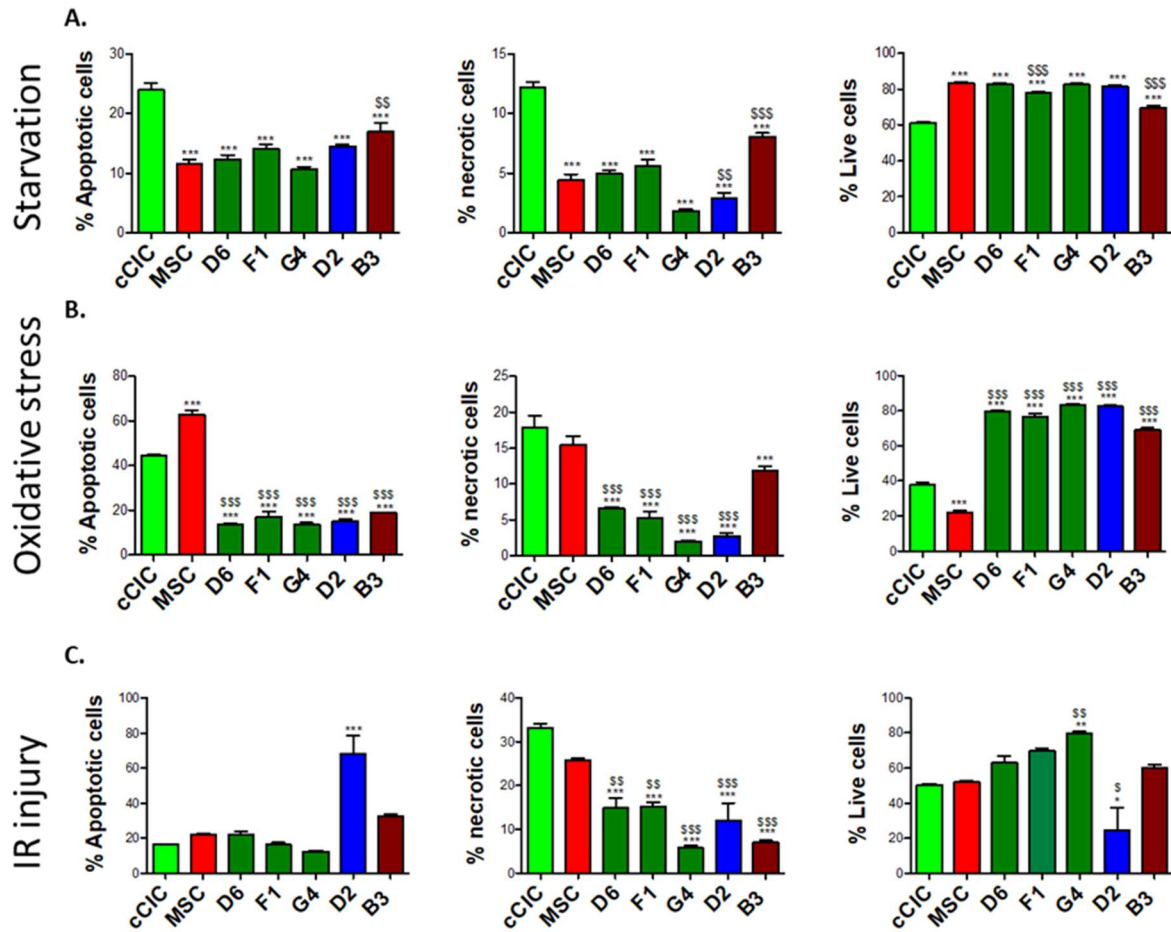


Figure 2.9. hCCs demonstrate enhanced survival in response to stress. Percentage of apoptotic, necrotic and live cells following A. serum starvation, B. oxidative stress, and C. IR injury. N=3 independent experiments. Statistical analysis was performed by Two-Way ANOVA multiple comparison with Tukey. *P<0.05 Vs cCIC, **P<0.001 Vs cCIC, ***P< 0.0001 Vs cCIC, \$P<0.05 Vs MSC, \$\$P<0.001 Vs MSC, \$\$\$P<0.0001 Vs MSC. Error bars are \pm SEM.

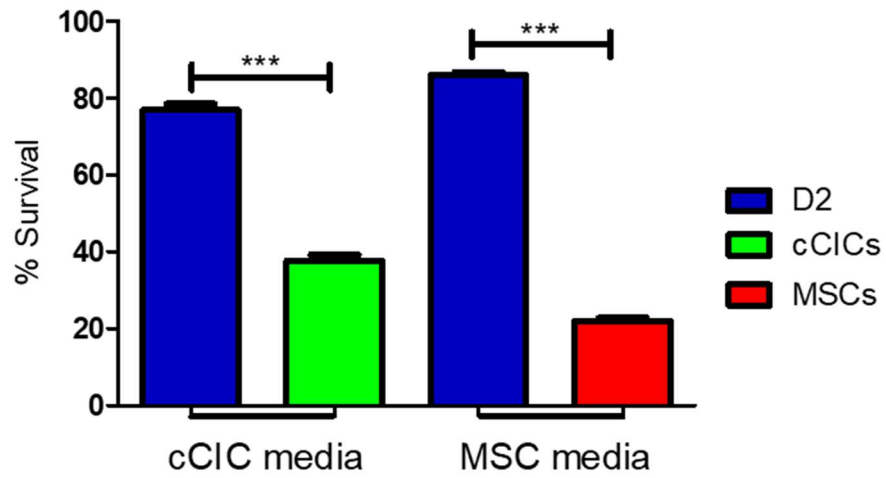


Figure 2.10. Percentage of survival (live cells) of D2 clones in cCIC media, cCICs in cCIC media, D2 clones in MSC media and MSCs in MSC media (from left to right) after treatment with hydrogen peroxide (350 $\mu\text{mol/L}$). Error bars are \pm SEM. *** $p < 0.001$

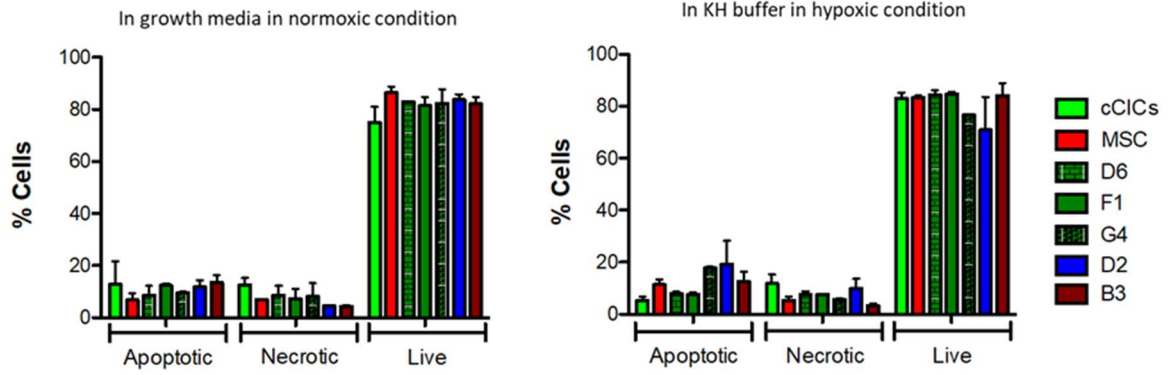


Figure 2.11. Percentage of apoptotic, necrotic and live cells. A. cultured in growth media in normoxic condition and B. subjected to KH buffer in hypoxic condition. Error bars are \pm SEM.

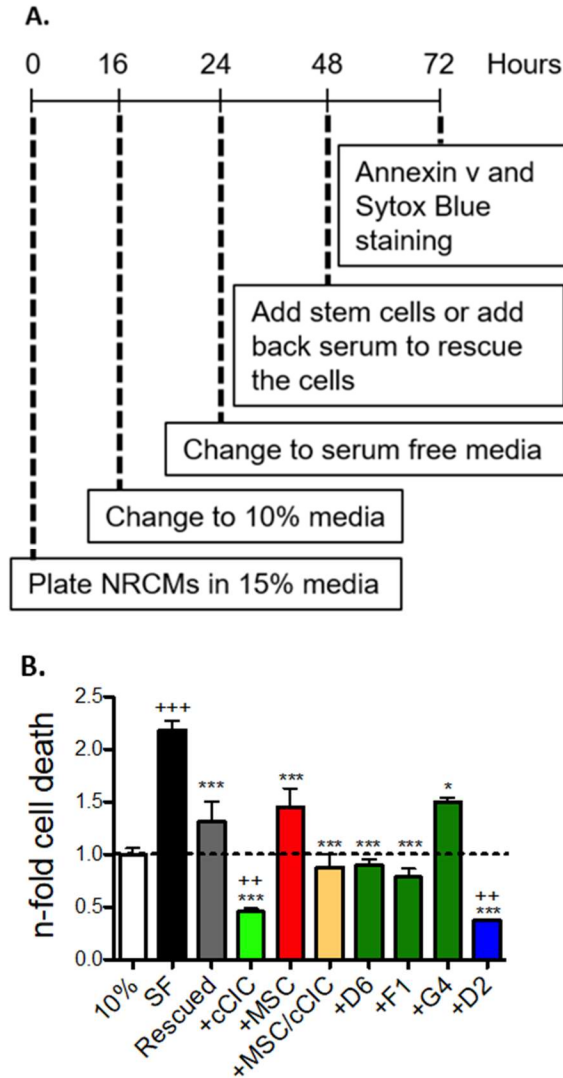


Figure 2.12. hCCs promote cardiomyocytes survival in response to serum deprivation. A. NRCM co-culture protocol. B. Cardiomyocytes cell death in 10% serum media (10%), serum free media (SF), rescued and in presence of cCICs, MSCs, combinatorial group of MSCs and cCICs (+MSCs/cCICs), D6, F1, G4 and D2. Values presented are fold change of Annexin v+ Sytox Blue+ cells relative to 10% serum media (also represented as dashed line, 1.0). N=3 independent experiments. Statistical analysis was performed by One-Way ANOVA multiple comparison with Dunnett. *P<0.05 Vs SF, ***P< 0.001 Vs SF, ++ P<0.01 Vs 10%, +++ P<0.001 Vs 10%.

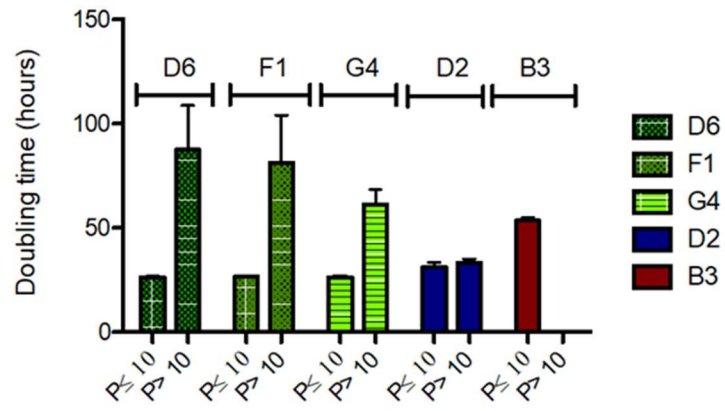


Figure 2.13. Cell doubling time of hCCs up to and after passage 10 in culture represented in hours. Error bars are \pm SEM.

REFERENCES

1. Li Q-H, Cao P, Vajravelu BN, Guo Y, Du J, Bolli R, Hong KU, Zhu X, Bhatnagar A, Book MJ, Nong Y, Al-Maqtari T. c-kit+ Cardiac Stem Cells Alleviate Post-Myocardial Infarction Left Ventricular Dysfunction Despite Poor Engraftment and Negligible Retention in the Recipient Heart. *PLoS One*. 2014; 9:e96725.
2. Sanganalmath SK, Bolli R. Cell Therapy for Heart Failure. *Circ Res*. 2013; 113:810-834.
3. Hare JM, Fishman JE, Gerstenblith G, DiFede Velazquez DL, Zambrano JP, Suncion VY, Tracy M, Ghersin E, Johnston P V., Brinker JA, Breton E, Davis-Sproul J, Schulman IH, Byrnes J, Mendizabal AM, Lowery MH, Rouy D, Altman P, Wong Po Foo C, Ruiz P, Amador A, Da Silva J, McNiece IK, Heldman AW. Comparison of allogeneic vs autologous bone marrow-derived mesenchymal stem cells delivered by transendocardial injection in patients with ischemic cardiomyopathy: The POSEIDON randomized trial. *JAMA - J Am Med Assoc*. 2012; 308:2369-2379.
4. Slaughter MS, Chugh AR, Rokosh DG, D'Amario D, Kajstura J, Solankhi NK, Sanada F, Hosoda T, Ikram S, Bolli R, Anversa P, Stoddard MF, Fahsah I, Elmore JB, Loughran JH, Goichberg P, Beache GM, Wagner SG, Leri A, Cappetta D. Cardiac stem cells in patients with ischaemic cardiomyopathy (SCIPIO): initial results of a randomised phase 1 trial. *Lancet*. 2011; 378:1847-1857.
5. Gerstenblith G, Johnston P V., Marbán L, Bonow RO, Marbán E, Mendizabal A, Lardo AC, Malliaras K, Wu E, Smith RR, Cingolani E, Makkar RR, Schuleri KH, Cheng K. Intracoronary Cardiosphere-Derived Cells After Myocardial Infarction. *J Am Coll Cardiol*. 2013; 63:110-122.
6. Williams AR, Hatzistergos KE, Addicott B, McCall F, Carvalho D, Suncion V, Morales AR, Da Silva J, Sussman MA, Heldman AW, Hare JM. Enhanced effect of combining human cardiac stem cells and bone marrow mesenchymal stem cells to reduce infarct size and to restore cardiac function after myocardial infarction. *Circulation*. 2013; 127:213-223.
7. Mitrani RD, Traverse JH, Chugh A, DiFede DL, March KL, Willerson JT, Bolli R, Sayre SL, Khan A, Bettencourt J, Lima JAC, Hare JM, Vojvodic RW, Perin EC, Simari RD, Moyé L, Hernandez-Schulman I, Henry TD, Loughran J, Cohen M, Ebert RF, Taylor DA, Yang PC, Pepine CJ. Rationale and Design of the CONCERT-HF Trial (Combination of Mesenchymal and c-kit + Cardiac Stem Cells As Regenerative Therapy for Heart Failure) . *Circ Res*. 2018; 122:1703-1715.
8. Quijada P, Salunga HT, Hariharan N, Cubillo JD, El-Sayed FG, Moshref M, Bala KM, Emathingier JM, De La Torre A, Ormachea L, Alvarez R, Gude NA, Sussman MA. Cardiac stem cell hybrids enhance myocardial repair. *Circ Res*. 2015; 117:695-706.
9. Fischer KM, Cottage CT, Wu W, Din S, Gude NA, Avitabile D, Quijada P, Collins BL, Fransioli J, Sussman MA. Enhancement of myocardial regeneration through genetic

engineering of cardiac progenitor cells expressing pim-1 kinase. *Circulation*. 2009; 120:2077-2087.

10. Mohsin S, Khan M, Toko H, Bailey B, Cottage CT, Wallach K, Nag D, Lee A, Siddiqi S, Lan F, Fischer KM, Gude N, Quijada P, Avitabile D, Truffa S, Collins B, Dembitsky W, Wu JC, Sussman MA. Human cardiac progenitor cells engineered with Pim-I kinase enhance myocardial repair. *J Am Coll Cardiol*. 2012; 60:1278-1287.

11. Korski KI, Kubli DA, Wang BJ, Khalafalla FG, Monsanto MM, Firouzi F, Echeagaray OH, Kim T, Adamson RM, Dembitsky WP, Gustafsson ÅB, Sussman MA. Hypoxia Prevents Mitochondrial Dysfunction and Senescence in Human c-Kit+ Cardiac Progenitor Cells. *Stem Cells*. 2019; 37:555-567.

12. Monsanto MM, Dembitsky WP, Ilves K, Kim T, White KS, Mohsin S, Fisher K, Sussman MA, Broughton K, Casillas A, Wang BJ, Khalafalla FG. Concurrent Isolation of 3 Distinct Cardiac Stem Cell Populations From a Single Human Heart Biopsy. *Circ Res*. 2017; 121:113-124.

13. Gude NA, Firouzi F, Broughton KM, Ilves K, Nguyen KP, Payne CR, Sacchi V, Monsanto MM, Casillas AR, Khalafalla FG, Wang BJ, Ebeid DE, Alvarez R, Dembitsky WP, Bailey BA, van Berlo J, Sussman MA. Cardiac c-Kit Biology Revealed by Inducible Transgenesis. *Circ Res*. 2018; 123:57-72.

14. Mohsin S, Khan M, Nguyen J, Alkatib M, Siddiqi S, Hariharan N, Wallach K, Monsanto M, Gude N, Dembitsky W, Sussman MA. Rejuvenation of human cardiac progenitor cells with pim-1 kinase. *Circ Res*. 2013; 113:1169-1179.

15. Samse K, Emathingier J, Hariharan N, Quijada P, Ilves K, Völkens M, Ormachea L, De La Torre A, Orogo AM, Alvarez R, Din S, Mohsin S, Monsanto M, Fischer KM, Dembitsky WP, Gustafsson ÅB, Sussman MA. Functional effect of Pim1 depends upon intracellular localization in human cardiac progenitor cells. *J Biol Chem*. 2015; 290:13935-13947.

16. Perlman RL. Mouse Models of Human Disease: An Evolutionary Perspective. *Evol Med Public Heal*. 2016; 2016:170-176.

17. Schoenfelder KP, Fox DT. The expanding implications of polyploidy. *J Cell Biol*. 2015; 209:485-491.

18. Coward J, Harding A. Size Does Matter: Why Polyploid Tumor Cells are Critical Drug Targets in the War on Cancer. *Front Oncol*. 2014; 4:123-137.

19. Avitabile D, Ormachea L, Tsai EJ, Sussman MA, Mohsin S, Monsanto M, Samse K, Joyo A, Hariharan N, Quijada P, De La Torre A, McGregor MJ. Nucleostemin Rejuvenates Cardiac Progenitor Cells and Antagonizes Myocardial Aging. *J Am Coll Cardiol*. 2015; 65:133-147.

20. Quijada P, Toko H, Fischer KM, Bailey B, Reilly P, Hunt KD, Gude NA, Avitabile

D, Sussman MA. Preservation of myocardial structure is enhanced by pim-1 engineering of bone marrow cells. *Circ Res.* 2012; 111:77-86.

21. Jagsi R, Jiang J, Momoh AO, Alderman A, Giordano SH, Buchholz TA, Pierce LJ, Kronowitz SJ, Smith BD. HHS Public Access. 2017; 263:219-227.

22. Blackwood EA, Thuerlauf DJ, Plate L, Glembotski CC, Paxman RJ, Wiseman RL, Azizi K, Kelly JW. Pharmacologic ATF6 activation confers global protection in widespread disease models by reprogramming cellular proteostasis. *Nat Commun.* 2019; 10:1-16.

23. Okabayashi FM, Okada Y, Tachibanat T. A Series of Hybrid Cells Containing Different Ratios of Parental Chromosomes Formed by Two Steps of Artificial Fusion. *Proceedings of the National Academy of Sciences.* 1971; 68:38-42.

24. Suetsugu A, Matsumoto T, Hasegawa K, Nakamura M, Kunisada T, Shimizu M, Saji S, Moriwaki H, Bouvet M, Hoffman RM. Color-coded Live Imaging of Heterokaryon Formation and Nuclear Fusion of Hybridizing Cancer Cells. *Anticancer Res.* 2016; 36:3827-3831.

25. Shirakata Y. Heparin-binding EGF-like growth factor accelerates keratinocyte migration and skin wound healing. *J Cell Sci.* 2005; 118:2363-2370.

26. Iwamoto R, Mekada E. ErbB and HB-EGF Signaling in Heart Development and Function. *Cell Struct Funct.* 2006; 31:1-14.

27. Yi S, Chen JR, Viallet J, Schwall RH, Nakamura T, Tsao MS. Paracrine effects of hepatocyte growth factor/scatter factor on non-small-cell lung carcinoma cell lines. *Br J Cancer.* 1998; 77:2162-2170.

28. ISLAM MR, YAMAGAMI K, YOSHII Y, YAMAUCHI N. Growth factor induced proliferation, migration, and lumen formation of rat endometrial epithelial cells in vitro. *J Reprod Dev.* 2016; 62:271-278.

29. Lee JG, Jung E, Heur M. Fibroblast growth factor 2 induces proliferation and fibrosis via SNAI1-mediated activation of CDK2 and ZEB1 in corneal endothelium. *J Biol Chem.* 2018; 293:3758-3769.

30. Gude NA, Sussman MA. Chasing c-Kit through the heart: Taking a broader view. *Pharmacol Res.* 2018; 127:110-115.

31. Khan M, Koch WJ. c-kit + Cardiac Stem Cells. *Circ Res.* 2016; 118:783-785.

32. Yan J, Bu L, Zhang L, Moon A, Razzaque S, Cai W, Zhou B, Huang G-Y, Jeong D, Cai C-L, Sultana N, Sheng W, Xu M, Hajjar RJ, Chen J. Resident c-kit+ cells in the heart are not cardiac stem cells. *Nat Commun.* 2015; 6:8701-8710.

33. Van Berlo JH, Kanisicak O, Maillet M, Vagnozzi RJ, Karch J, Lin SCJ, Middleton RC, Marbán E, Molkentin JD. C-kit+ cells minimally contribute cardiomyocytes to the

heart. *Nature*. 2014; 509:337-341.

34. Vajravelu BN, Hong KU, Al-Maqtari T, Cao P, Keith MCL, Wysoczynski M, Zhao J, Moore JB, Bolli R. C-Kit promotes growth and migration of human cardiac progenitor cells via the PI3K/AKT and MEK-ERK Pathways. *PLoS One*. 2015; 10:e0140798.

35. Smith AJ, Torella A, Shone V, Lewis FC, Cristiano F, Gritti G, Nadal-Ginard B, Scalise M, Vicinanza C, Ellison-Hughes GM, Terracciano CM, Torella D, Marotta P, Britti D, Indolfi C, Cianflone E, Veltri P, Aquila I, Mancuso T, Couch L, Marino F, Sacco W. Adult cardiac stem cells are multipotent and robustly myogenic: c-kit expression is necessary but not sufficient for their identification. *Cell Death Differ*. 2017; 24:2101-2116.

36. Ellison GM, Vicinanza C, Smith AJ, Aquila I, Leone A, Waring CD, Henning BJ, Stirparo GG, Papait R, Scarfò M, Agosti V, Viglietto G, Condorelli G, Indolfi C, Ottolenghi S, Torella D, Nadal-Ginard B. Adult c-kit^{pos} cardiac stem cells are necessary and sufficient for functional cardiac regeneration and repair. *Cell*. 2013; 154:827-842.

37. Sussman MA, Tuck S, Gude N, Cottage CT, Muraski J, Alvarez R, Bailey B, Avitabile D, Fischer KM, Quijada P, Collins B. Cardiac Progenitor Cell Cycling Stimulated by Pim-1 Kinase. *Circ Res*. 2010; 106:891-901.

38. Monsanto M, White K, Fisher K, Wang J SM. CardioClusters: Harnessing the Power of Multi-lineage Cardiac Stem Cells. *Circ Res*. 2018; 121:A355 (Abstract).

39. Carrera-Quintanar L, Bernad A, Samper E, Torres Y, Benguría A, Pérez RA, Ramírez JC, Roche E, Dopazo A, Enríquez JA, Torres R, Estrada JC. Human mesenchymal stem cell-replicative senescence and oxidative stress are closely linked to aneuploidy. *Cell Death Dis*. 2013; 4:e691.

40. Peterson SE, Westra JW, Rehen SK, Young H, Bushman DM, Paczkowski CM, Yung YC, Lynch CL, Tran HT, Nickey KS, Wang YC, Laurent LC, Loring JF, Carpenter MK, Chun J. Normal human pluripotent stem cell lines exhibit pervasive mosaic aneuploidy. *PLoS One*. 2011; 6:e23018.

41. Dong F, Harvey J, Finan A, Weber K, Agarwal U, Penn MS. Myocardial CXCR4 expression is required for mesenchymal stem cell mediated repair following acute myocardial infarction. *Circulation*. 2012; 126:314-324.

42. Herrmann JL, Wang Y, Meldrum DR, Abarbanell AM, Poynter JA, Manukyan MC, Weil BR, Brewster BD. Intracoronary Mesenchymal Stem Cells Promote Postischemic Myocardial Functional Recovery, Decrease Inflammation, and Reduce Apoptosis via a Signal Transducer and Activator of Transcription 3 Mechanism. *J Am Coll Surg*. 2011; 213:253-260.

43. Shi B, Wang Y, Zhao R, Long X, Deng W, Wang Z. Bone marrow mesenchymal stem cell-derived exosomal miR-21 protects C-kit⁺ cardiac stem cells from oxidative injury through the PTEN/PI3K/Akt axis. *PLoS One*. 2018; 13:e0191616.

44. Angelos MG, Noor M, Dougherty JA, Kumar N, Khan M, Chen C-A, Khan M. Extracellular Vesicles Released by Human Induced-Pluripotent Stem Cell-Derived Cardiomyocytes Promote Angiogenesis. *Front Physiol.* 2018; 9:1794-1807.
45. Moore JB, Tang XL, Zhao J, Fischer AG, Wu WJ, Uchida S, Gumpert AM, Stowers H, Wysoczynski M, Bolli R. Epigenetically modified cardiac mesenchymal stromal cells limit myocardial fibrosis and promote functional recovery in a model of chronic ischemic cardiomyopathy. *Basic Res Cardiol.* 2018; 114:3-26.
46. Balbi C, Bollini S. Fetal and perinatal stem cells in cardiac regeneration: Moving forward to the paracrine era. *Placenta.* 2017; 59:96-106.
47. Cowan CA, Atienza J, Melton DA, Eggan K. Developmental Biology: Nuclear reprogramming of somatic cells after fusion with human embryonic stem cells. *Science* (80-). 2005; 309:1369-1373.
48. Davani S. Mesenchymal Progenitor Cells Differentiate into an Endothelial Phenotype, Enhance Vascular Density, and Improve Heart Function in a Rat Cellular Cardiomyoplasty Model. *Circulation.* 2003; 108:253-258.

Chapter 2, with slight modifications, is a reprint of the material as it appears in Journal of the American Heart Association, 2020. Human CardioChimeras: Creation of a Novel “Next-Generation” Cardiac Cell. Fareheh Firouzi, Sarmistha Sinha Choudhury, Kathleen Broughton, Adriana Salazar, Barbara Bailey, Mark A. Sussman. The dissertation author was the primary author and investigator on this manuscript.

CHAPTER 3

PIM1 Promotes Survival of Cardiomyocytes by Upregulating c-Kit Protein Expression

INTRODUCTION

Capacity of the adult mammalian heart to regenerate following injury is severely limited¹⁻³. Myocardial mass of the heart is 70% cardiomyocytes, the contractile units of the heart, which withdraw from cell cycle during postnatal growth^{4,5}. Pathologic injury such as myocardial infarction (MI) causes extensive cardiomyocyte death and compromised cardiac function. In response, the heart undergoes maladaptive remodeling accompanied by biochemical, molecular, structural, and metabolic changes placing chronic strain on cardiomyocytes and ultimately leading to heart failure⁶. Therefore, enhancing cardiomyocyte survival represents an important strategy for blunting myocardial deterioration and cardiac failure following pathological damage.

The cardioprotective role of PIM1 serine threonine kinase has been extensively studied⁷⁻¹⁰. PIM kinases are a family of highly conserved, constitutively active serine/threonine kinases with PIM1 being the highest expressed isoform in the myocardium^{9,11-13}. PIM1 regulates many cellular processes crucial for antagonizing cellular senescence including cell cycle progression, survival signaling, anti-apoptotic signaling, preservation of mitochondrial integrity, telomere preservation, and blunting pathological hypertrophy^{8,9,14}. Myocardial infarction injury as represented by decreased infarct size and improved contractile performance were mediated by cardiac specific overexpression of human PIM1 in transgenic mice⁹. Furthermore, PIM1 overexpressing hearts displayed blunting of cardiac hypertrophy, decrease in apoptosis markers, and maintenance of cardiac function following transverse aortic constriction (TAC) pressure overload compared to TAC banded non-transgenic controls⁹. In contrast, PIM1 knockout mice displayed increased cardiomyocyte apoptosis and decreased contractile function in

response to MI and TAC^{8,9}. Collectively, these studies demonstrate a powerful role for PIM1 in cardioprotection.

Similar to PIM1, c-Kit receptor tyrosine kinase also mediates cardioprotective activity¹⁵. c-Kit is expressed in diverse cardiac cell populations including endothelial cells, mesenchymal stem cells, and cardiomyocytes¹⁶. In response to adrenergic stress in vitro, cardiomyocytes upregulate c-Kit, implicating c-Kit in promotion of survival signaling¹⁷. Functionally, binding of c-Kit ligand, Stem Cell Factor (SCF) induces c-Kit receptor dimerization, phosphorylation, and activation of the Ras-Raf-MEK-ERK and the PI3K-Akt pathways^{18,19}. Activation of ERK promotes cardiomyocyte survival in response to pressure overload, MI, and oxidative stress²⁰⁻²². Activation of Akt promotes phosphorylation and inactivation of pro-apoptotic proteins²³. Taken together, these results point to a cardioprotective cascade induced by c-Kit activity.

PIM1 regulates c-Kit protein level in hematopoietic stem cells, altering cellular biological properties including colony forming capacity²⁴. The present study was designed to delineate the relationship between PIM1 and c-Kit in cardiomyocytes to reveal a cardioprotective signaling cascade contributing to amelioration of cardiomyopathic injury. Findings from this study demonstrate that PIM1 upregulates c-Kit expression post-transcriptionally in cardiomyocytes. PIM1 interacts with c-Kit at the protein level offering a potential mechanism of PIM1-mediated regulation of c-Kit expression. Furthermore, cardiomyocytes with elevated c-Kit expression demonstrate enhanced resistance to oxidative stress in vitro. Collectively, the findings of this study establish a novel signaling relationship for PIM1/c-Kit-mediated cardiomyocyte survival.

METHODS

Animal Experiments

All animal protocols were approved by the Institutional Animal Care and Use Committee of San Diego State University and conform to the Guide for the Care and Use of Laboratory Animals published by the US National Institutes of Health. Transgenic mice with cardiac specific overexpression of human PIM1 (PIM1) and global deletion of PIM1, PIM2, and PIM3 (PIM-TKO) have been described before^{9,25}. Non-transgenic (NTg) and gender matched mice of the same strain (FVB) were used as controls. Adult mice aged 4-6 months were used for the study.

Isolation and Culture of Adult Mouse Cardiomyocytes

Cardiomyocytes were isolated from FVB mice as previously described²⁶. Briefly, mice were anesthetized with a xylazine/ketamine solution and injected with Heparin (100U/kg) (Sigma-Aldrich; H3393) intraperitoneally to prevent blood clots. The chest was opened, and the aortic arch was isolated. Curved forceps were used to push 4-0 suture underneath the aorta. A small incision was made at the aortic branch and a cannula was inserted into the aorta then tied securely with the suture. The cannula was attached to a Langendorff apparatus and was perfused until all blood was cleared from the heart. The heart was then digested with using buffer containing Collagenase II (230U/mL) (Worthington; LS004147) for 12 minutes. Hearts were gently teased apart using forceps and triturated until no large tissue remained. The cell suspension was transferred to a T-75 flask and calcium was gradually introduced over a 30-minute interval to a final concentration of 900 μ M. Following calcium introduction, cardiomyocytes were either lysed for protein or were pre-plated on laminin (ThermoFisher; 23017015) coated dishes

at a density of 50,000 cells/mL. After 2 hours, cardiomyocytes were cultured in serum free media overnight at 37°C following which pharmacological treatments or cell death experiments were conducted.

Viral Infections

Cardiomyocytes were infected with adenovirus encoding enhanced green fluorescent protein (eGFP) or mouse c-Kit-GFP (VectorBuilder; VB190910-1241cgg) at an MOI of 100 for 48 hours. GFP and c-Kit overexpression were confirmed via immunoblot.

Pharmacological Treatments

Cardiomyocytes were plated at a density of 100,000 cells per 35mm dishes. The next day, cardiomyocytes were treated with 200 ng/mL murine stem cell factor (SCF) (Peprotech; 250-03) for one hour. For the cell death assay, cardiomyocytes were pre-treated with 0.5 μ M Imatinib (R&D Systems; 5906) for 2 hours.

Immunoblot

Cells were lysed in ice cold radioimmunoprecipitation assay (RIPA) buffer (ThermoFisher; 89900) containing protease and phosphatase inhibitor cocktails (Sigma-Aldrich; P8340, P5726, P2850). Protein concentrations were analyzed and normalized by Bradford Assay and lysates were prepared by addition of NuPAGE LDS Sample Buffer (ThermoFisher; NP0007) and 100 μ M dithiothreitol (Bio-Rad; 161-0611). Samples were sonicated and boiled then loaded onto a 4-12% NuPAGE Bis-Tris gel (ThermoFisher; NP0321BOX) and run in MOPS buffer (ThermoFisher; NP0001) for 80 minutes at 150V. Proteins were transferred onto an Immobilon-FL Polyvinylidene difluoride membrane

(EMD Millipore; IPFL0010) for 2 hours at 30 mA following which the membrane was blocked with Odyssey Blocking Buffer (Li-Cor; 927-50000) for one hour at room temperature and incubated with primary antibodies prepared in blocking buffer with 0.2% Tween-20 overnight at 4 °C. Secondary antibodies prepared in blocking buffer were applied for 2 hours at room temperature. Fluorescent signal was detected using an Odyssey CLx imaging system (Li-Cor) and bands were quantified using Image Studio. Primary antibodies used are listed in table 3.1.

Quantitative RT-PCR

RNA was isolated using Quick-RNA Miniprep Kit (Zymo Research; R1054) following the manufacturer's instructions. RNA concentrations were determined using a Nanodrop 2000 spectrophotometer (ThermoFisher) and cDNA was synthesized using iScript cDNA synthesis kit (Bio-Rad; 1708890). Reactions were prepared in triplicate using 6.5ng cDNA per reaction and iQ SYBER Green (Bio-Rad; 1708880) on a CFX Real-Time PCR thermocycler (Bio-Rad). Samples were normalized to 18S and data were analyzed by $\Delta\Delta C_t$ method. Primer sequences used are as follows:

c-Kit Forward: ATTGTGCTGGATGGATGGAT

c-Kit Reverse: GATCTGCTCTGCGTCCTGTT

Co-Immunoprecipitation

PIM1 hearts were transferred to a 5 mL round bottom tube containing 1 mL of lysis buffer composed of Tris-HCl, pH 7.4 (50 mM), NaCl (150 mM), EDTA (1 mM), EGTA (1 mM) and protease and phosphatase inhibitors (Sigma-Aldrich). Hearts were finely minced using a Polytron Homogenizer (ThomasSci) at 22,000 RPM for 3 seconds. The

homogenates were transferred to a 1.7 mL microcentrifuge tube and Triton X-100 was added to a final concentration of 1%. The tissue homogenates were vortexed then incubated on ice for 45 minutes. Debris was cleared from the homogenates by centrifugation at 20,000 x g at 4°C. The lysates were precleared by addition of 20 µl Protein A agarose beads (Santa Cruz Biotechnology; sc-2001) on a rotator at 4°C for 30 minutes. The beads were pelleted by centrifugation at 1,000 x g for 5 minutes and the supernatant was transferred to a fresh microcentrifuge tube on ice. An aliquot of the sample was taken as the “pre-immunoprecipitation” sample. Primary antibody was added to the lysates and was incubated on a rotator at 4 °C overnight. Antibodies are listed in table 3.1. The following day, 20 µl Protein A agarose beads were added to the lysates on a rotator for 2 hours. The beads were pelleted by centrifugation at 1,000 x g for 5 minute and the supernatant was saved as the “post-immunoprecipitation supernatant”. The beads were washed by resuspending in 1 mL of ice-cold phosphate-buffered saline (PBS), following which the beads were centrifuged. The washes were repeated for a total of 3 times. The bead pellet was suspended in NUPAGE LDS sample buffer (ThermoFisher; NP0007) containing 100 µM dithiothreitol (Bio-Rad; 161-0611) and the beads were boiled at 95°C for 5 minutes. The sample was centrifuged at 20,000 x g at room temperature for 5 minutes and the samples were loaded on a gel for immunoblot analysis.

Proximity Ligation Assay

Cardiomyocytes were isolated and plated on 8 well glass chamber slides. Cells were fixed in a 4% formaldehyde solution for 20 minutes at room temperature then were permeabilized in a 0.1% Triton-X solution for 15 minutes. The proximity ligation assay

was performed according to the manufacturer's instructions (Sigma Aldrich; DUO92104-1KT). Briefly, cardiomyocytes were blocked using Duolink Blocking Solution in a heated humidity chamber for 60 minutes at 37 °C. Primary antibody was diluted in Duolink Antibody Diluent and added to the wells. The slides were incubated with primary antibody overnight in a humidity chamber at 4 °C. The following day, the slides were washed twice for 5 minutes each using Wash Buffer A. The plus and minus probes were applied to the wells and the slides were incubated in a humidity chamber for 60 minutes at 37 °C. The slides were washed twice for 5 minutes each using wash Buffer A following which the ligation solution was added and incubated for 30 minutes at 37 °C. After two 5-minute washes using Wash Buffer A, the amplification solution was added to the wells and the slides were incubated for 100 minutes at 37 °C. The slides were washed twice for 10 minutes each using Wash Buffer B, followed by one last wash in 0.01x Wash Buffer B for 1 minute. The slides were then mounted with a coverslip using Mounting Medium with 4',6-diamidino-2-phenylindole (DAPI) and were imaged using a Leica SP8 confocal microscope.

Cell Death Assay

Cardiomyocytes were isolated and plated on 35 mm dishes. Following viral or pharmacological treatment, cells were treated with 10 μ M H₂O₂ (Sigma Aldrich; H1009) for 3 hours. TO-PRO-3 (ThermoFisher; T3605) was added to the wells in a 1:10,000 dilution and cells were immediately imaged using a Leica SP8 confocal microscope.

Statistical Analyses

Statistical analyses were performed using Student's t-test, one way-ANOVA or two-way ANOVA with Tukey's multiple comparison test on GraphPad Prism v5.0. A value of $p < 0.05$ was considered statistically significant.

RESULTS

PIM1 upregulates c-Kit protein expression

PIM1 regulates c-Kit expression in hematopoietic stem cells²⁴, but this relationship has not been examined in the myocardial context. Therefore, c-Kit protein level was measured in whole heart lysates from PIM1 and PIM-triple knockout (TKO) mice by immunoblot. PIM1 overexpression is driven downstream of the alpha myosin heavy chain promoter which results in cardiomyocyte specific overexpression of PIM1. PIM1 hearts displayed significantly elevated c-Kit expression compared to non-transgenic (NTg) hearts (Figure 3.1A, Figure 3.2A) whereas PIM-TKO hearts displayed significantly lower c-Kit expression compared to NTg (Figure 3.1B, Figure 3.2B). To further validate the role of PIM1 in the regulation of c-Kit expression, cardiomyocytes were isolated and analyzed for c-Kit expression via immunoblot. PIM1 cardiomyocytes displayed a 2.5-fold increase in c-Kit expression compared to NTg cardiomyocytes (Figure 3.1C, Figure 3.2C). c-Kit mRNA level was analyzed by RT-qPCR revealing no significant difference between PIM1 and NTg cardiomyocytes, consistent with the premise that PIM1 does not regulate c-Kit at the transcriptional level (Figure 3.1D). Overall, these results demonstrate that PIM1 regulates c-Kit expression post-transcriptionally in adult murine cardiomyocytes.

PIM1 interacts with c-Kit

Regulation of c-Kit expression by PIM1 occurs post-transcriptionally [24, Figure 3.1], therefore potential association between PIM1 and c-Kit proteins in heart lysates was assessed by co-immunoprecipitation (IP) of c-Kit and PIM1 followed by immunoblotting (Figure 3.3A, Figure 3.4). PIM1 overexpressing whole heart input lysates displayed elevated expression of PIM1, c-Kit, and SRC. Levels of PIM1 were decreased in post-IP

supernatant following pull down with PIM1 antibody, validating depletion of PIM1 from heart lysate. PIM1 and c-Kit were enriched in the IP: PIM1 sample, as evidenced by the prominent bands corresponding to PIM1 protein and c-Kit (Figure 3.3A) confirming a protein association between PIM1 and c-Kit. No c-Kit was detected in the negative control indicating that c-Kit was only enriched in association with PIM1 IP. Protein expression of SRC, a tyrosine kinase that has no known interaction with PIM1 was also analyzed as a negative-interaction protein control. PIM1 IP failed to show association with SRC protein supporting specificity of PIM1:c-Kit interaction. Further corroboration of PIM1:c-Kit association, a proximity ligation assay (PLA) was performed on isolated PIM1 cardiomyocytes. PLA demonstrates a physical association and protein-protein interaction of two separate molecules within 40nm (Figure 3.3B). Proximity between PIM1 and c-Kit was detected in cardiomyocytes as indicated by the red fluorescence which displayed a significantly higher number of spots of proximity compared to the negative controls (Figure 3.5). Taken together, these results demonstrate that PIM1 interacts with c-Kit at the protein level in cardiomyocytes.

Cardioprotective signaling downstream of c-Kit is elevated in PIM1 cardiomyocytes

c-Kit receptor activation is mediated by binding of Stem Cell Factor (SCF) that activates cardioprotective PI3k-Akt and MAPK/ERK pathways^{20,22,23,27}. Signal cascades downstream of c-Kit receptor activation by SCF was assessed to determine cardioprotective signaling upregulation in PIM1 versus normal cardiomyocytes. Isolated cardiomyocytes from PIM1 overexpressing and non-transgenic (NTg) hearts were treated with SCF and levels of activated ERK1/2 and AKT measured over a one-hour time course by immunoblot. Cardiomyocytes from both groups responded to SCF treatment with

activation of AKT or ERK signaling (Figure 3.6) unaffected by overexpression of c-Kit (Figure 3.1C). In contrast, PIM1 cardiomyocytes displayed significantly increased ERK1/2 activation at the 15-minute time point compared to NTg cardiomyocytes (Figure 3.6A, Figure 3.7A). AKT was not significantly different between PIM1 and NTg cardiomyocytes over the time course (Figure 3.6B, Figure 3.7B). In summary, PIM1 cardiomyocytes responded to SCF treatment by activating both ERK and AKT, but only ERK1/2 activation was enhanced by the presence of PIM1.

Elevated c-Kit expression enhances resistance against oxidative stress in cardiomyocytes

c-Kit activity is cardioprotective²⁸, raising the possibility that elevated c-Kit expression enhances survival of cardiomyocytes independent of PIM1. Elevation of c-Kit protein was mediated by adenoviral overexpression in cardiomyocytes (Figure 3.8A). Validation of adenoviral expression of GFP and c-Kit was confirmed via immunoblot (Figure 3.8B, Figure 3.9). After viral transduction to induce protein overexpression, the cardiomyocytes were treated with H₂O₂ and cell death was determined using TO-PRO-3 (Figure 3.8C). Cell viability was comparable between c-Kit overexpressing cardiomyocytes compared to the GFP controls at baseline (Figure 3.8D). Viability was significantly higher in c-Kit overexpressing cardiomyocytes following H₂O₂-induced stress compared to the GFP cardiomyocytes, although both groups showed comparable live cells at baseline prior to exposure (Figure 3.8C, D-Vehicle only). Collectively, these results demonstrate that elevated c-Kit expression protects cardiomyocytes against oxidative stress.

PIM1 and c-Kit act independently to confer cardioprotection

The cardioprotective role of PIM1 is well established^{8-10,29-31} but involvement of c-Kit in PIM1-mediated cardioprotection has not been elucidated. Involvement of c-Kit in PIM1-mediated cardioprotection was assessed in cardiomyocytes subjected to oxidative stress following treatment with imatinib, an inhibitor of c-Kit activity³². Isolated cardiomyocytes were pretreated with imatinib for 2 hours, then challenged with H₂O₂ for 3 hours (Figure 3.10A). Cell viability was determined by quantitation of TO-PRO-3 stained cardiomyocytes (Figure 3.10B). Viability was comparable between PIM1 and NTg cardiomyocytes at baseline prior to H₂O₂-mediated stress (Figure 3.10C) and imatinib treatment had no effect on cell viability. In comparison, viability was significantly higher following H₂O₂ exposure in PIM1 cardiomyocytes compared to NTg cells. Pretreatment with imatinib significantly decreased cell viability following H₂O₂ challenge in PIM1 and NTg cardiomyocytes compared to H₂O₂ alone. However, PIM1 cardiomyocytes retain higher cell viability compared to NTg even after imatinib-blocking of c-Kit signaling. Taken together, these results are consistent with PIM1 and c-Kit acting independently and synergistically to protect cardiomyocytes from oxidative stress.

DISCUSSION

Decades of cardioprotective signal transduction studies have produced an intricate web of relationships between mediators of cardiomyocyte survival. Our group were pioneers in establishing PIM1-mediated cardioprotection in over a decade of studies^{8,9,16,29,30,33–35} that was subsequently reinforced by studies from other researchers^{7,10,36,37}. Similarly, cardioprotection is also conferred by c-Kit activity^{17,32,38}, with c-Kit biology inextricably linked to myocardial homeostasis^{39,40}. Synergism between PIM1 and c-Kit in cardioprotective signaling could be inferred from fundamental biological roles in hematopoietic cells for both PIM1^{11,41,42} and c-Kit^{6,43} as well as the ability of PIM1 to increase c-Kit gene translation²⁴. Following these precedents, this study establishes the link between c-Kit and PIM1 in cardiomyocyte protection from oxidative stress in vitro. Specifically, PIM1 interacts with c-Kit protein to increase c-Kit expression which subsequently promotes ERK activity. These findings provide novel insights into PIM1 mediated signal transduction mechanisms of cardioprotection.

Collectively, the present study along with previously published reports reinforce the crucial role of PIM1 in promoting cardioprotective signaling. Overexpression of PIM1 in neonatal rat cardiomyocytes (NRCM) upregulated anti-apoptotic proteins BCL-XL and BCL-2 and inactivated pro-apoptotic protein BAD by phosphorylation⁹. Further, PIM1 overexpression protected mitochondrial integrity and decreased mitochondrial swelling in NRCM after hydrogen peroxide treatment¹⁴. In vivo studies also demonstrated the cardioprotective role of PIM1. PIM1 knockout mice displayed decreased contractile function and increased apoptotic death in response to MI and TAC^{8,9}. Conversely, mice with cardiac specific overexpression of PIM1 displayed decreased apoptotic cell death

after MI, blunting of hypertrophy, decreased infarct size after MI, and preserved contractility⁹.

Independent of PIM1, elevated levels of c-Kit enhance resistance to oxidative stress in vitro by promoting downstream expression of activated ERK. The Ras-Raf-MEK-ERK cascade has been implicated in promoting survival of cardiomyocytes in response to oxidative stress^{17,19,21,44,45}.

While the present study introduces a link between PIM1 and c-Kit in cardiomyocytes, the mechanism of PIM1 mediated upregulation of c-Kit remains to be elucidated. A previous report demonstrating PIM1 regulation of c-Kit in hematopoietic cells found regulation to be at the translational level²⁴. Knockout of PIM1 did not affect transcription of c-Kit gene, but PIM1 expression enhanced c-Kit 35S methionine labeling and increased ribosomal incorporation of c-Kit mRNA²⁴. Possibilities for how PIM1 exerts potentiation of c-Kit expression could include direct protein-protein interaction as well as post-translational modifications and stabilization of c-Kit analogous to the effect of PIM1 upon RelA/P65 phosphorylation⁴⁶. The potential of PIM1 to phosphorylate c-Kit is one of several possibilities based upon our findings to be investigated in the future.

In summary, PIM1 upregulates c-Kit protein expression to promote protection in cardiomyocytes, consistent with cumulative evidence of cardioprotection as well as preservation of a more “youthful” phenotype mediated by PIM1 overexpression^{9,29,34,47}. Reinforcement of c-Kit activity by PIM1 could account for the ability of PIM1 to antagonize cellular senescence^{33,47} and serve as the basis for future studies. Mechanistic understanding of PIM1 mediated cardioprotection could provide valuable information towards protection of cardiomyocytes to promote cardiac repair.

TABLES

Table 3.1. Antibody list

| Antibody | Catalog Number | Dilution | Application |
|-----------------|------------------------|-----------------|--------------------|
| PIM1 | ThermoFisher 39-4600 | 1:500 | IB, Co-IP |
| PIM1 | ThermoFisher 710504 | 1:100 | PLA |
| c-Kit | R&D AF1356 | 1:200, 1:100 | IB, PLA |
| GAPDH | Millipore Sigma MAB374 | 1:5000 | IB |
| SRC | Abcam Ab47405 | 1:500 | IB |
| pERK1/2 | CST 9101 | 1:500 | IB |
| ERK1/2 | CST 9102 | 1:500 | IB |
| pAkt (Ser473) | CST 9271 | 1:500 | IB |
| Akt | CST 9272 | 1:500 | IB |
| GFP | Rockland 600-101-215 | 1:1000 | IB |

FIGURES

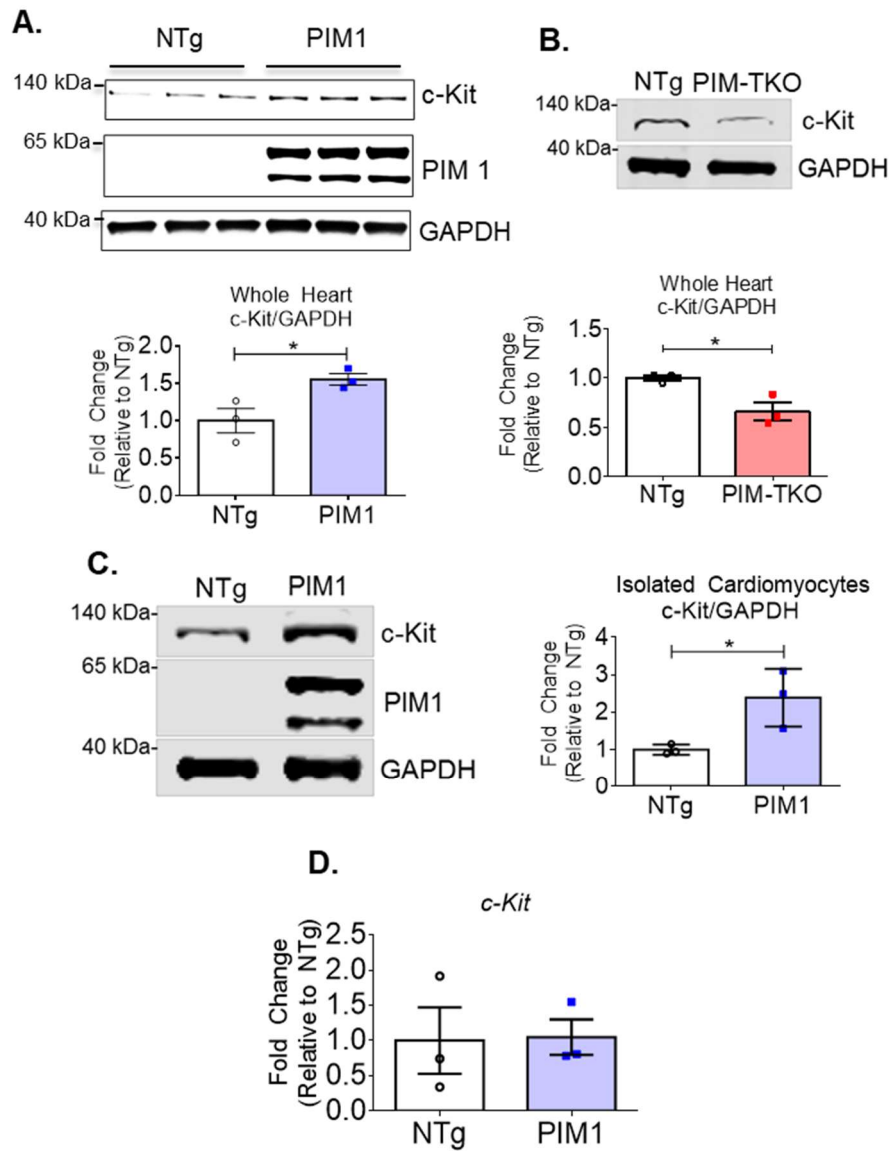


Figure 3.1. PIM1 upregulates c-Kit protein expression. A. Immunoblot analysis showing expression of c-Kit in PIM1 vs NTg whole heart lysates with quantification below. N=3, Error bars represent SEM, * $p < 0.05$ vs untreated as measured by Student t test. B. Immunoblot analysis showing expression of c-Kit in PIM-TKO vs NTg whole heart lysates with quantification shown below. N=3, Error bars represent SEM, * $p < 0.05$ vs untreated as measured by Student t test. C. Immunoblot analysis showing c-Kit expression in cardiomyocytes isolated from PIM1 overexpressing hearts vs NTg with quantification on the right. N=3, Error bars represent SEM, * $p < 0.05$ vs untreated as measured by Student t test. D. Gene expression of c-Kit in cardiomyocytes isolated from PIM1 and NTg hearts as revealed by qPCR. N=3, Error bars represent SEM.

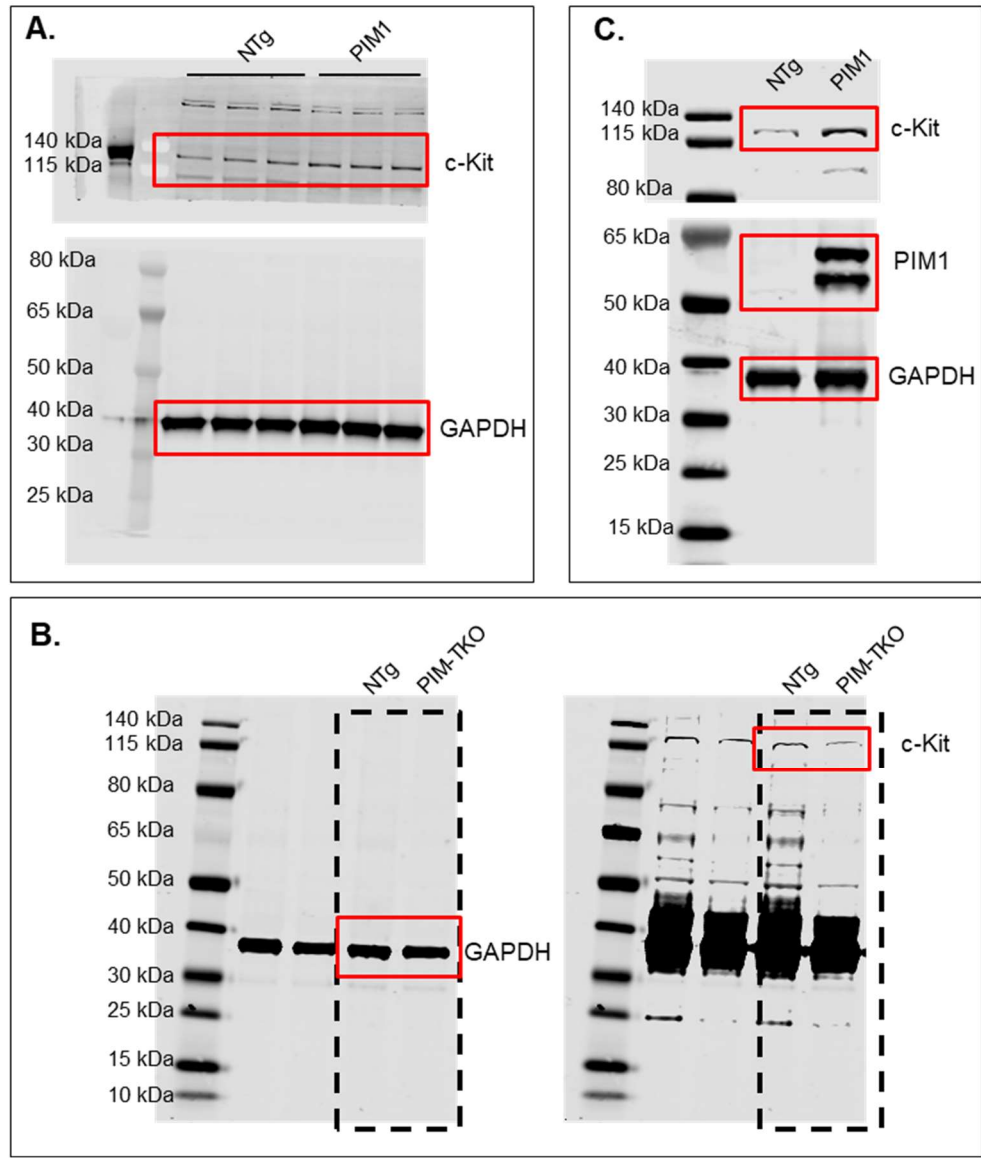


Figure 3.2. Full blot of cropped image presented in Figure 3.1A., Figure 3.1B, and Figure 3.1C of the manuscript.

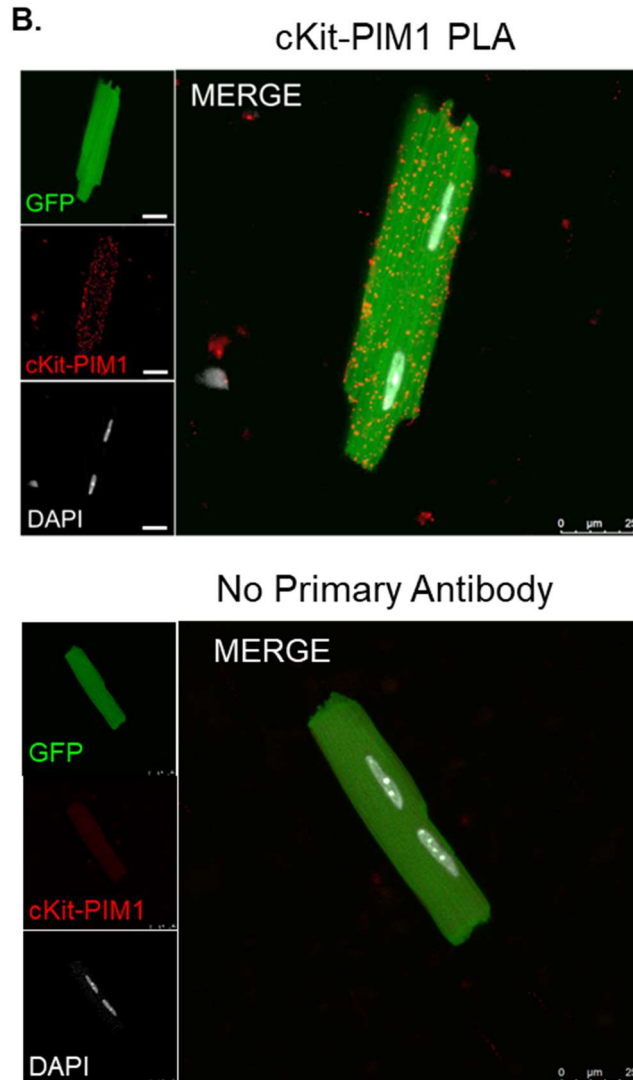
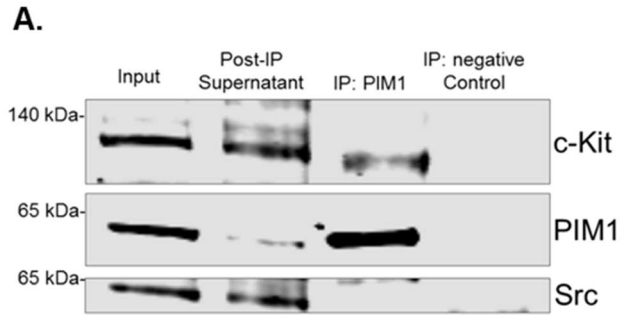


Figure 3.3. PIM1 interacts with c-Kit. A. Immunoblot analysis of a co-immunoprecipitation using whole heart lysates from PIM1 hearts in which PIM1 was pulled down. B. Interaction between PIM1 and c-Kit as determined by proximity ligation assay (top panel) and in the absence of primary antibody (bottom panel). Proximity events are shown as red dots.

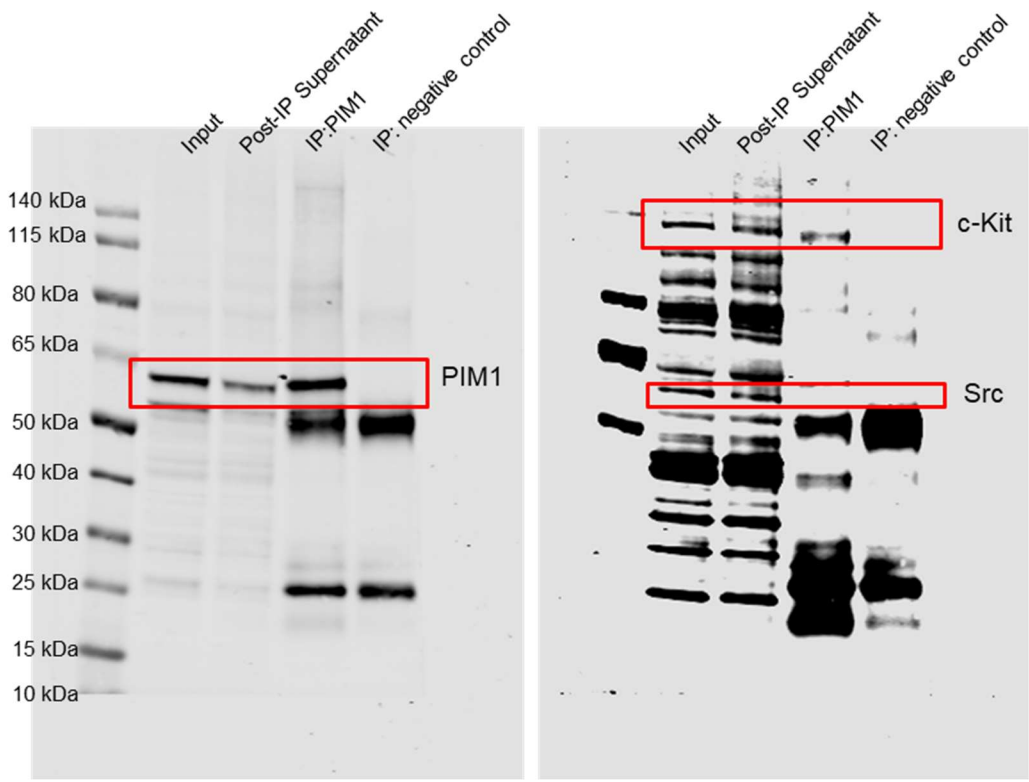


Figure 3.4. Full blot of cropped image presented in Figure 3.3A of the manuscript.

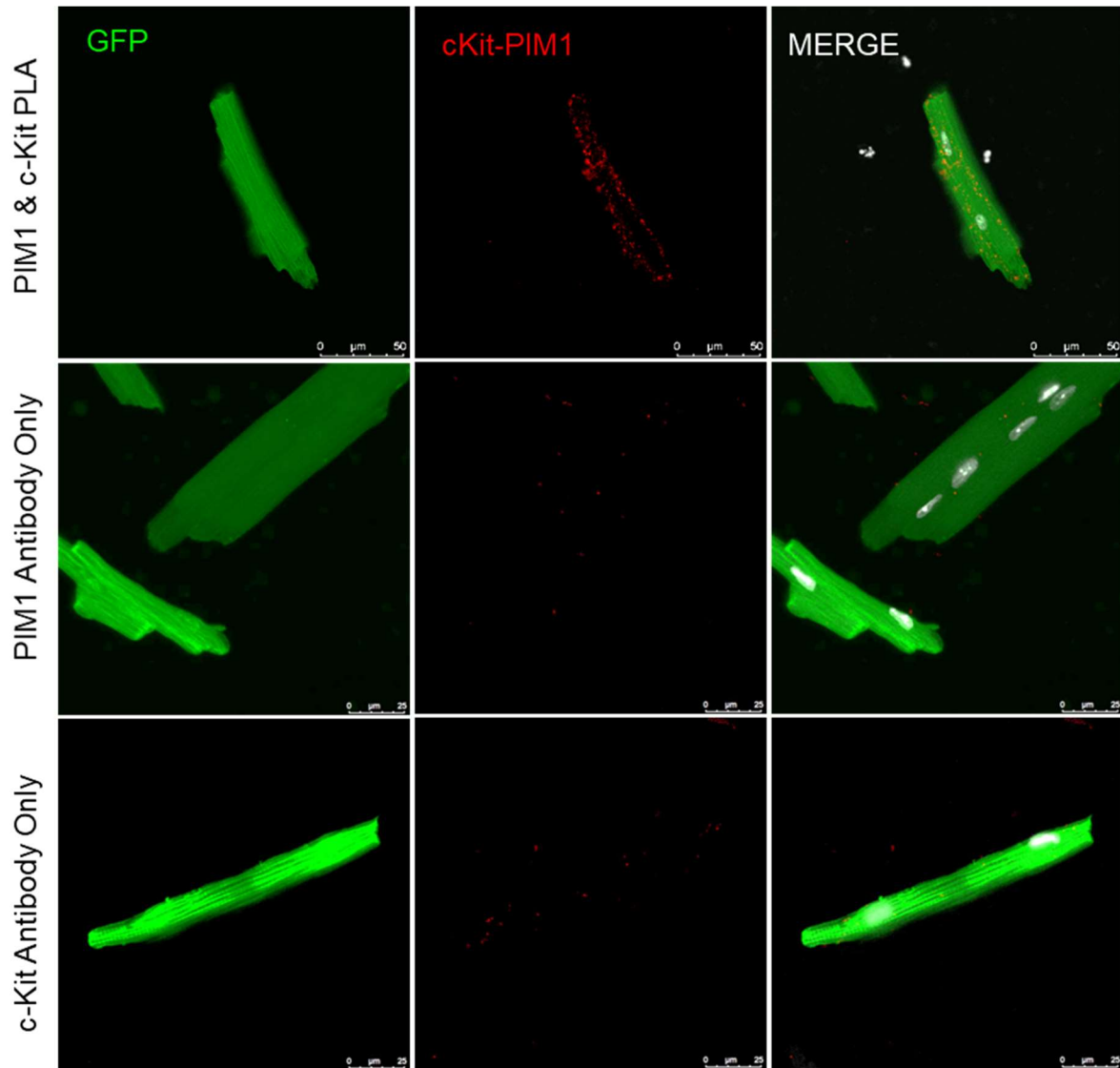


Figure 3.5. Negative controls for the Proximity Ligation Assay. Endogenous GFP is shown in green, the PLA signal is shown in red and DAPI is shown in gray.

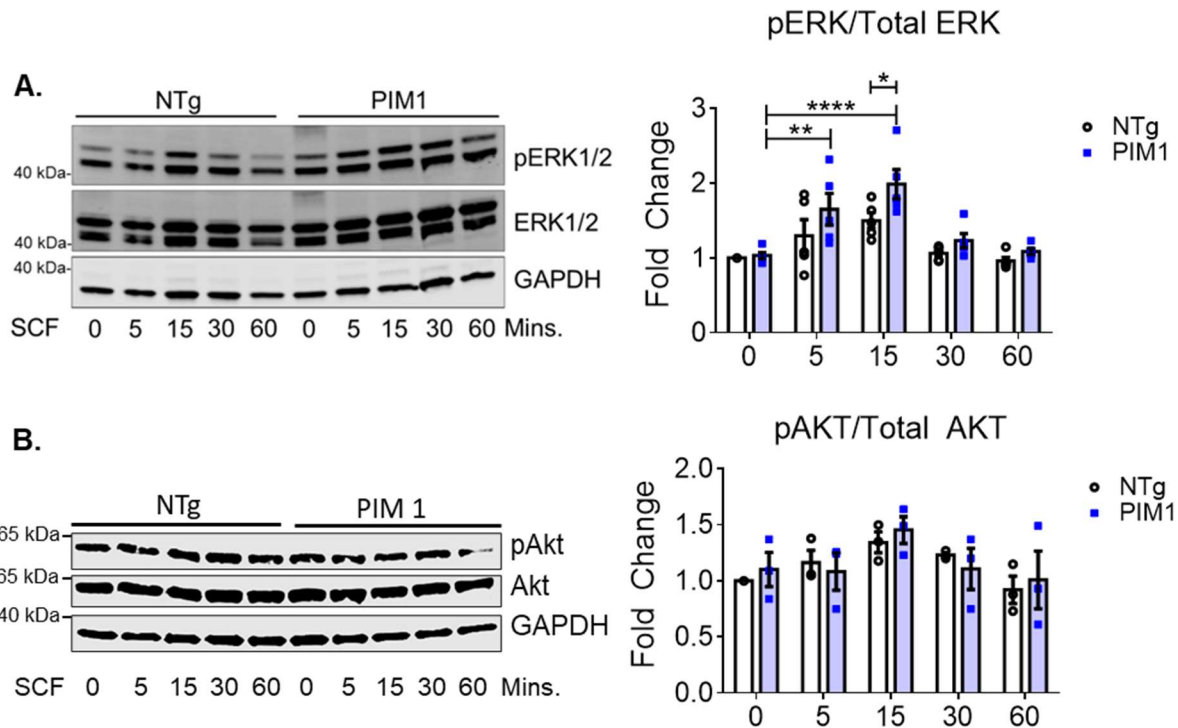


Figure 3.6. Cardioprotective signaling downstream of c-Kit is elevated in PIM1 cardiomyocytes. A. Immunoblot analysis of activated ERK1/2 and B. activated AKT in NTg and PIM1 cardiomyocytes following treatment with SCF over 60 minutes. Quantification is shown on the right. N=5, Error bars represent SEM, * $p < 0.05$, ** $p < 0.01$ and *** $p < 0.001$ as measured by two-way ANOVA multiple comparison with Tukey.

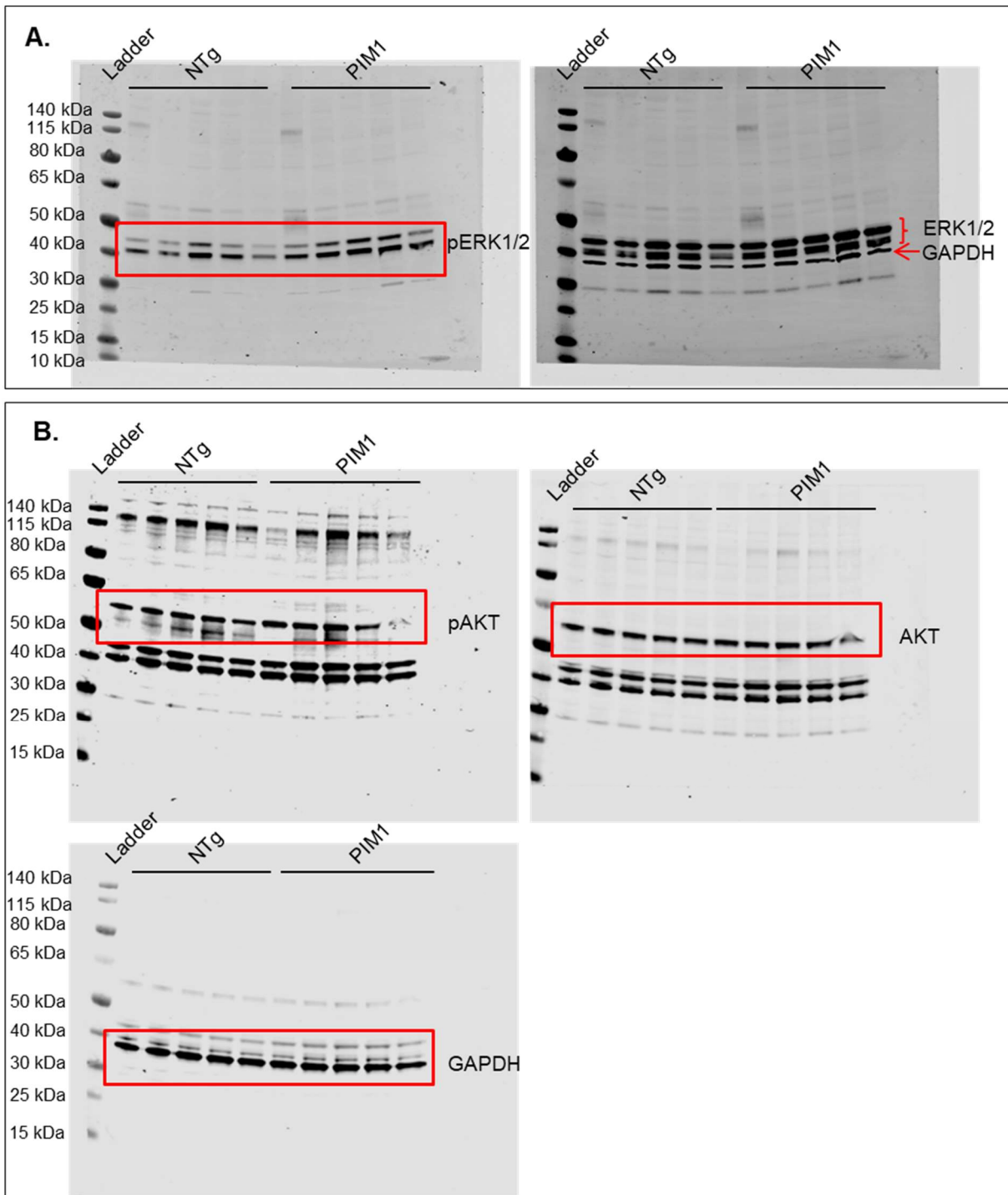


Figure 3.7. Full blot of cropped image presented in Figure 3.6A and Figure 3.6B of the manuscript.

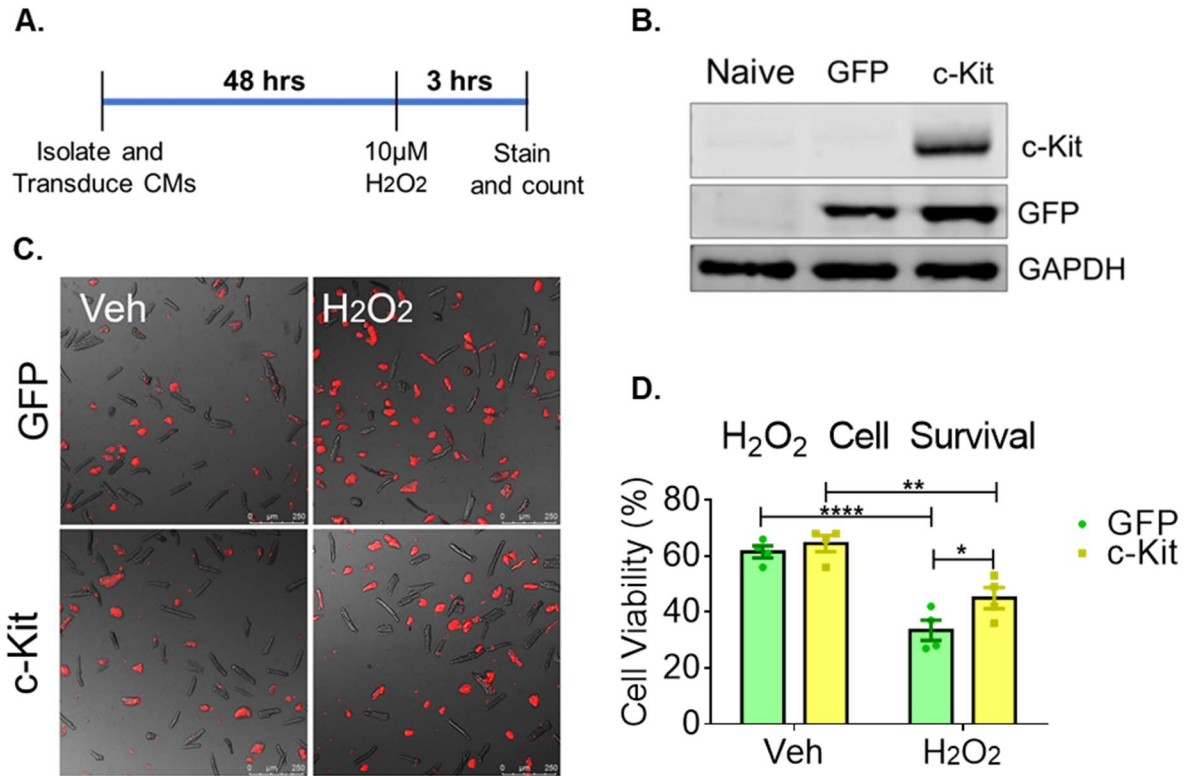


Figure 3.8. Cardiomyocytes with elevated c-Kit expression demonstrate enhanced resistance against oxidative stress. A. Schematic showing the treatment procedure. B. Immunoblot analysis of isolated cardiomyocytes transduced with GFP or c-Kit-GFP. C. Fluorescent images of TO-PRO-3 staining on GFP or c-Kit expressing cardiomyocytes treated with vehicle or H₂O₂ overlaid with brightfield images depicting dead or dying cells in red. D. Quantification of cell viability counted from fluorescent images. N=4, 300-600 cardiomyocytes counted per group, error bars represent SEM, *p<0.05, **p<0.01 and ***p<0.001 as measured by two-way ANOVA multiple comparison with Tukey.

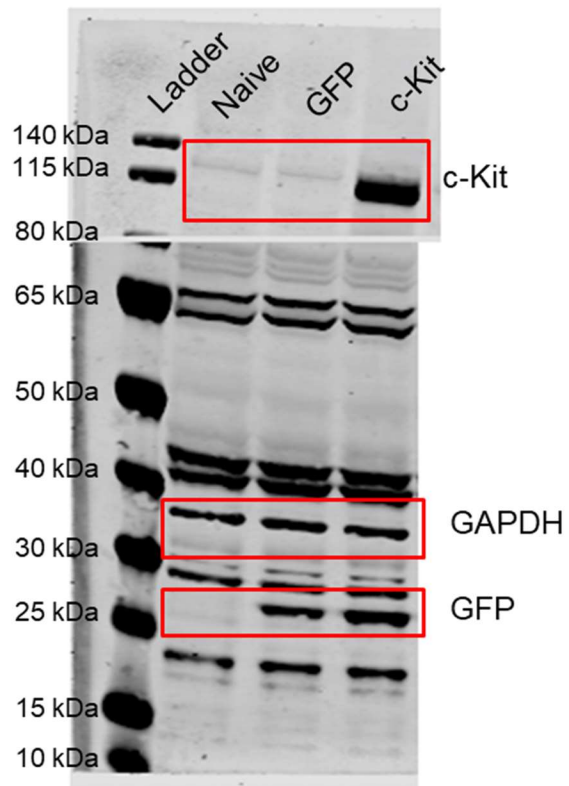


Figure 3.9. Full blot of cropped image presented in Figure 3.8B of the manuscript.

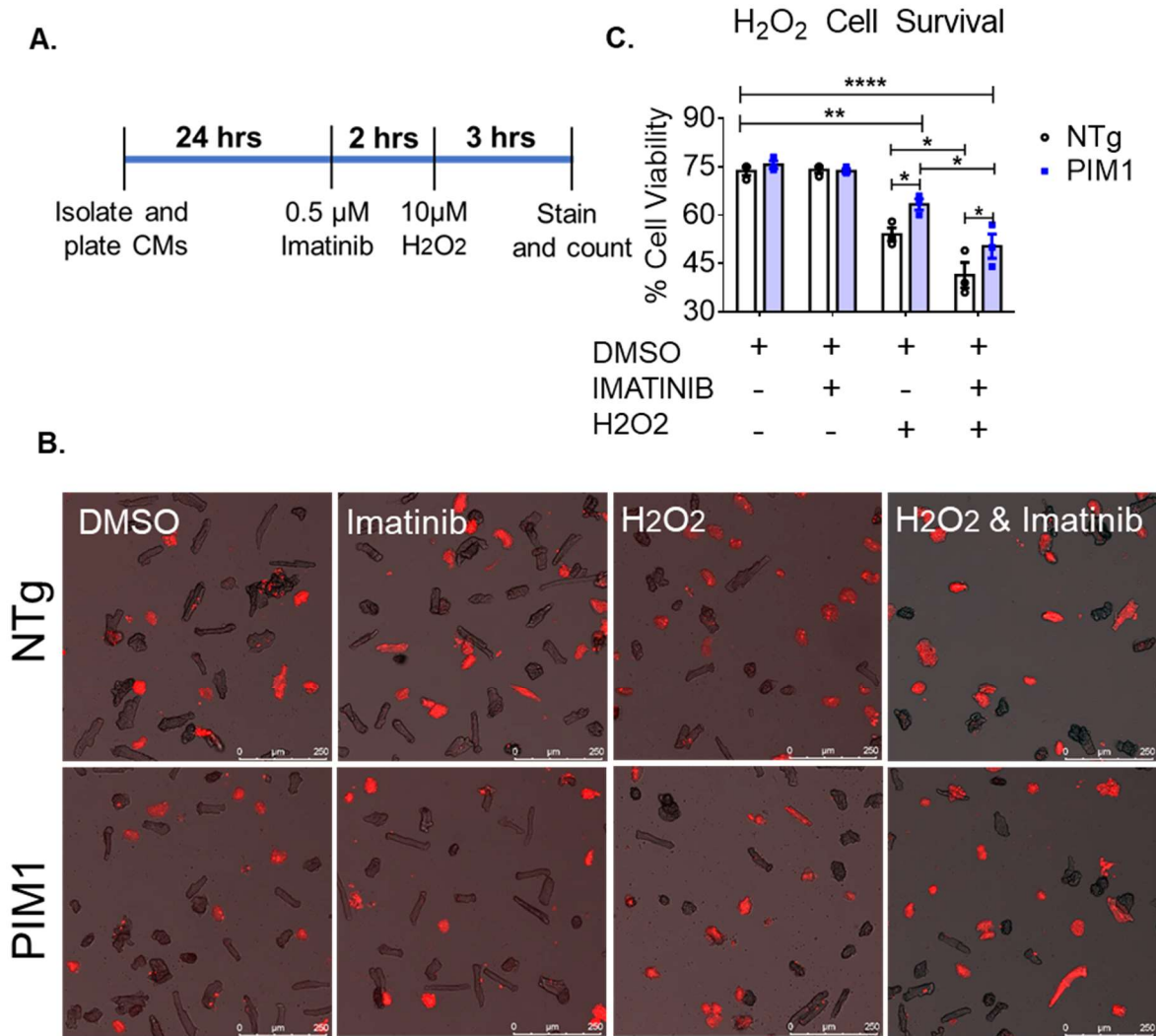


Figure 3.10. PIM1 and c-Kit act independently to confer cardioprotection. A. schematic showing the treatment procedure. B. Representative images of NTg and PIM1 cardiomyocytes stained with TO-PRO-3. Cells depicted in red are counted as non-viable cells. C. Quantification of cell viability counted from fluorescent images. N=5, 300-600 cardiomyocytes counted per group, error bars represent SEM, * $p < 0.05$, ** $p < 0.01$ and *** $p < 0.001$ as measured by two-way ANOVA multiple comparison with Tukey.

REFERENCES

1. Li F, Wang X, Capasso JM, Gerdes AM. Rapid transition of cardiac myocytes from hyperplasia to hypertrophy during postnatal development. *J Mol Cell Cardiol.* 1996;28:1737–1746.
2. Zebrowski DC, Engel FB. The cardiomyocyte cell cycle in hypertrophy, tissue homeostasis, and regeneration. *Rev Physiol Biochem Pharmacol.* 2013;165:67–96.
3. Zebrowski DC, Vergarajauregui S, Wu CC, Piatkowski T, Becker R, Leone M, Hirth S, Ricciardi F, Falk N, Giessl A, Just S, Braun T, Weidinger G, Engel FB. Developmental alterations in centrosome integrity contribute to the post-mitotic state of mammalian cardiomyocytes. *Elife.* 2015;4:e05563.
4. Kang MJ, Kim JS, Chae SW, Koh KN, Koh GY. Cyclins and cyclin dependent kinases during cardiac development. *Mol Cells.* 1997;7:360–6.
5. Poolman RA, Gilchrist R, Brooks G. Cell cycle profiles and expressions of p21(CIP1) and p27(KIP1) during myocyte development. *Int J Cardiol.* 1998;67:133–142.
6. Tham YK, Bernardo BC, Ooi JYY, Weeks KL, McMullen JR. Pathophysiology of cardiac hypertrophy and heart failure: signaling pathways and novel therapeutic targets. *Arch Toxicol.* 2015;89:1401–1438.
7. Kulandavelu S, Karantalis V, Fritsch J, Hatzistergos KE, Loescher VY, McCall F, Wang B, Bagno L, Golpanian S, Wolf A, Grenet J, Williams A, Kupin A, Rosenfeld A, Mohsin S, Sussman MA, Morales A, Balkan W, Hare JM. Pim1 Kinase Overexpression Enhances ckit+ Cardiac Stem Cell Cardiac Repair Following Myocardial Infarction in Swine. *J Am Coll Cardiol.* 2016;68:2454–2464.
8. Muraski JA, Fischer KM, Wu W, Cottage CT, Quijada P, Mason M, Din S, Gude N, Alvarez R, Rota M, Kajstura J, Wang Z, Schaefer E, Chen X, MacDonnel S, Magnuson N, Houser SR, Anversa P, Sussman MA. Pim-1 kinase antagonizes aspects of myocardial hypertrophy and compensation to pathological pressure overload. *Proc Natl Acad Sci U S A.* 2008;105:13889–13894.
9. Muraski JA, Rota M, Misao Y, Fransioli J, Cottage C, Gude N, Esposito G, Delucchi F, Arcarese M, Alvarez R, Siddiqi S, Emmanuel GN, Wu W, Fischer K, Martindale JJ, Glembotski CC, Leri A, Kajstura J, Magnuson N, Berns A, Beretta RM, Houser SR, Schaefer EM, Anversa P, Sussman MA. Pim-1 regulates cardiomyocyte survival downstream of Akt. *Nat Med.* 2007;13:1467–1475.
10. Zhu HH, Wang XT, Sun YH, He WK, Liang JB, Mo BH, Li L. Pim1 Overexpression Prevents Apoptosis in Cardiomyocytes after Exposure to Hypoxia and Oxidative Stress via Upregulating Cell Autophagy. *Cell Physiol Biochem.* 2018;49:2138–2150.
11. An N, Lin Y-W, Mahajan S, Kellner JN, Wang Y, Li Z, Kraft AS, Kang Y. Pim1 Serine/Threonine Kinase Regulates the Number and Functions of Murine Hematopoietic

Stem Cells. *Stem Cells*. 2013;31:1202–1212.

12. Qian KC, Wang L, Hickey ER, Studts J, Barringer K, Peng C, Kronkaitis A, Li J, White A, Mische S, Farmer B. Structural basis of constitutive activity and a unique nucleotide binding mode of human Pim-1 kinase. *J Biol Chem*. 2005;280:6130–6137.

13. Wang Z, Bhattacharya N, Weaver M, Petersen K, Meyer M, Gapter L, Magnuson NS. Pim-1: A serine/threonine kinase with a role in cell survival, proliferation, differentiation and tumorigenesis. *J Vet Sci*. 2001;2:167.

14. Borillo GA, Mason M, Quijada P, Völkers M, Cottage C, McGregor M, Din S, Fischer K, Gude N, Avitabile D, Barlow S, Alvarez R, Truffa S, Whittaker R, Glassy MS, Gustafsson AB, Miyamoto S, Glembotski CC, Gottlieb RA, Brown JH, Sussman MA. Pim-1 kinase protects mitochondrial integrity in cardiomyocytes. *Circ Res*. 2010;106:1265–1274.

15. Smith AL, Ellison FM, McCoy JP, Chen J. c-Kit expression and stem cell factor-induced hematopoietic cell proliferation are up-regulated in aged B6D2F1 mice. *Journals Gerontol - Ser A Biol Sci Med Sci*. 2005;60:448–456.

16. Fischer KM, Cottage CT, Wu W, Din S, Gude NA, Avitabile D, Quijada P, Collins BL, Fransioli J, Sussman MA. Enhancement of myocardial regeneration through genetic engineering of cardiac progenitor cells expressing pim-1 kinase. *Circulation*. 2009;120:2077–2087.

17. Gude NA, Firouzi F, Broughton KM, Ilves K, Nguyen KP, Payne CR, Sacchi V, Monsanto MM, Casillas AR, Khalafalla FG, Wang BJ, Ebeid DE, Alvarez R, Dembitsky WP, Bailey BA, Van Berlo J, Sussman MA. Cardiac c-Kit biology revealed by inducible transgenesis. *Circ Res*. 2018;123:57–72.

18. Linnekin D. Early signaling pathways activated by c-Kit in hematopoietic cells. *Int J Biochem Cell Biol*. 1999;31:1053–1074.

19. Lips DJ, Bueno OF, Wilkins BJ, Purcell NH, Kaiser RA, Lorenz JN, Voisin L, Saba-El-Leil MK, Meloche S, Pouysségur J, Pagès G, De Windt LJ, Doevendans PA, Molkenkin JD. MEK1-ERK2 Signaling Pathway Protects Myocardium From Ischemic Injury In Vivo. *Circulation*. 2004;109:1938–1941.

20. Li XM, Ma YT, Yang YN, Liu F, Chen BD, Han W, Zhang JF, Gao XM. Downregulation of survival signalling pathways and increased apoptosis in the transition of pressure overload-induced cardiac hypertrophy to heart failure. *Clin Exp Pharmacol Physiol*. 2009;36:1054–1061.

21. Song YH, Cai H, Zhao ZM, Chang WJ, Gu N, Cao SP, Wu ML. Icariin attenuated oxidative stress induced-cardiac apoptosis by mitochondria protection and ERK activation. *Biomed Pharmacother*. 2016;83:1089–1094.

22. Yeh CC, Fan Y, Xu Y, Yang YL, Simpson PC, Mann MJ. Shift toward greater

pathologic post-myocardial infarction remodeling with loss of the adaptive hypertrophic signaling of alpha1 adrenergic receptors in mice. *PLoS One*. 2017;12:e0188471.

23. Datta SR, Dudek H, Xu T, Masters S, Haian F, Gotoh Y, Greenberg ME. Akt phosphorylation of BAD couples survival signals to the cell- intrinsic death machinery. *Cell*. 1997;91:231–241.

24. An N, Cen B, Cai H, Song JH, Kraft A, Kang Y. Pim1 kinase regulates c-Kit gene translation. *Exp Hematol Oncol*. 2016;5:31–38.

25. Mikkers H, Nawijn M, Allen J, Brouwers C, Verhoeven E, Jonkers J, Berns A. Mice Deficient for All PIM Kinases Display Reduced Body Size and Impaired Responses to Hematopoietic Growth Factors. *Mol Cell Biol*. 2004;24:6104–6115.

26. Moyzis AG, Najor RH, Cortez MQ, Gustafsson ÅB, Kubli DA, Lee Y. PINK1 Is Dispensable for Mitochondrial Recruitment of Parkin and Activation of Mitophagy in Cardiac Myocytes. *PLoS One*. 2015;10:e0130707.

27. Ma HP, Ma XN, Ge BF, Zhen P, Zhou J, Gao YH, Xian CJ, Chen KM. Icariin attenuates hypoxia-induced oxidative stress and apoptosis in osteoblasts and preserves their osteogenic differentiation potential in vitro. *Cell Prolif*. 2014;47:527–539.

28. Di Siena S, Gimmelli R, Nori SL, Barbagallo F, Campolo F, Dolci S, Rossi P, Venneri MA, Giannetta E, Gianfrilli D, Feigenbaum L, Lenzi A, Naro F, Cianflone E, Mancuso T, Torella D, Isidori AM, Pellegrini M. Activated c-Kit receptor in the heart promotes cardiac repair and regeneration after injury. *Cell Death Dis*. 2016;7:e2317–e2317.

29. Fischer KM, Cottage CT, Konstandin MH, Völkers M, Khan M, Sussman MA. Pim-1 kinase inhibits pathological injury by promoting cardioprotective signaling. *J Mol Cell Cardiol*. 2011;51:554–558.

30. Liu N, Wang BJ, Broughton KM, Alvarez R, Siddiqi S, Loaiza R, Nguyen N, Quijada P, Gude N, Sussman MA. PIM1-minicircle as a therapeutic treatment for myocardial infarction. *PLoS One*. 2017;12:e0173963.

31. Mohsin S, Khan M, Toko H, Bailey B, Cottage CT, Wallach K, Nag D, Lee A, Siddiqi S, Lan F, Fischer KM, Gude N, Quijada P, Avitabile D, Truffa S, Collins B, Dembitsky W, Wu JC, Sussman MA. Human cardiac progenitor cells engineered with Pim-I kinase enhance myocardial repair. *J Am Coll Cardiol*. 2012;60:1278–1287.

32. Vajravelu BN, Hong KU, Al-Maqtari T, Cao P, Keith MCL, Wysoczynski M, Zhao J, Moore JB, Bolli R. C-Kit promotes growth and migration of human cardiac progenitor cells via the PI3KAKT and MEK-ERK Pathways. *PLoS One*. 2015;10:e0140798.

33. Ebeid DE, Khalafalla FG, Broughton KM, Monsanto MM, Esquer CY, Sacchi V, Hariharan N, Korski KI, Moshref M, Emathingier J, Cottage CT, Quijada PJ, Nguyen JH, Alvarez R, Völkers M, Konstandin MH, Wang BJ, Firouzi F, Navarrete JM, Gude NA,

Goumans M-J, Sussman MA. Pim1 maintains telomere length in mouse cardiomyocytes by inhibiting TGF β signalling. *Cardiovasc Res*. 2020;116:cvaa066.

34. Mohsin S, Khan M, Nguyen J, Alkatib M, Siddiqi S, Hariharan N, Wallach K, Monsanto M, Gude N, Dembitsky W, Sussman MA. Rejuvenation of human cardiac progenitor cells with pim-1 kinase. *Circ Res*. 2013;113:1169–1179.

35. Quijada P, Toko H, Fischer KM, Bailey B, Reilly P, Hunt KD, Gude NA, Avitabile D, Sussman MA. Preservation of myocardial structure is enhanced by pim-1 engineering of bone marrow cells. *Circ Res*. 2012;111:77–86.

36. Hu S, Yan G, Xu H, He W, Liu Z, Ma G. Hypoxic preconditioning increases survival of cardiac progenitor cells via the pim-1 kinase-mediated anti-apoptotic effect. *Circ J*. 2014;78:724–731.

37. Katare R, Caporali A, Zentilin L, Avolio E, Sala-Newby G, Oikawa A, Cesselli D, Beltrami AP, Giacca M, Emanuelli C, Madeddu P. Intravenous gene therapy with PIM-1 via a cardiotropic viral vector halts the progression of diabetic cardiomyopathy through promotion of prosurvival signaling. *Circ Res*. 2011;108:1238–1251.

38. Marino F, Scalise M, Cianflone E, Mancuso T, Aquila I, Agosti V, Torella M, Paolino D, Mollace V, Nadal-Ginard B, Torella D. Role of c-Kit in Myocardial Regeneration and Aging. *Front Endocrinol (Lausanne)*. 2019;10:371–385.

39. Gude NA, Sussman MA. Chasing c-Kit through the heart: Taking a broader view. *Pharmacol Res*. 2018;127:110–115.

40. Li M, Naqvi N, Yahiro E, Liu K, Powell PC, Bradley WE, Martin DIK, Graham RM, Dell'Italia LJ, Husain A. c-kit is required for cardiomyocyte terminal differentiation. *Circ Res*. 2008;102:677–685.

41. Hammerman PS, Fox CJ, Birnbaum MJ, Thompson CB. Pim and Akt oncogenes are independent regulators of hematopoietic cell growth and survival. *Blood*. 2005;105:4477–4483.

42. Pircher TJ, Zhao S, Geiger JN, Joneja B, Wojchowski DM. Pim-1 kinase protects hematopoietic FDC cells from genotoxin-induced death. *Oncogene*. 2000;19:3684–3692.

43. Blume-Jensen P, Janknecht R, Hunter T. The Kit receptor promotes cell survival via activation of PI 3-kinase and subsequent Akt-mediated phosphorylation of Bad on Ser136. *Curr Biol*. 2004;8:779–785.

44. Bueno OF, Molkentin JD. Involvement of extracellular signal-regulated kinases 1/2 in cardiac hypertrophy and cell death. *Circ Res*. 2002;91:776–781.

45. Ulm S, Liu W, Zi M, Tsui H, Chowdhury SK, Endo S, Satoh Y, Prehar S, Wang R, Cartwright EJ, Wang X. Targeted deletion of ERK2 in cardiomyocytes attenuates hypertrophic response but provokes pathological stress induced cardiac dysfunction. *J*

Mol Cell Cardiol. 2014;72:104–116.

46. Nihira K, Ando Y, Yamaguchi T, Kagami Y, Miki Y, Yoshida K. Pim-1 controls NF- κ B signalling by stabilizing RelA/p65. *Cell Death Differ.* 2010;17:689–698.

47. Samse K, Emathinger J, Hariharan N, Quijada P, Ilves K, Völkers M, Ormachea L, De La Torre A, Orogo AM, Alvarez R, Din S, Mohsin S, Monsanto M, Fischer KM, Dembitsky WP, Gustafsson ÅB, Sussman MA. Functional effect of Pim1 depends upon intracellular localization in human cardiac progenitor cells. *J Biol Chem.* 2015;290:13935–13947.

Chapter 3, with slight modifications, is a reprint of the material as it appears in *Cells*, 2020. PIM1 Promotes Survival of Cardiomyocytes by Upregulating c-Kit Protein Expression. David E Ebeid, Fareheh Firouzi, Carolina Y Esquer, Julian M Navarrete, Bingyan J Wang, Natalie A Gude, Mark A Sussman. The dissertation author was the co-first author and investigator on this manuscript.

CHAPTER 4

'Youthful' Phenotype of c-Kit⁺ Cardiac Fibroblasts

INTRODUCTION

Fibroblasts constitute the primary subtype of cardiac nonmyocyte populations^{1,2}. Functional diversity including (but not limited to) myocardial development, structural and mechanical homeostasis, and pathological remodeling³⁻⁵ necessitates fundamental characterization of cardiac fibroblasts (CFs) to glean insights into normal cardiac biology coupled with potential therapeutic interventions to mitigate myocardial damage and aging. However, advancement of CF biology has been limited by 1) molecular heterogeneity within CF population, 2) understudied biological properties of CF subpopulations and, 3) rudimentary understanding of gene expression signatures underlying their functional plasticity. Molecular markers that define phenotypic and functional properties would refine delineation of CF subsets responsible for biological responses in development, injury, and aging.

c-Kit is a type III receptor tyrosine kinase present in different cells throughout various adult tissues⁶⁻⁸. In the heart, c-Kit⁺ cells encompass multiple cell types including cardiomyocytes as well as cardiac interstitial cells (CICs) involved in myocardial homeostasis and reparative remodeling⁹⁻¹². Mechanistically, binding of stem cell factor (SCF) ligand induces c-Kit receptor dimerization, phosphorylation, and activation of downstream signaling targets^{7,13}. Outcomes of c-Kit activation are cell type-specific and include cellular activities such as proliferation, survival, cell differentiation and migration^{8,12,14}.

c-Kit is expressed in fibroblast subtypes in several tissues and organs including aorta, lung, and liver¹⁵⁻¹⁸. In the lung, a subpopulation of fibroblasts upregulates c-Kit in response to pathological injury while lacking myofibroblast associated markers such as

α -SMA and collagen I¹⁶. In addition, cultured fibroblasts with induced c-Kit expression resulted in “rejuvenation” of cells with youthful biological traits such as smaller cell size and higher proliferative capacity¹⁹. Nevertheless, biological significance of c-Kit and functional contribution of c-Kit signaling within the CFs population remains obscure. Based upon substantial experience of our laboratory studying cardiac c-Kit biology^{12,20–24}, the present study examines c-Kit signaling within CICs of fibroblast lineage.

CF is a challenging population of cells to study due in part to the lack of unique marker proteins. Simply put, multiple cell types express most fibroblast markers⁴. However, there are organ-specific characteristics to distinguish fibroblasts in different tissues. For example, in human and mouse cardiac tissue Discoidin domain-containing receptor 2 (DDR2): a collagen-induced receptor tyrosine kinase is expressed mainly by fibroblasts^{1,25}. Therefore, DDR2 was used as the primary marker of the CF population that served as the basis for our investigation of c-Kit biology. Findings of the present study document phenotypic properties in the DDR2⁺ CF population relative to c-Kit expression and reveal that youthful pre-committed characteristics are coincident with c-Kit⁺ in CF.

METHODS

Mouse models

Three-month-old FVB/J mice and inducible c-Kit reporter mouse models (named CKH2B) were used. As described previously¹², CKH2B transgenic mouse was created by crossing a c-Kit-rtTA mouse line; harboring rtTA transcription factor under the control of c-Kit promoter, with a TRE-H2BEGFP line; with tetracycline responsive H2BEGFP reporter construct. Doxycycline treatment of double transgenic mice drives expression of H2BEGFP construct with active c-Kit promoter. In vivo, H2BEGFP reporter expression was induced by administering 0.2 mg/ml doxycycline in the drinking water for up to four days.

Myocardial infarction

All animal procedures and experiments were approved by the Institutional Animal Care and Use Committee at San Diego State University (IACUC). Mice were housed on ventilated racks provided with ambient temperature of 70–72 °F, on a 12-h light dark cycle. Myocardial infarction (MI) was induced on FVB/J strain mice under 2% isoflurane as previously reported²¹. Briefly, a small incision was made between the 3rd and 4th ribs and the heart was squeezed out by gently pressing the thorax. The left anterior descending artery (LAD) was then ligated at the distal diagonal branch with a 7–0 silk suture. Infarction was confirmed by paling of anterior left myocardium wall. Squeezing heart out of the chest and placing it back in the chest without ligation of the LAD was considered a sham surgery. Seven days post MI or sham surgery, hearts were either retro-perfused and fixed in formalin for paraffin processing or lysed for protein collection and immunoblotting.

CIC isolation and expansion

CICs were isolated from 3-month-old FVB/J mice or CKH2B mouse models following enzymatic dissociation (Liberase™ DH Research Grade, 26 U/ ml, Sigma-Aldrich, 5466202001) of the whole heart on a Langendorff apparatus (Radnoti, 158831) as previously described²². For young vs old cell analysis, CICs were isolated from 1.5-month-old and 9-month-old mice respectively. Cell suspension was then passed through a 100-micron nylon mesh and cardiomyocytes were separated by centrifugation for 2 minutes at 150 x g. Total non-myocyte CICs were either directly analyzed by flow cytometry or cultured at 37 °C in 5% CO₂ incubator in growth media [DMEM/F12 supplemented with 10% FBS and 1% Penicillin-Streptomycin-Glutamine (100X)] for subsequent analysis (Figure 4.1A). Cultured CICs were used at p3 for the experiments. In vitro, H2BEGFP reporter expression was induced by administering 0.1 mg/ml doxycycline at 1:1000 dilution in growth media for 24 hours.

Flow cytometry and cell sorting

Freshly isolated CICs were blocked in 10% HS in 1X PBS on ice for 30 minutes. Following, cells were washed with wash buffer (0.5% BSA in 1X PBS) and incubated with antibodies on ice for 30 minutes. For fixed cell analysis, cells were suspended in 4% paraformaldehyde for 10 minutes at room temperature prior to blocking and antibody staining. Post antibody incubation, cells were washed with wash buffer, resuspended in 300 µl wash buffer and analyzed and/or sorted based on surface expression of c-Kit and DDR2 by flow cytometry [BD FACS Melody™ cell sorter or BD FACS Canto™ (BD Biosciences)]. To deplete for CD45, cell suspension was incubated with CD45-labeled beads (Miltenyi Biotec, catalog #130-052-301) and sorted according to the manufacturer's

protocol. CD45⁻ population was then stained for c-Kit and DDR2. Unstained and isotype controls were used to establish gating strategies and baseline fluorescence levels. Antibodies and dilutions are listed in table 4.1.

Immunohistochemistry and confocal microscopy

Heart tissues from uninjured, sham and MI mice were fixed in formalin and processed for paraffin embedding as previously described¹⁰. For immunolabeling, 5µm-sections were deparaffinized and subjected to antigen retrieval (10mM citrate pH 6.0). Endogenous peroxidase activity was quenched in 3% H₂O₂ in 1X PBS for 30 minutes. Tissues were incubated with primary antibodies overnight followed by secondary antibody incubation for 90 minutes. Nuclei were stained with 4',6-diamidino-2-phenylindole, (DAPI) diluted in 1X PBS at room temperature for 15 minutes and slides were coverslipped with Vectashield mounting media. Images were captured on a Leica SP8 confocal microscope and ImageJ software (National Institutes of Health) was used to quantify staining intensity presented as a percentage of the area of each image. Antibodies and dilutions are listed in table 4.1.

Immunoblotting

Whole heart tissue and cultured cells were homogenized in lysis buffer containing protease and phosphatase inhibitor cocktails (Sigma-Aldrich; P8340, P5726, P2850). Bradford assay was performed to analyze and normalize protein concentrations and lysates were prepared by addition of NuPAGE LDS Sample Buffer (ThermoFisher; NP0007) and 100 µM dithiothreitol (Bio-Rad; 161-0611). Samples were sonicated and boiled for 5 minutes at 95 °C and stored at -80 °C. Proteins were separated on a 4–12% NuPAGE Bis-Tris gel (ThermoFisher; NP0321BOX) and transferred onto a polyvinylidene

fluoride membrane. Nonspecific binding sites were blocked using Odyssey blocking buffer (LICOR, 927-60001) and proteins were labeled with primary antibodies in 0.2% Tween in Odyssey blocking buffer overnight. After multiple washes, blots were incubated with secondary antibodies in 0.2% Tween 20 in Odyssey blocking buffer for 1.5 hours at room temperature and scanned using the LICOR Odyssey CLx scanner. Quantification was performed using ImageJ software. Antibodies and their dilutions are listed in table 4.1.

Immunocytochemistry and confocal microscopy

Three CIC populations of c-Kit⁺ DDR2⁻, c-Kit⁻ DDR2⁺ and c-Kit⁺ DDR2⁺ were plated on a 2-well chamber slide (10,000 per well). Cells were fixed in 4% paraformaldehyde for 20 minutes, washed in 1% Tween in 1X PBS and blocked in 10% HS in 1X PBS. Phalloidin staining was performed at room temperature for 1.5 hours. Nuclei were stained with DAPI diluted in 1X PBS at room temperature for 15 minutes. Cells were imaged using a Leica TCS SP8 confocal microscope. Antibodies and dilutions are listed in table 4.1. For nucleation status measurement, images of phalloidin-stained cells were used to count the number of nuclei per cell in each group.

Senescence-associated beta-galactosidase (SA- β -Gal) staining

Three populations of CICs were seeded on a 6-well plate at a density of 20,000 cells per well. Senescence detection kit (Abcam, ab65351) was used per manufacturer's instruction. Briefly, cells were washed in 1X PBS and fixed in fixative Solution for 10 - 15 minutes at room temperature. Next, cells were incubated with staining solution including X-gal for 1 hour at 37°C. Cells were observed under microscope for development of blue color and imaged using a Leica DMI6000 live imaging microscope. Images were

processed using ImageJ software (National Institutes of Health) and number of SA- β -Gal⁺ cells was counted.

Morphology measurement

Bright field images of the three CIC populations of c-Kit⁺ DDR2⁻, c-Kit⁺ DDR2⁺ and c-Kit⁺ DDR2⁺ were obtained using a LEICA DM IL microscope and cell boundaries were outlined by image analysis using ImageJ software (National Institutes of Health). Cell surface area, length to width ratio and roundness were determined as previously described²³.

Proliferation assay and doubling time

Three populations of CICs were seeded on 12-well plates in quintuplicate at a density of 20,000 cells per well. At 3 time points (days 1, 4, and 7) cells were dissociated and counted manually using a hemocytometer. Cell proliferation rate was determined for each cell population as fold change over day 1. Cell doubling time was calculated for each group using online population doubling time software (http://www.doubling-time.com/compute_more.php).

Cell motility measurement

Three populations of CICs were plated on a 6-well plate at a density of 20,000 cells per well. Time-lapse video microscopy was conducted using Leica DMI6000 live imaging microscope equipped with a 37°C temperature-controlled stage with a humidified atmosphere containing 5% CO₂ to allow the cells to remain viable during the image acquisition. Images were acquired with a 30-second time interval over the course of 96 hours and compiled into time-lapse videos. Four cells from each time-lapse video

corresponding to each population of cells were manually tracked using ImageJ software and their velocity of movement ($\mu\text{M/s}$) was calculated.

scRNA-Seq

Freshly isolated single cell suspensions were loaded on a Chromium™ Controller (10x Genomics) and single-cell RNA-seq libraries were prepared using Chromium™ Single Cell 3' Library & Gel Bead Kit v3 (10x Genomics; Item 1000075) following manufacturer's protocol. Concentration and fragment size distribution of each library were tested with Bioanalyzer (Agilent High Sensitivity DNA Kit, #Cat. 5067-4626; average library size: 450-490 bp). The sequencing libraries were quantified by quantitative PCR (KAPA Biosystems Library Quantification Kit for Illumina platforms P/N KK4824) and Qubit 3.0 with dsDNA HS Assay Kit (Thermo Fisher Scientific). Sequencing libraries were submitted to the UCSD IGM Genomics Core for sequencing (NovaSeq 6000). For single cell selection and quality control, the raw data was processed with the Cell Ranger pipeline (10X Genomics; version 3.0.1, Figure 4.7). Sequencing reads were aligned to the 10x mouse genome mm10. Cells with fewer than 200 genes were filtered out to avoid inclusion of empty droplets in downstream analysis. Based on UMI and gene detection distribution droplet multiplets were excluded using the Interquartile Range Rule (Values over the third quartile and 1.5 the interquartile range are considered outliers). Cell with more than 20% of mitochondrial gene UMI count and genes detected in fewer than three cells were filtered out using Seurat R Package (v4.0.4)²⁴. The first 12 principal components were significant to perform dimensionality reduction. Preparations derived from cell surface sorting strategy yielded 12286 barcoded cells for analysis, from which 3603 corresponded to c-Kit⁺ DDR2⁻, 2755 corresponded to c-Kit⁻ DDR2⁺, 4546

corresponded to CND c-Kit⁺ DDR2⁺, and 1382 corresponded to c-Kit⁺ DDR2⁺ CD45⁻. Final removal of unwanted sources of variation and batch effect corrections was performed using Seurat R Package (v4.0.4)²⁴. Dimensionality reduction and unsupervised clustering approximately 2000 variable genes were selected based on their expression and dispersion. Prior dimensionality reduction, data was scaled to mean expression equal to 0 and variance across cells equal to 1. Principal component analysis was performed on the scaled data as a linear dimensionality reduction approach. The first 12 most significant principal components (PCs) were selected for non-linear dimensional reduction (PCA, tSNE and UMAP; Figure 4.9A) and unsupervised clustering using complementary methods including supervised PC selection, Jackstraw statistical and heuristic approaches. Clusters were validated by concurrent expression of housekeeping genes (Gapdh, Actb, Rplp0, B2m and Ywhaz; Figure 4.9B). Differential expression analysis was done using Wilcoxon rank sum test and selecting for a threshold of 0.05 for an adjusted p-value and a log (FC) >0.25 was used to define statistically significant and differentially expressed genes (DEGs). Gene ontology (GO) enrichment analysis for DEGs lists derived from c-Kit⁺ DDR2⁻, c-Kit⁻ DDR2⁺, CND c-Kit⁺ DDR2⁺ and c-Kit⁺ DDR2⁺ CD45⁻ cells was performed using enrichGO and compareCluster functions of clusterProfiler (3.16.1) R package²⁵. GO terms were selected with p-value cutoff of 0.05 using BH method. RNA velocity and pseudotime analysis RNA velocity was performed to explore transitional states of c-Kit⁺ DDR2⁻, c-Kit⁻ DDR2⁺, CND c-Kit⁺ DDR2⁺ and c-Kit⁺ DDR2⁺ CD45⁻ derived cells. Expression data from 12286 cells was used to generate a cds object to process through monocle3²⁶. Analysis was performed using 12 PCs for dimensionality reduction and trajectory inference. Gene expression module scores for single cells were calculated

for Secretary Associated Senescence Phenotype factors (SASPs), and Growth Factors, using the AddModuleScore function in the Seurat R package. SASP and growth factors are listed in table 4.2. Cell Cycle score and analysis was performed as described by the Satija group based upon cell cycle markers developed for scRNA-seq analysis²⁷. scRNA-Seq data generated in this study has been uploaded to the Gene Expression Omnibus (GEO) database (GSE188804).

Statistical analysis

All data are expressed as mean \pm SEM. Statistical significance was assessed using Student t-test for comparison between two groups and one-way or two-way ANOVA for multiple comparisons, followed by the Tukey or Bonferroni post hoc tests to compare groups with a control group in GraphPad Prism version 5.0. $P < 0.05$ was considered statistically significant.

RESULTS

c-Kit promoter is active in cardiac fibroblasts *in vitro*

To identify c-Kit gene expression in CFs, non-myocyte CICs were isolated from a previously described CKH2B reporter mouse model. Cultured CICs were treated with doxycycline for 24 hours to induce EGFP reporter expression in cells with active c-Kit promoter. Subsequently, cells were immunolabeled for EGFP and fibroblast markers and analyzed through flow cytometry (Figure 4.1B). EGFP⁺ cells comprised about 70% of cultured CICs (Figure 4.1C). EGFP colocalized with DDR2 and vimentin in approximately 50% and 40% of CIC population, respectively (Figure 4.1D-E). In addition, TCF21; an essential transcription factor for CF function²⁸; and periostin; a marker of activated fibroblast with essential role in regulating collagen organization²⁹ are expressed in a subset of EGFP⁺ CICs (TCF21, 21.77%; periostin, 9.26%) (Figure 4.1F-G). Taken together, EGFP reporter is expressed in cultured transgenic CFs.

c-Kit promoter is active in cardiac fibroblasts *in vivo*

Culture condition impacts cellular gene expression profile and biological properties^{30,31}. Correspondingly, cells cultured in two different growth media adapted for c-Kit⁺ CICs decreased DDR2 expression and coincidence with EGFP compared to cells cultured in fibroblast and endothelial progenitor cell (EPC) growth media (Figure 4.2A-D). To avoid influence of culture conditions, H2BEGFP reporter expression was induced *in vivo* with doxycycline in the drinking water for up to four days followed by isolation and analysis of the freshly isolated CICs for DDR2 expression and colocalization with EGFP (Figure 4.3A). EGFP⁺ cells comprised more than half of the freshly isolated CICs (Figure 4.3B-C) with coincidence with DDR2 in about 30% of the total population (Figure 4.3D-

E). These results provide further evidence that c-Kit promoter is active in transgenic DDR2⁺ CFs.

c-Kit protein is expressed in a subset of cardiac fibroblast population and diminishes with physiological aging

c-Kit promoter activation does not necessarily correlate with c-Kit protein expression^{12,32}. Consistently, half of the EGFP⁺ CICs from the doxycycline treated hearts are labeled for c-Kit protein (Figure 4.4A-B). To determine c-Kit protein expression within CF population, freshly isolated CICs from WT mice were immunolabeled for DDR2 along with c-Kit and analyzed via flow cytometry (Figure 4.4C-D). Approximately, 30% of CICs express either c-Kit or DDR2 with coincidence of the two markers in 8% of the total population (Figure 4.5A). Immunolabeling of paraffin sections confirms c-Kit protein expression in DDR2⁺ CFs (Figure 4.5B). Colocalization of c-Kit and DDR2 is mainly identified in the cells along the epicardial border. Aging influence upon c-Kit and DDR2 coincidence in freshly isolated CICs from young and old mice reveals increased presence of c-Kit⁻ DDR2⁺ CFs consistent with the fibrotic remodeling of senescent hearts (Young, 12.5%; old, 34.0%). Notably, c-Kit⁺ DDR2⁺ CFs diminished in the aged hearts (Young, 10.3%; old, 3.9%), similar to c-Kit⁺ DDR2⁻ CICs (Young, 12.2%; old, 3.4%). Cumulatively, these data confirm presence of c-Kit in CF population and demonstrate age-associated reduction in c-Kit expressing CFs (Figure 4.5C).

c-Kit and DDR2 expression as well as coincidence upregulate following pathological damage

c-Kit upregulates in response to myocardial damage and promotes survival in multiple cell types^{12,33,34}. Tissue sections from uninjured and infarcted hearts were

immunolabeled for c-Kit and DDR2 to determine the impact of pathological damage on DDR2 expression and colocalization with c-Kit. Consistent with previous findings, c-Kit expression increased in the injured hearts (Uninjured, 0.18%; sham, 0.15%; MI, 0.59% Area). Similarly, DDR2 substantially upregulated in infarcted heart sections (Uninjured, 0.24%; sham, 0.20%; MI, 5.0% Area). Moreover, c-Kit and DDR2 colocalization is elevated approximately threefold (Uninjured, 2.7%; sham, 2.0%; MI, 5.6% Area) indicative of expansion for this cell subtype in the injured heart (Figure 4.6A-C). As opposed to uninjured tissue sections, coincidence of c-Kit and DDR2 is detected in interstitium along with epicardial region in the damaged heart. Immunoblot of tissue lysates from uninjured and infarcted hearts confirms enhanced expression of c-Kit and DDR2 upon myocardial infarction (Figure 4.6D).

Transcriptomic phenotype of c-Kit expressing CFs

Single-cell RNA sequencing (scRNA-seq) was used to evaluate phenotypic differences of freshly isolated CICs based upon surface presence of c-Kit and / or DDR2 alone or in combination (Figure 4.7). Consistent with previous reports in lung, skin and liver^{35,36}, a large fraction of freshly isolated c-Kit⁺ DDR2⁺ CFs express CD45 (Figure 4.8) indicative of their hematopoietic origin. Accordingly, CD45 depletion was performed on double positive derived cells and transcriptional phenotype of the non-hematopoietic double positive CFs (c-Kit⁺ DDR2⁺ CD45⁻) was analyzed along with CD45-non-depleted (CND) c-Kit⁺ DDR2⁺ fibroblast population. Dimensionality reduction and unsupervised clustering revealed 16 clusters (Clusters 0-15) segregated according to transcriptional phenotype (Figure 4.10A-B, and Figure 4.9). Dimensionality reduction projections of single cell data revealed distinct distribution of c-Kit⁺ DDR2⁻ cells (shown in red) and three

CIC populations of fibroblast lineage: 1. c-Kit⁻ DDR2⁺ (shown in green), 2. c-Kit⁺ DDR2⁺ CD45⁻ (shown in purple) and CND c-Kit⁺ DDR2⁺ (shown in teal) (Figure 4.10C). Differential expression analysis reveals transcriptional differences across all populations, with 375 differentially expressed genes (DEGs) identified on c-Kit⁺ DDR2⁻, 820 DEGs on c-Kit⁻ DDR2⁺ CFs, 947 DEGs on c-Kit⁺ DDR2⁺ CD45⁻ CFs and 630 DEGs on CND c-Kit⁺ DDR2⁺ cells (Figure 4.10D). The CND c-Kit⁺ DDR2⁺ population displays a unique expression profile compared to all other populations. c-Kit⁺ DDR2⁺ CD45⁻ CFs display an expression profile relatively similar to c-Kit⁺ DDR2⁻ and c-Kit⁻ DDR2⁺ cells. DEGs derived from differential expression analysis were used as input for gene ontology (GO) analysis. GO term analysis of biological processes reveals enrichment of various ontologies associated with cardiac development on the c-Kit⁺ DDR2⁻ population, while the c-Kit⁻ DDR2⁺ population displays enrichment on ECM and fibril organization consistent with fibroblast phenotype (Figure 4.10E). Expression profile of the CND c-Kit⁺ DDR2⁺ population was enriched for GO terms associated to myeloid, leucocyte, lymphocyte and hemopoiesis consistent with hematopoietic origin. Expression profile of c-Kit⁺ DDR2⁺ CD45⁻ CFs reveals mild enrichment (<0.02 ratio) on GO terms associated with antigen presentation via MHCI (Figure 4.10E). Pseudotime analysis using Monocle3 established progression of cells from distinct origins in a single transcriptional trajectory, pseudotime abstract units were calculated, and directionality of the system was authenticated (Figure 4.10F-H). Based upon literature^{4,36-38} nodes 1 and 2, corresponding to clusters 7 and 1 respectively, were selected as origins of transcriptional progression for the cells. Pseudotime analysis confirms CND c-Kit⁺ DDR2⁺ CFs of hematopoietic origin in a transitional state toward c-Kit⁻ DDR2⁺ as well as c-Kit⁺ DDR2⁺ CD45⁻ CFs. In addition,

cells derived from the c-Kit⁺ DDR2⁻ and c-Kit⁺ DDR2⁺ CD45⁻ groups position on cluster 7, progress towards terminal leaves of the pseudotime plot via cluster 4 which is mainly composed of c-Kit⁻ DDR2⁺ population (Figure 4.10F-H). Together, these results reveal c-Kit expressing CF population (c-Kit⁺ DDR2⁺ CD45⁻) in a transitional state toward c-Kit⁻ DDR2⁺ CFs.

c-Kit expressing CFs transcriptionally associate with higher cell cycle progression and lower senescence-associated secretory phenotype

Assessment of cell cycle progression on all populations was performed through cell cycle scoring previously developed using markers for scRNA-Seq analysis²⁷ (Figure 4.11A-C). Interestingly, c-Kit⁺ DDR2⁻ and c-Kit⁺ DDR2⁺ CD45⁻ groups had comparable cell cycle profiles. The c-Kit⁺ DDR2⁺ CD45⁻ CFs display a 2.8-fold increase in G2M, while CFs without c-Kit expression (c-Kit⁻ DDR2⁺) show a ~1.5-fold increase upon cells restricted to G1 (Figure 4.11B). Expression of Senescence Associated Secretory Phenotype (SASP) factors³⁹ was also surveyed. c-Kit⁺ DDR2⁻ cells express most of the soluble receptors/ligands (Icam1, Il6st). Growth factors and regulators (Kitl, Cxcl12, Ngf, Igfbp3, Igfbp4, Igfbp6 and Igfbp7) were mostly overexpressed in c-Kit⁻ DDR2⁺ and c-Kit⁺ DDR2⁺ CD45⁻ CFs, while overexpression of interleukins (Il1B), chemokines (Cxcl1, Cxcl2, Ccl3) and proteases (Ctsb) was characteristic in CND c-Kit⁺ DDR2⁺ population (Figure 4.11C). Further confirmation using expression of 33 genes generated SASP (26 genes) and growth factor (18 genes) scores for each cell in our dataset (see methods). c-Kit⁺ DDR2⁺ CD45⁻ CFs score lower for SASP targets similar to c-Kit⁺ DDR2⁻, while maintaining a score similar to c-Kit⁻ DDR2⁺ CFs for growth factor expression (Figure 4.11D-E).

Collectively, these results demonstrate a transcriptome associated with higher cell cycle progression and lower SASP for c-Kit expressing CFs.

c-Kit expressing CFs are morphologically distinct

Based upon surface expression of c-Kit and DDR2, three CIC populations of c-Kit⁺ DDR2⁻, c-Kit⁻ DDR2⁺ and c-Kit⁺ DDR2⁺ were concurrently isolated, cultured and characterized in vitro. Phalloidin staining reveals morphological variation between the three populations (Figure 4.12A). Cell morphology measurements of area, length to width (L/W) ratio and roundness for each population confirms their distinct morphologies. DDR2⁺ CFs without c-Kit expression exhibits significantly larger cell area (c-Kit⁺ DDR2⁻, 0.011 x10⁴; c-Kit⁻ DDR2⁺, 0.28 x10⁴; c-Kit⁺ DDR2⁺, 0.03 x10⁴ μM²), lower L/W ratio (c-Kit⁺ DDR2⁻, 4.5; c-Kit⁻ DDR2⁺, 1.3; c-Kit⁺ DDR2⁺, 3.1) and higher level of roundness (c-Kit⁺ DDR2⁻, 0,08; c-Kit⁻ DDR2⁺, 0.38; c-Kit⁺ DDR2⁺, 0.09) compared to the other two populations of c-Kit⁺ DDR2⁻ and c-Kit⁺ DDR2⁺ (Figure 4.12B).

Cellular senescence is attenuated in c-Kit expressing CFs

Enlarged and irregular cell shape is a hallmark of senescence in cultured cells⁴⁰. Therefore, senescence associated cellular properties were assessed in the cultured CIC populations. Beside nuclear enlargement, c-Kit⁻ DDR2⁺ CICs demonstrate higher levels of binucleation. A large fraction of the c-Kit⁻ DDR2⁺ population is binucleated (40%) as opposed to c-Kit⁺ DDR2⁻ and c-Kit⁺ DDR2⁺ populations with 13% and 9.5% binucleated cells, respectively (Figure 4.13A). Binucleated cells go through premature senescence⁴¹ which was assayed using SA-β-Gal staining (Figure 4.13B). Compared to c-Kit⁺ DDR2⁻ and c-Kit⁺ DDR2⁺ CICs, a significantly higher proportion of c-Kit⁻ DDR2⁺ population exhibits SA-βGal accumulation (c-Kit⁺ DDR2⁻, 21.2%; c-Kit⁻ DDR2⁺, 51.4%; c-Kit⁺ DDR2⁺,

30.6%). In addition, cellular senescence marker P53 is highly expressed in c-Kit⁻ DDR2⁺ CICs with nearly sixfold increase in expression level relative to c-Kit⁺ DDR2⁻ and c-Kit⁺ DDR2⁺ populations (Figure 4.13C).

Self-renewal and cellular motility are enhanced in c-Kit expressing CFs

P53 is associated with inhibition of cell cycle progression as well as suppression of cell polarization and cellular motility^{42,43}. To understand the functional impact of senescence, the three populations of cultured CICs were assayed for proliferative characteristics and cellular motility. Proliferation rate of c-Kit⁻ DDR2⁺ population is significantly reduced with an average fold-change (FC) of 3.99 over the course of 7 days in culture reflected in a doubling time of 71 hours. Interestingly, c-Kit expressing DDR2⁺ CICs exhibit the greatest proliferative capacity with an average FC of 9.32 and a doubling time of 45 hours, exceeding even that of c-Kit⁺ DDR2⁻ with a FC of 6.99 and a doubling time of 51 hours (Figure 4.14A-B). Consistent with proliferation assay results, time-lapse video microscopy evidently demonstrates reduced cell spreading and cellular movement in c-Kit⁻ DDR2⁺ cell culture. Measurement of cell motion velocity confirms reduced cell motility in c-Kit⁻ DDR2⁺ CICs and illustrates a trend toward an elevated cell movement in c-Kit⁺ DDR2⁺ population (c-Kit⁺ DDR2⁻, 147.1; c-Kit⁻ DDR2⁺, 43.9; c-Kit⁺ DDR2⁺, 181.4 $\mu\text{M}/\text{S}$) (Figure 4.14C). Collectively, in vitro characterization validates distinct phenotypic and biological properties of c-Kit expressing CFs.

c-Kit expressing CFs are enriched for signaling genes implicated in proliferation and cell migration

Biological distinctions corresponding to underlying molecular mechanisms between the three CIC populations were assessed with respect to activated ERK1/2 and

pro-caspase-3 using protein lysates. ERK1/2 is associated with protective and proliferative signaling in a plethora of cell types³⁴. Likewise, caspase-3 confers nonapoptotic effects such as regulating proliferation and cell motility involving non-proteolytic functions exerted by its pro-domains^{44,45}. c-Kit expressing DDR2⁺ CFs highly express activated ERK1/2 with approximately 2-fold and 3-fold increase levels relative to c-Kit⁺ DDR2⁻ and c-Kit⁻ DDR2⁺ CICs, respectively. Similarly, pro-caspase-3 protein expression is upregulated in c-Kit⁺ DDR2⁺ CICs by 64% and 88% compared to c-Kit⁺ DDR2⁻ and c-Kit⁻ DDR2⁺ CICs. In contrary, activated ERK1/2 and pro-caspase-3 is significantly downregulated in c-Kit⁻ DDR2⁺ CICs compared to both c-Kit⁺ DDR2⁻ and c-Kit⁺ DDR2⁺ populations (Figure 4.14D-E). Overall, these data reflect pro-proliferative and pro-migratory properties of c-Kit expressing CFs.

DISCUSSION

The consensus outcome from decades of myocardial therapeutic interventions targeting fibroblasts⁴⁶⁻⁵¹ uncovers CF heterogeneity as a challenge for fundamental understanding of CF biology and advancement of treatment strategies. Therefore, characterization of CF subpopulations defined by patterns of protein expression and associated functional activities represents the frontier of fibroblast-based cardiac research and development. While the critical role of c-Kit signaling in myocardial biology and response to pathological damage is established, assessment of c-Kit biology within CF population has not been addressed. Findings presented here report biological significance of c-Kit in CF population. Presence of c-Kit identifies a subset of CFs with youthful and pre-committed cell phenotype.

Presence of c-Kit in fibroblasts derived from skin and liver upon isolation and expansion *in vitro*¹⁷ is consistent with H2BEGFP reporter expression indicative of c-Kit promoter activation in CFs isolated from the c-Kit transgenic reporter mouse heart (Figure 4.1B-G). *Ex vivo* expansion can alter cellular phenotype including expression of molecular markers^{30,31}. Similarly, transgenic fibroblasts exhibited variation in EGFP and DDR2 expression as well as colocalization (Figure 4.2A-D) depending upon media formulation. In comparison to *in vitro* findings, adult fibroblasts *in vivo* express c-Kit mainly in lung tissue as well as liver and aorta^{16,18,52,53}. Correspondingly, freshly isolated DDR2⁺ CFs from the CKH2B mouse exhibited c-Kit promoter activation, albeit at a lower level compared to cultured CFs (Figure 4.3A-E). Analysis of c-Kit protein expression in freshly isolated adult CFs by flow cytometry demonstrated coincidence of DDR2 and c-Kit in 8%

of total CICs (Figure 4.5A-B and Figure 4.4D). Notably, c-Kit expressing CF subpopulation diminished in the aged mice (Figure 4.5C).

The percentage of cells expressing DDR2, c-Kit, and/or EGFP showed variation because of multiple factors including 1) c-Kit protein and mRNA expression levels don't directly correlate^{32,54}, 2) c-Kit exhibits a highly dynamic expression pattern; cells transiently express c-Kit protein while labeled with H2BEGFP with a reported half-life of several months *in vivo*^{12,55,56}, and 3) intracellular c-Kit expression and internalized c-Kit exhibit differences in live vs. fixed cells that influences assay sensitivity¹². Collectively, these factors can readily explain detection of c-Kit in half of EGFP⁺ CICs from Doxy treated hearts (Figure 4.4A-B).

More than a decade of intense research has concluded that c-Kit biology in the cardiac context is relevant to a transitional cardiac cell population exhibiting heterogeneous expression characterized by temporal and spatial variations^{31,57}. Under normal conditions c-Kit⁺ cells reside mainly in subepicardial regions as well as interstitial spaces with an epicardial to endocardial gradient⁵⁸⁻⁶⁰. Epicardial activation upon injury leads to c-Kit upregulation, proliferation, and migration of epicardial-derived cells (EPDCs) through epithelial-mesenchymal transition (EMT), giving rise to mainly noncardiomyocyte lineages with presumptive roles in myocardial repair^{31,60}. EPDCs are considered the main source of CFs^{4,61} undergoing EMT and differentiate into cardiac interstitial fibroblasts⁶² under the influence of PDGF, FGF and TGF signaling. Presence of c-Kit⁺ DDR2⁺ cells exclusively along epicardial border in heart sections from uninjured mice (Figure 4.5A, Figure 4.6A) contrasts with abundant colocalization of c-Kit and DDR2 in interstitium (along with epicardial region) in infarcted heart sections (Figure 4.6B). In

the lung, a transitional non-myofibroblastic population with a presumed protective role in response to pathological damage was linked to a fibroblast subset with active c-Kit signaling¹⁶. Similarly, myocardial damage following infarction prompted increased c-Kit⁺ and DDR2⁺ and coinciding with a peak at 7 days post MI, consistent with a protective role for cardiac c-Kit⁺ and DDR2⁺ cells (Figure 4.6C-D).

scRNA-seq revealed transcriptional diversity within freshly isolated CIC populations based upon surface c-Kit⁺ and/or DDR2⁺. Fibroblasts and fibrocytes with a hematopoietic origin have been identified in lung, skin and liver^{35,36,63}. Hematopoietic-derived fibroblasts express CD45 along with fibroblast markers such as DDR2 and collagen I exhibit transitional precursor cell traits and contribute to pathological response⁶⁴⁻⁶⁶. In the heart, CD45⁺ fibroblast precursor population was detected upon myocardial damage, although hematopoietic progenitor cell contribution to the CF population is considered very limited under normal conditions of development and aging^{3,67-69}. In our hands, CD45 expression and hematopoietic lineage accounted for a considerable fraction of freshly isolated c-Kit⁺ DDR2⁺ CF population (Figure 4.8A). Possibly due to the distinct origin of CND c-Kit⁺ DDR2⁺, a unique expression profile (Figure 4.10D) enriched for GO terms associated with a hematopoietic lineage (Figure 4.10E) is evident relative to other populations. CND c-Kit⁺ DDR2⁺ CICs appear to be in a transitional state toward CFs based upon pseudotime trajectory analysis (Figure 4.10F-H). CD45 depletion prior to the selection for c-Kit⁺ DDR2⁺ CFs yields c-Kit⁺ DDR2⁺ CD45⁻ CFs with a transcriptome similar to both c-Kit⁺ DDR2⁻ and c-Kit⁻ DDR2⁺ CICs (Figure 4.10D). GO term analysis of biological processes suggested their potential role in immune response (Figure 4.10E). Moreover, pseudotime trajectory analysis of freshly isolated

CICs revealed a subpopulation of c-Kit⁺ cells (cluster 7) in a transitional state progressing toward c-Kit⁻ DDR2⁺ CFs.

c-Kit⁺ DDR2⁺ CD45⁻ cells exhibited higher G2/M and lower SASP scores, resembling c-Kit⁺ DDR2⁻ CICs, while maintained a similar score to c-Kit⁻ DDR2⁺ CICs for growth factor expression (Figure 4.11). Overall, phenotypic characteristics such as 1) comprising a subpopulation of proliferating cells, 2) transcriptome profile similar to both c-Kit⁺ DDR2⁻ as well as c-Kit⁻ DDR2⁺ CICs along with the results of the pseudotime analysis suggest a transitional phenotype for c-Kit expressing CFs (c-Kit⁺ DDR2⁺ CD45⁻).

Characterization of isolated DDR2⁺ CFs with and without c-Kit illustrated discrete morphological phenotypes. The c-Kit⁻ CFs displayed a large stellate-shaped morphology with long cytoplasmic extensions (Figure 4.12A, Figure 4.13A) corresponding to a myofibroblast phenotypic trait⁷⁰. Consistently, cell morphology measurements of area, roundness, and L/W ratio were significantly distinct in c-Kit⁻ DDR2⁺ cells compared to c-Kit⁺ DDR2⁺ and c-Kit⁺ DDR2⁻ populations (Figure 4.12A-B). TGF- β , a key regulator of fibroblasts to myofibroblast trans-differentiation, induces cellular binucleation⁷¹. Studies also showed that TGF- β signaling reduced expression of c-Kit and SCF in lung fibroblasts⁷². Remarkably, DDR2⁺ CFs without c-Kit expression exhibited higher level of binucleation (Figure 4.13A). Senescence following binucleation⁷³ is an established myofibroblast transition post fibrosis⁷⁴. Senescent myofibroblasts contribute to ECM degradation and cardiac dysfunction^{39,75}. c-Kit⁻ DDR2⁺ culture was highly senescent determined by significantly greater SA- β -Gal activity and P53 expression (Figure 4.13A-C). Functionally, c-Kit⁻ DDR2⁺ population demonstrated considerably lower proliferative

capacity and cell motility, whereas proliferation rate and motility of c-Kit expressing DDR2⁺ population were enhanced exceeding that of c-Kit⁺ DDR2⁻ CICs (Figure 4.14A-C). Overall, these observations associate c-Kit signaling with fibroblast morphology and biological activities such as proliferation and migration^{19,52,76}. c-Kit confers protective and proliferative properties partially via ERK and AKT downstream signaling pathways⁷. In the myocardial context, c-Kit activation enhanced phosphorylation of ERK1/2 in myocytes as well as cCICs and promoted cell survival and proliferation¹². Under basal conditions, ERK1/2 was highly expressed and activated in the c-Kit⁺ DDR2⁺ culture as opposed to c-Kit⁻ DDR2⁺ cells (Figure 4.14D). Recently, caspase-3 has emerged to participate in non-apoptotic functions such as differentiation, proliferation, and cell migration^{45,77,78}. During heart development, caspase-3 deficiency reduced expression of genes implicated in cell cycle progression and impaired cardiomyocyte proliferation⁷⁹. In mouse embryonic fibroblasts (MEFs), pro-caspase-3 regulates cell morphology and mediates cell migration independent of its catalytic activity⁴⁴. Similarly, pro-caspase-3 nonenzymatically suppresses ROS production and mitochondrial dysfunction^{80,81}. Correspondingly, c-Kit expressing DDR2⁺ CFs significantly upregulated pro-caspase-3 (Figure 4.14E), indicative of a potential contribution of pro-caspase-3 to cell proliferation and motility. Taken together, in vitro characterization of the DDR2⁺ CFs with or without c-Kit demonstrated correlation of c-Kit expression with a youthful biological phenotype.

Recent studies challenge straightforward fibroblast to myofibroblast trans-differentiation and indicate greater heterogeneity of cell state and functional complexity within CF population^{74,82,83}. Fibroblast subsets from distinct origins with unique gene expression profiles differentially mediate development of fibrotic responses and post-

fibrotic processes⁴. Three fates for activated fibroblasts include: 1) ECM production, 2) senescence or apoptosis, or 3) re-acquisition of resting phenotype⁶¹. Based upon these fibroblast fate outcomes, selection favoring CF subpopulations with preferentially reduced ECM production, decreased maladaptive fibrotic remodeling, and pre-senescent state is a desirable goal. Alternatively, elimination of fibroblasts with undesirable phenotypic attributes by senolytic approaches^{84,85} could be advantageous for preservation of “youthful” c-kit⁺ CFs described in this report. The debut of c-Kit biology within DDR2⁺ CFs detailed herein shows c-Kit expressing CFs are morphologically and functionally distinct with pro-proliferative and pro-migratory phenotypes, linking c-Kit to CF polarization toward a pre-committed state (Figure 4.15). This report is the first to our knowledge evaluating c-Kit biology within CF population and provides valuable insight regarding CF heterogeneity.

TABLES

Table 4.1. List of Antibodies

| Marker | Company | # Catalog | Species | Dilution | Application |
|-------------------|----------------|-------------|---------|----------|-------------|
| α -actinin | Sigma | A7811 | Mouse | 1:100 | IHC |
| c-Kit | R&D | AF1356 | Goat | 1:50 | IHC |
| c-Kit-PE-Vio 770 | Milteni biotec | 130-125-226 | Rat | 1:50 | Flow |
| CD45 | R&D | AF114 | Goat | 1:500 | WB |
| CD45-FITC | Invitrogen | 11-0451-82 | Rat | 1:100 | Flow |
| DDR2 | Invitrogen | PA5-27752 | Rabbit | 1:50 | IHC |
| DDR2 | Invitrogen | PA5-27752 | Rabbit | 1:200 | WB |
| c-Kit | R&D | AF1356 | Goat | 1:50 | WB |
| DDR2-APC | LS-bio | LS-C255959 | Rabbit | 1:100 | Flow |
| ERK1/2 | Cell signaling | 9107s | Mouse | 1:250 | WB |
| GAPDH | Sicgen | AB0067-200 | Goat | 1:3000 | WB |
| p53 | Abcam | ab131442 | Rabbit | 1:500 | WB |
| P-ERK1/2 | Cell signaling | 9101s | Rabbit | 1:500 | WB |
| Periostin | Invitrogen | PA5-34641 | Rabbit | 1:100 | Flow |

Table 4.1. List of Antibodies-Continued

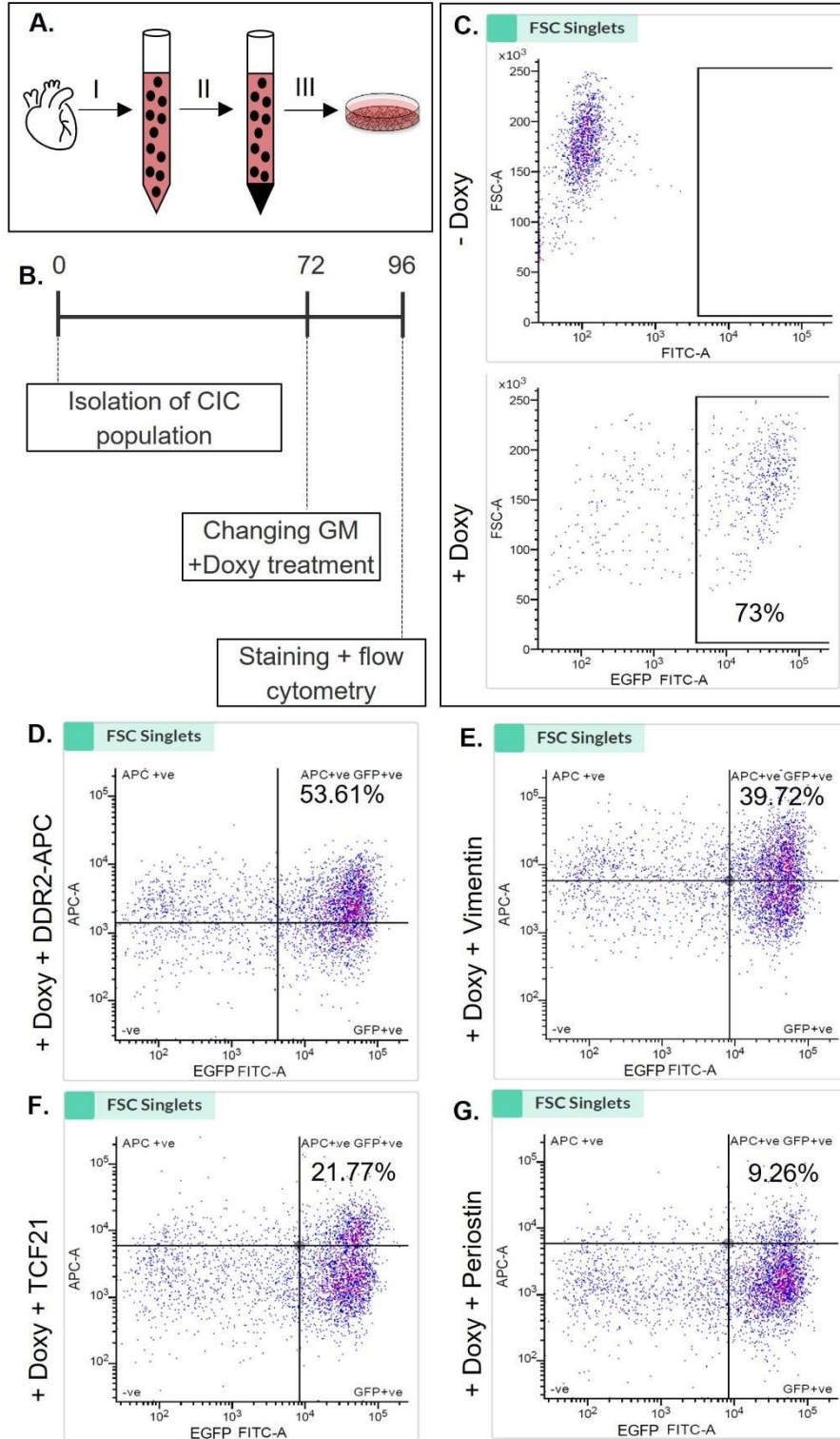
| Marker | Company | # Catalog | Species | Dilution | Application |
|----------------|-------------------|-----------|---------|----------|-------------|
| Pro-caspase 3 | Cell signaling | 9662s | Rabbit | 1:500 | WB |
| Phalloidin 488 | Life technologies | A12379 | N/A | 1:500 | ICC |
| TCF21 | Invitrogen | PA5-68595 | Rabbit | 1:100 | Flow |
| Vimentin | Invitrogen | PA1-10003 | Chicken | 1:100 | Flow |

Table 4.2. List of SASPs and Growth Factors

| SASPs | Growth Factors |
|-----------|----------------|
| IL6 | AREG |
| IL1B | EREG |
| MIF | NRG1 |
| NRG1 | EGF |
| FGF2 | FGF2 |
| HGF | HGF |
| FGF7 | FGF7 |
| VEGFA | VEGFA |
| ANG | ANG |
| CXCL12 | KITLG |
| IGFBP3 | CXCL12 |
| IGFBP4 | PIGF |
| IGFBP6 | NGF |
| IGFBP7 | IGFBP2 |
| MMP1 | IGFBP3 |
| TIMP2 | IGFBP4 |
| SERPINE1 | IGFBP6 |
| PLAT | IGFBP7 |
| CTSB | |
| ICAM1 | |
| ICAM3 | |
| TNFRSF11B | |
| TNFRSF1A | |
| FAS | |
| IL6ST | |
| EGFR | |

FIGURES

Figure 4.1. Transgenic cardiac fibroblasts express EGFP upon Doxy treatment in vitro. **A.** CIC isolation protocol: following enzymatic digestion of the heart (I), cardiomyocytes were separated (II) and total CICs were cultured for further analyses (III). **B.** CICs were cultured for 72 hours followed by Doxy treatment for 24 hours. Next, cells were collected, fixed and stained for GFP and fibroblasts markers. GM: growth medium. **C-G,** Flow cytometry plots showing expression of EGFP reporter and fibroblast markers in cultured CICs.



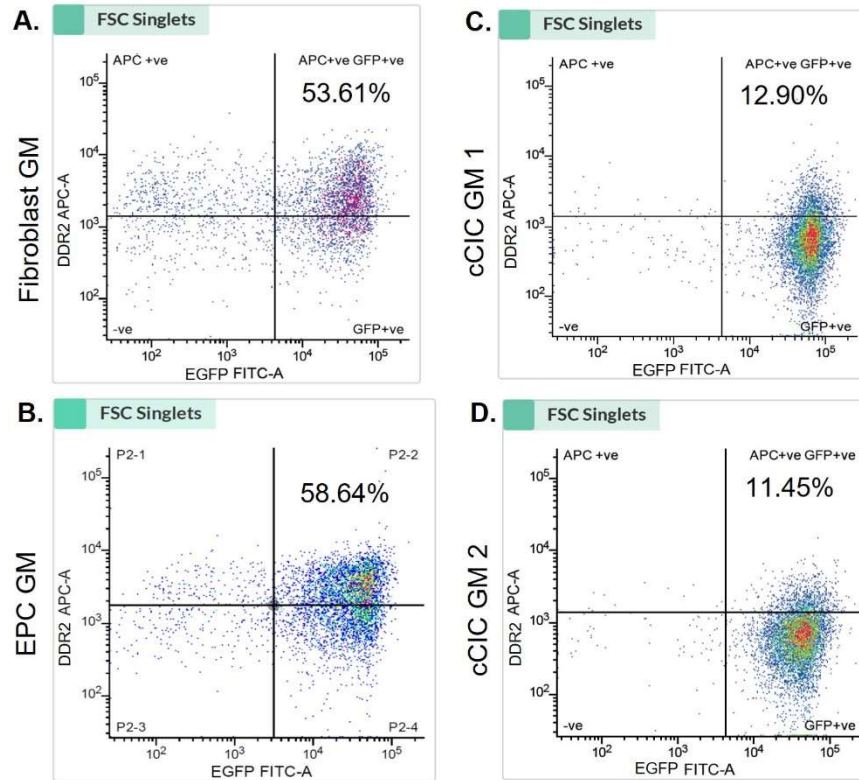


Figure 4.2. DDR2 expression and coincidence with EGFP adapt to culture media. A-D. Flow cytometry plots for DDR2 staining in fixed CICs cultured in fibroblast, EPC and two different cCIC growth media. GM: growth medium, EPC: Epithelial Progenitor Cells, cCICs: c-Kit⁺ Cardiac Interstitial Cells

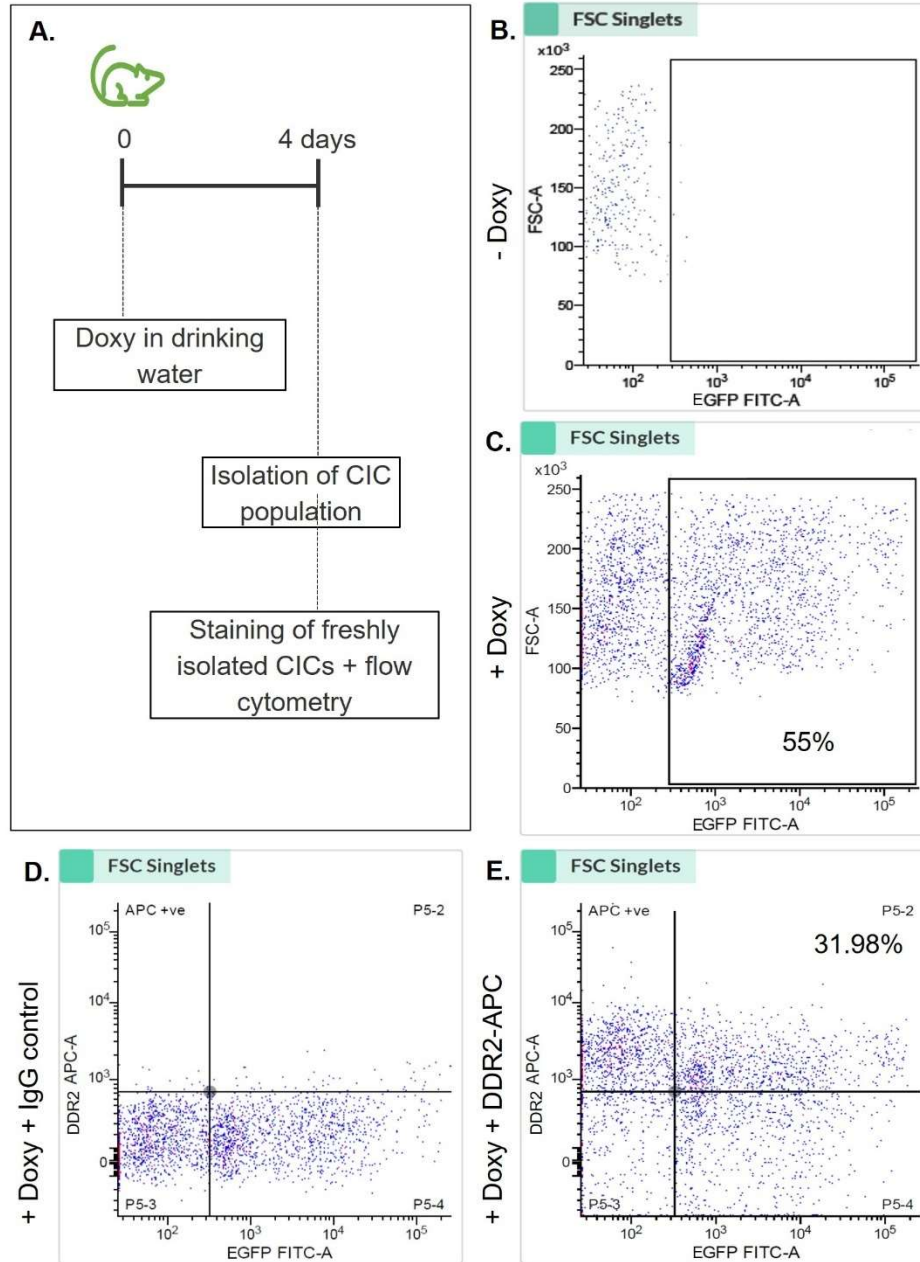


Figure 4.3. Transgenic cardiac fibroblasts express EGFP upon Doxy treatment *in vivo*. A. Transgenic mice imbibed Doxy for four days. Next, CICs were isolated, fixed, stained and analyzed via flow cytometry. B-E. Fellow cytometry plots showing expression of EGFP reporter and DDR2 in freshly isolated cells.

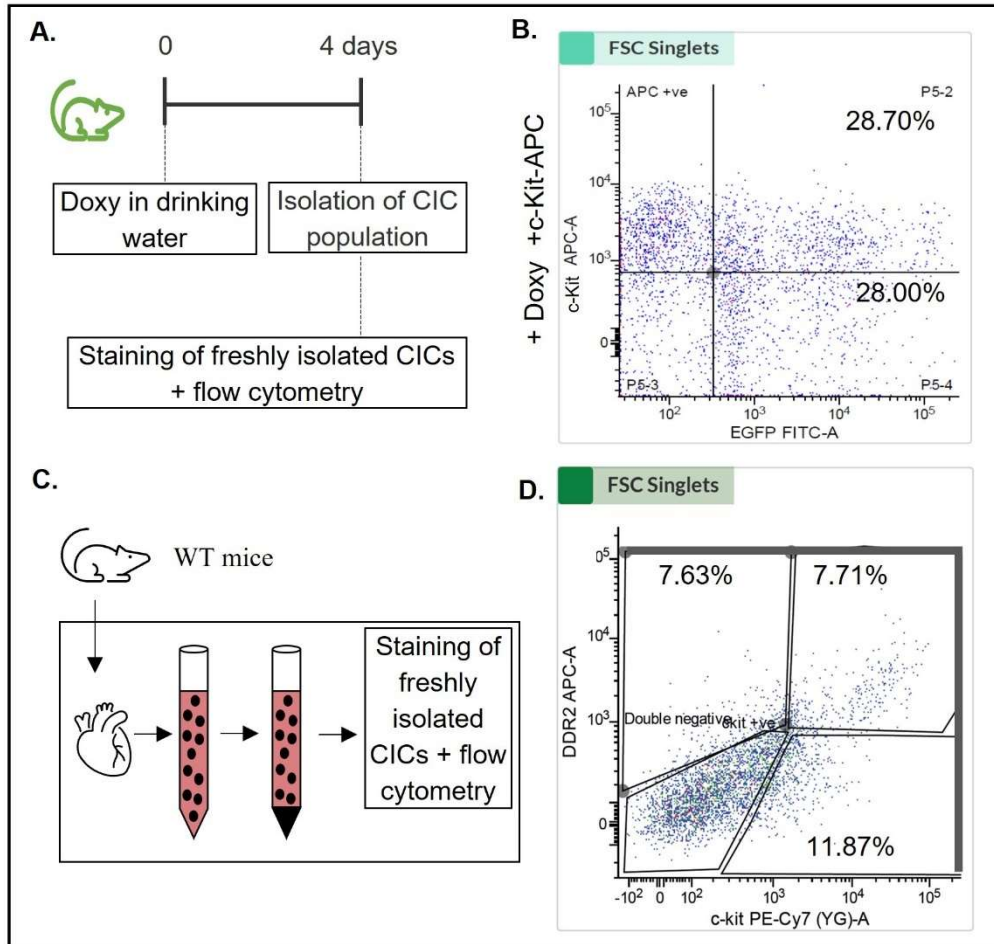


Figure 4.4. c-Kit protein colocalization with EGFP and DDR2. **A.** Transgenic mice imbibed Doxy for four days. Next, CICs were isolated, fixed, stained and analyzed via flow cytometry. **B.** Flow cytometry plot showing expression of EGFP reporter and c-Kit in freshly isolated cells. **C.** CICs isolated from WT murine hearts were stained for c-Kit and DDR2 and analyzed via flow cytometry. **D.** Flow cytometry plot showing expression of c-Kit and DDR2 in freshly isolated cells. WT: wildtype.

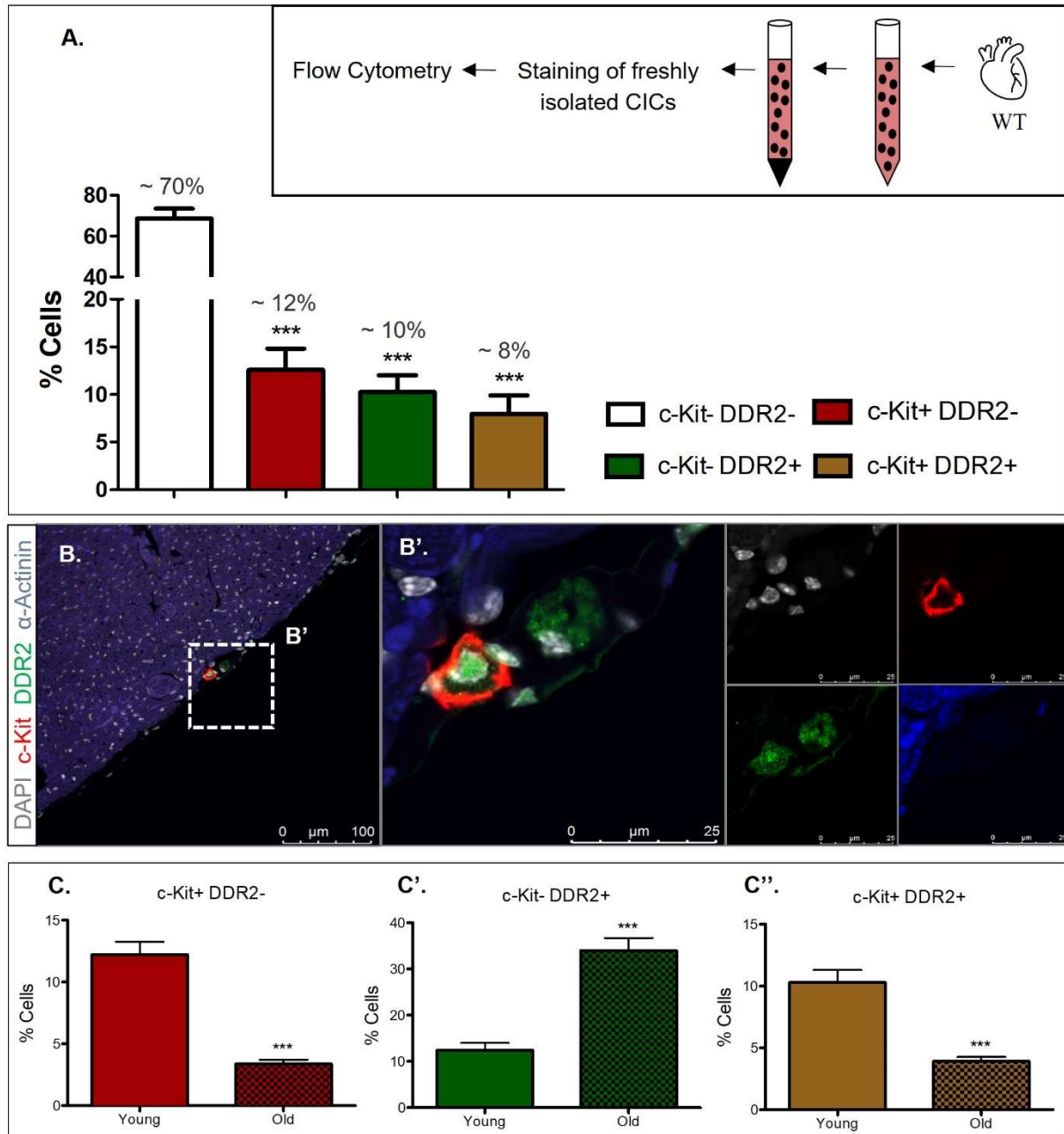


Figure 4.5. c-Kit protein is present in a subset of cardiac fibroblast population. **A.** CICs isolated from WT murine hearts were stained for c-Kit and DDR2 and analyzed via flow cytometry. Quantification shows percentage of cells expressing c-Kit and DDR2 in CICs from n of 7 independent isolations analyzed via flow cytometry. Error bars represent \pm SEM. *** $p < 0.001$ vs c-Kit⁻ DDR2⁻ as measured by one-way ANOVA followed by the Tukey post hoc test **B.** IHC for c-Kit (red) and DDR2 (green) on WT heart section. Right panels show higher magnification of a cell expressing both c-Kit and DDR2 shown within white dotted box (B'). DAPI (gray) was used to visualize nuclei. α -Actinin (blue) was used as the cardiac label. WT: Wild type. **C-C''** CICs isolated from young (1.5-month-old) and old (9-month-old) murine hearts were stained for c-Kit and DDR2 and analyzed via flow cytometry. Quantification represents n of 6 experimental replicates from 4 mice (2 per age). Error bars represent \pm SEM. *** $p < 0.001$

Figure 4.6. Expression as well as coincidence of c-Kit and DDR2 increase in response to myocardial infarction. A. IHC for c-Kit (red) and DDR2 (green) on uninjured WT heart sections. Right panels show higher magnification of a cell expressing both c-Kit and DDR2 shown within white dotted box (a'). WT: wildtype. **B.** IHC for c-Kit (red) and DDR2 (green) on 7-day post MI heart section. Right panels show higher magnification of a cluster of cells expressing both c-Kit and DDR2 shown within white dotted box (b'). MI: myocardial infarction. DAPI (gray) was used to visualize nuclei. α -Actinin (blue) was used as the cardiac label. **C-C''.** Quantification of c-Kit and DDR2 expression as well as colocalization presented as the percentage of area of each image. Dashed line represents sham group. Error bars represent \pm SEM. * $p < 0.05$ and *** $p < 0.001$ vs sham group as measured by one-way ANOVA followed by the Tukey post hoc test. **D-D''.** Immunoblot analysis showing expression of c-Kit and DDR2 in whole heart lysates from uninjured and 7-day post MI mice. GAPDH is the loading control. Dashed line represents uninjured group. Error bars represent \pm SEM. *** $p < 0.001$ vs uninjured as measured by Student t test.

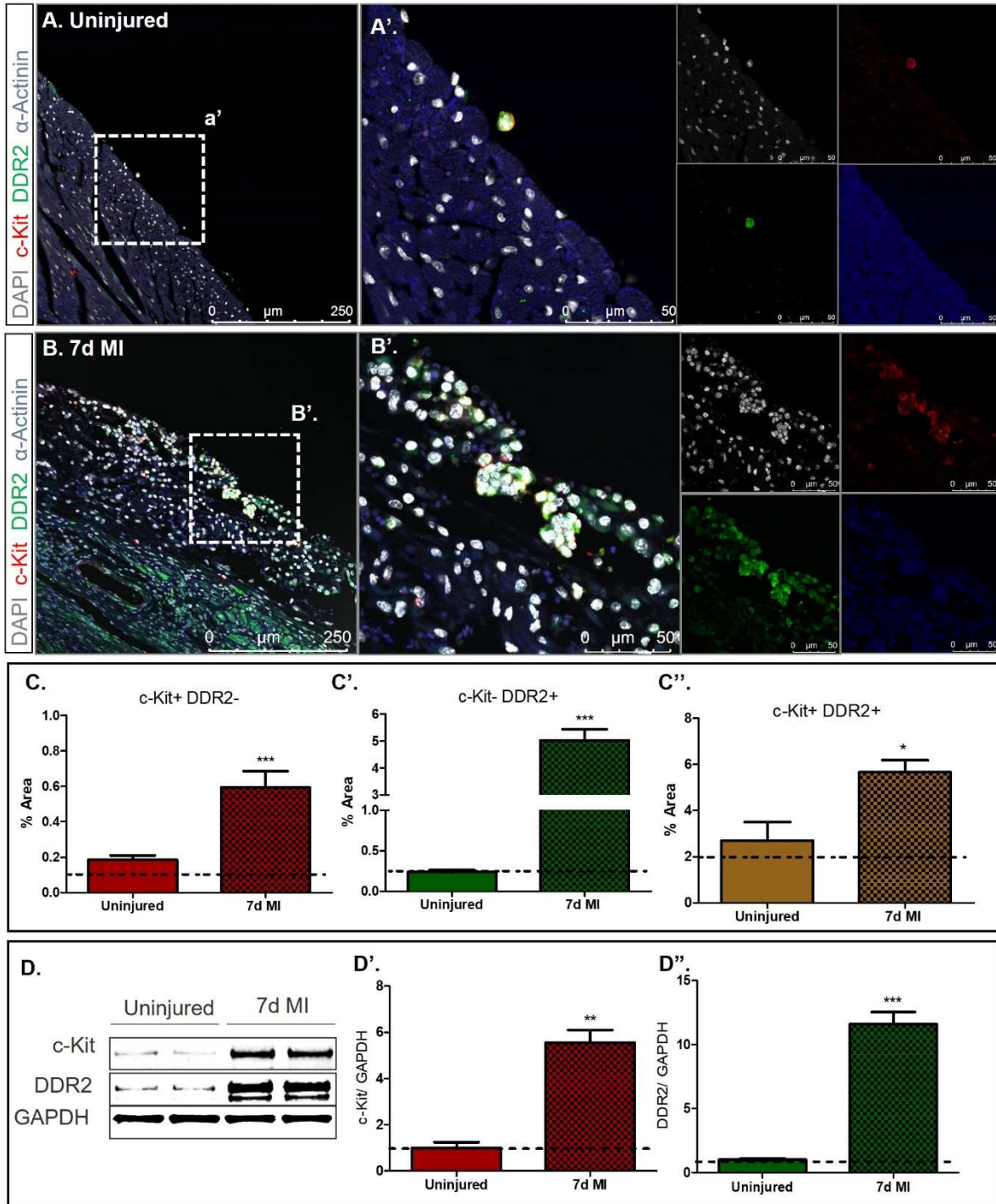
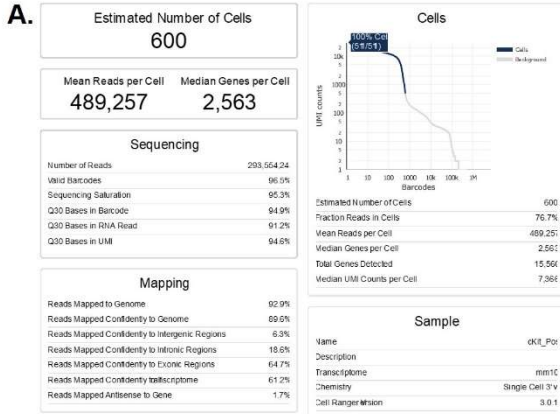
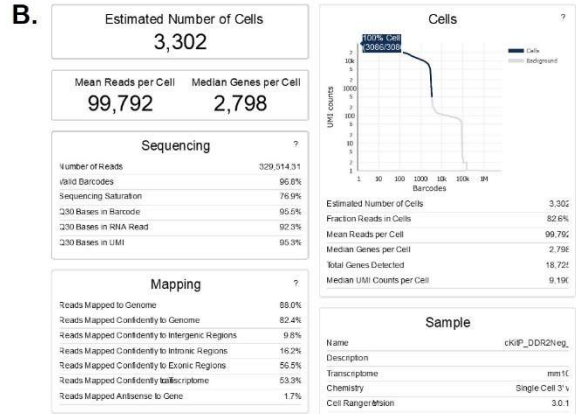


Figure 4.7. Quality control for scRNA-seq experiment. A-E. CellRanger 3.0.1 quality control summary for c-Kit+ DDR2-, c-Kit- DDR2+, CND c-Kit+ DDR2+ and c-Kit+ DDR2+ CD45-. **F.** CellRanger 3.0.1 Library aggregation summary. CND: CD45-non-depleted.

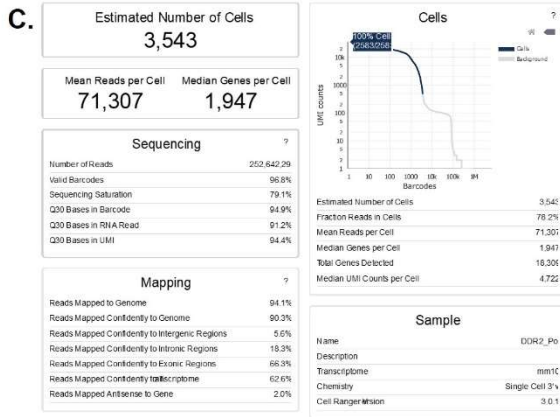
c-Kit+ DDR2-



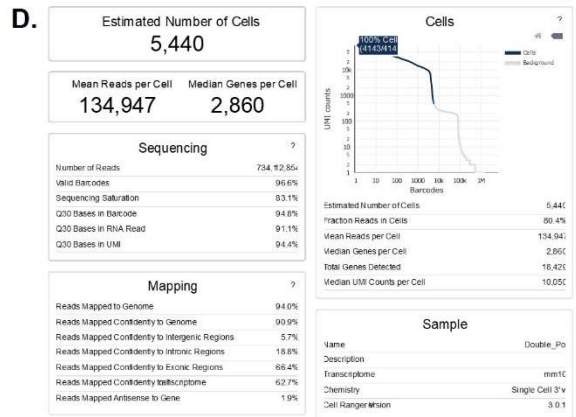
c-Kit+ DDR2-



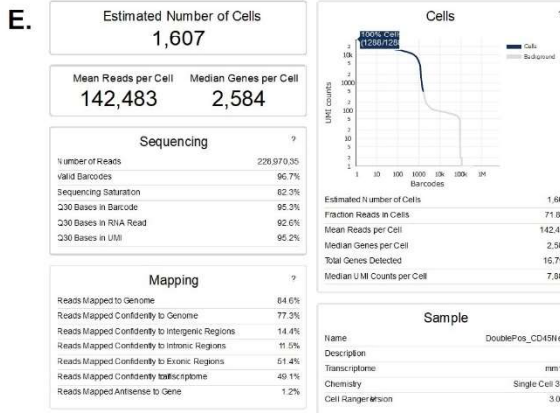
c-Kit- DDR2+



CND c-Kit+ DDR2+



c-Kit+ DDR2+ CD45-



c-Kit- DDR2- CD45- Aggr



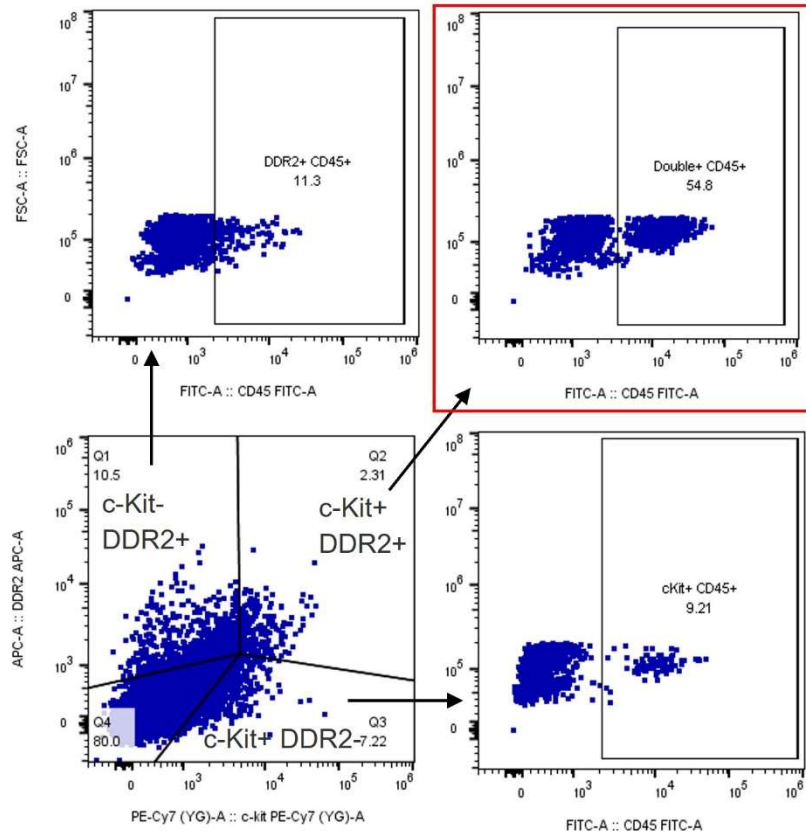


Figure 4.8. CD45 expression in freshly isolated CICs. Fellow cytometry plots depicting CD45 expression in freshly isolated CICs of c-Kit+ DDR2-, c-Kit- DDR2+ and c-Kit+ DDR2+ populations.

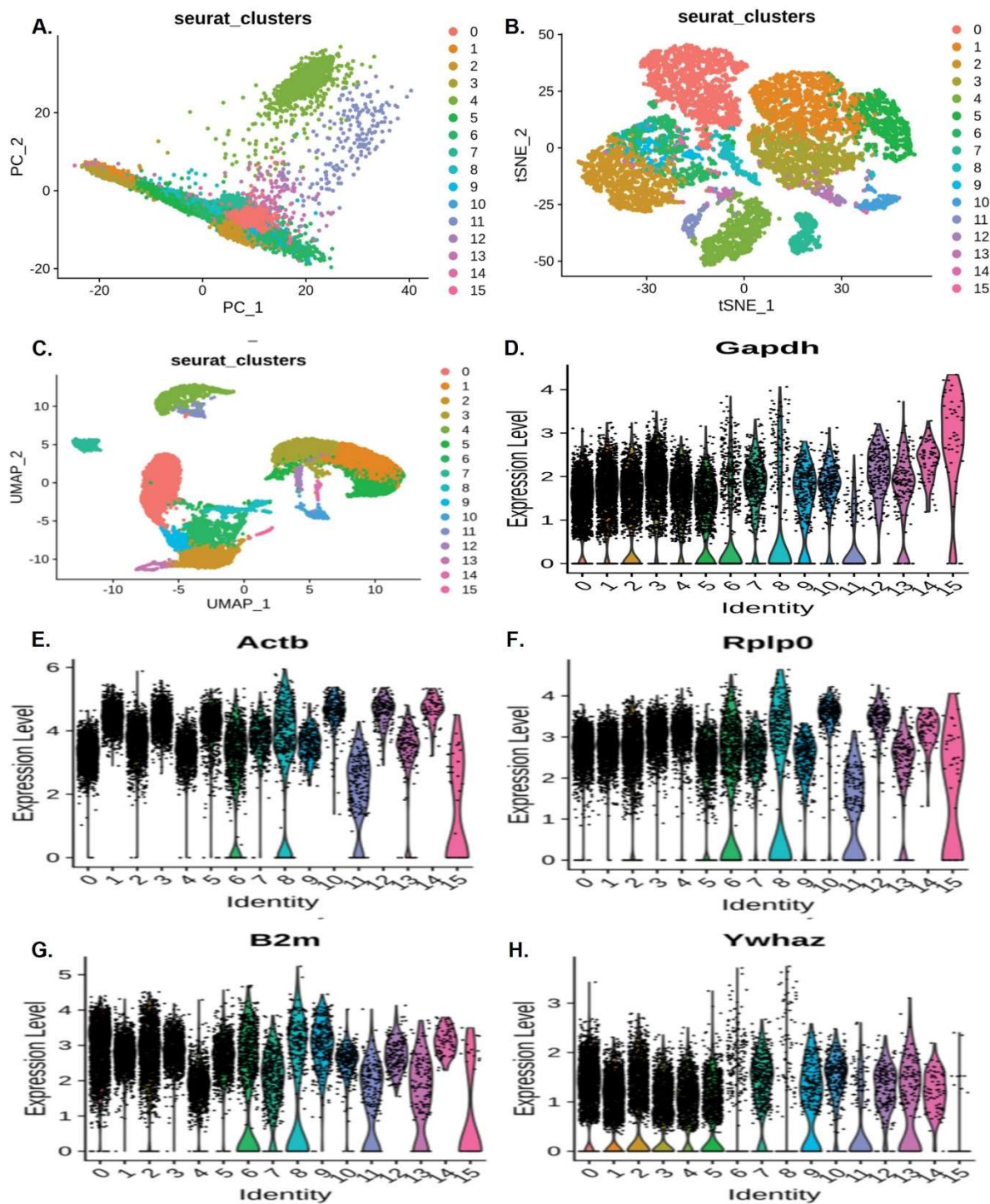


Figure 4.9. Unsupervised clustering reveals 16 clusters. A-C. Dimensionality reduction projections of single cell data color coded by detected unsupervised clusters: Principal component analysis (PCA; Top panel), t-Distributed Stochastic Neighbor Embedding (t-SNE; middle panel) and Uniform Manifold Approximation and Projection (UMAP; Bottom panel). D-H. Violin plots indicating expression of *Gapdh*, *Actb*, *Rplp0*, *B2m* and *Ywhaz*.

Figure 4.10. c-Kit⁺ cardiac fibroblasts are transitional in the transcriptional trajectory. **A.** UMAP projection of cardiac interstitial c-Kit⁺ DDR2⁻, c-Kit⁻ DDR2⁺, CND c-Kit⁺ DDR2⁺ or c-Kit⁺ DDR2⁺ CD45⁻ cells color-coded according to unsupervised clustering of gene signatures. **B.** Cell contributions of each population normalized to input of each clusters as shown in UMAP. **C.** Dimensionality reduction projections of single cell data color-coded by population of origin. **D.** Heatmap representing the differential expressed genes from each isolated population (DEGs in parenthesis). **E.** GO terms results from Gene Ontology analysis annotated by Biological Process. Circle diameter represents the gene ratio, while significance level is color-coded according to heatmap scale. **F-H.** Monocle generated UMAP projection of cells color-coded according to cluster (F), population of origin (G) and calculated pseudotime units (H). Pseudotime transcriptional trajectory visualized by line across UMAP projection. Origin indicated by white number one circle. Nodes annotated in black circles and leaves numbered in gray.

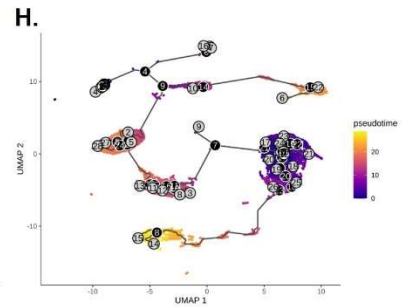
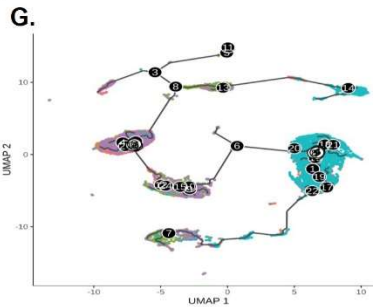
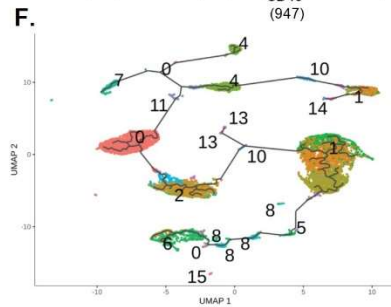
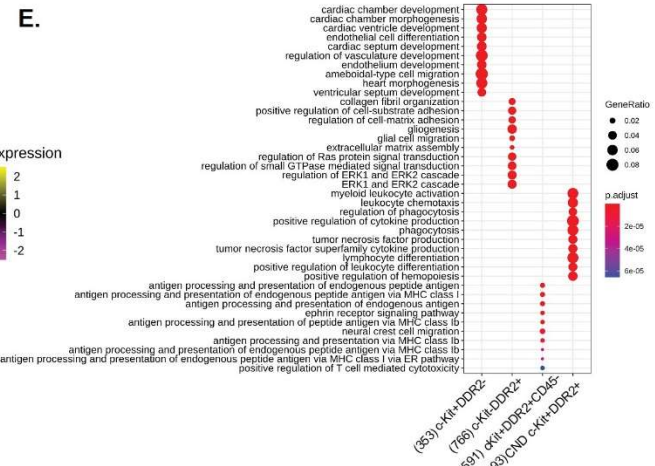
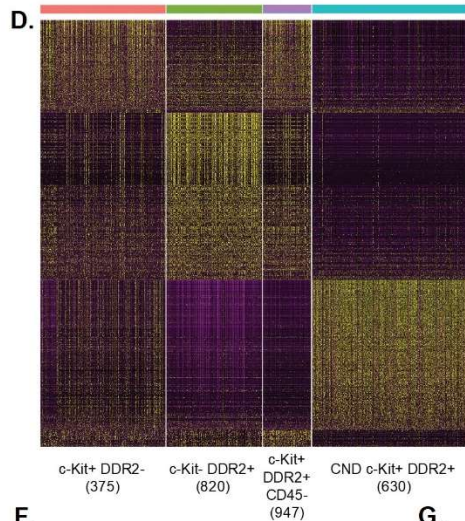
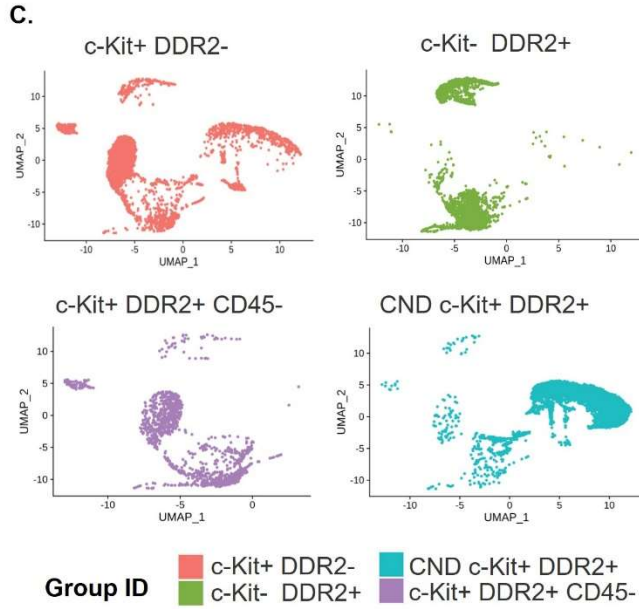
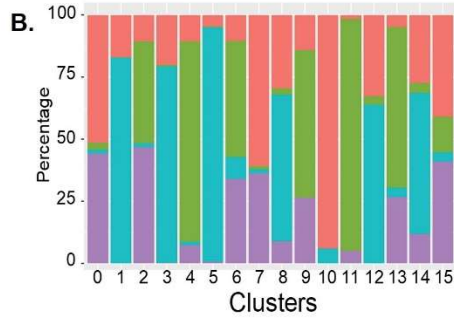
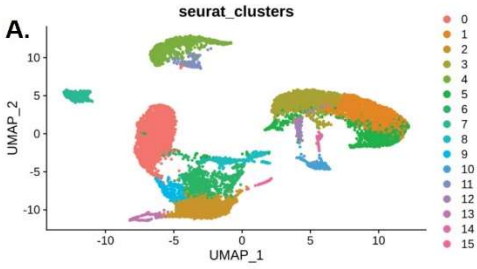
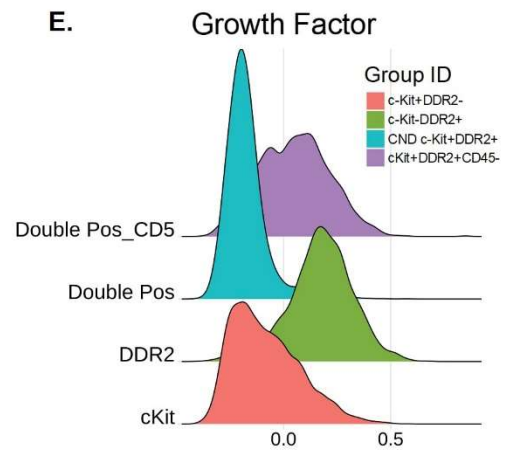
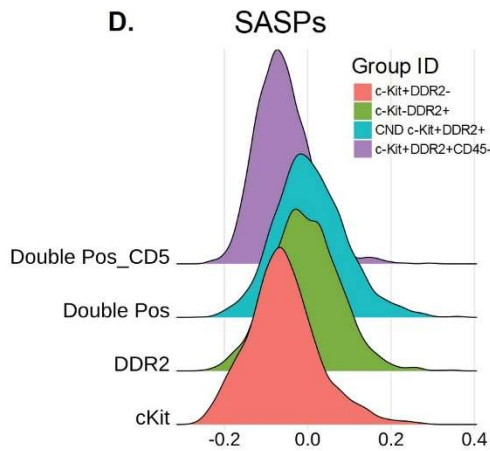
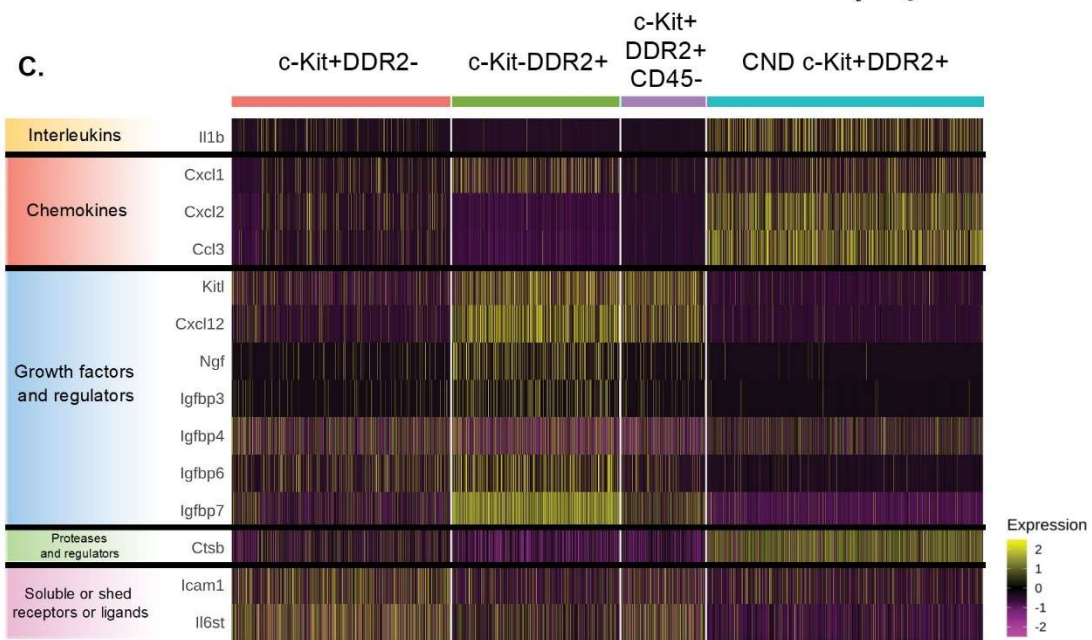
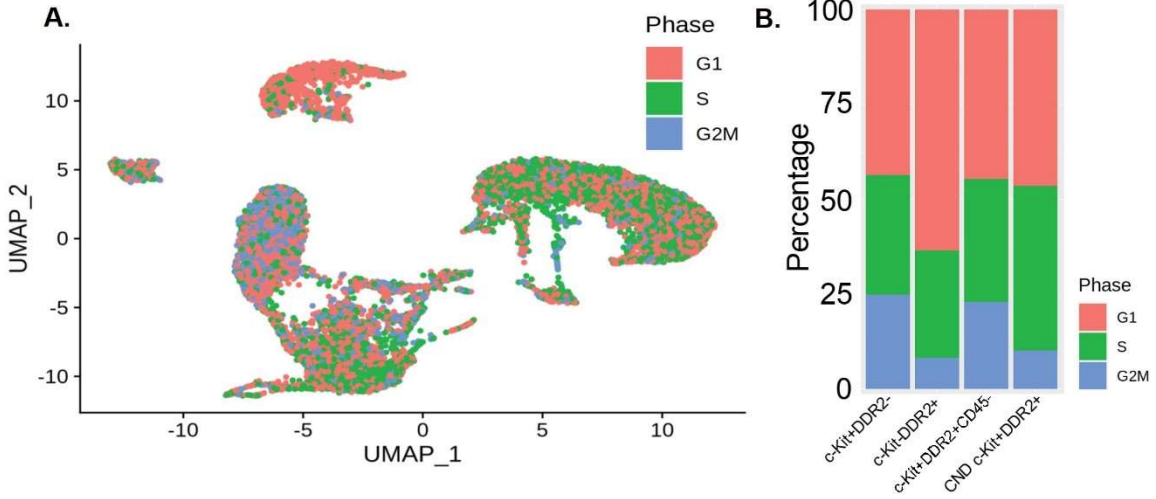


Figure 4.11. c-Kit⁺ cardiac fibroblasts are transcriptionally associated with higher cell cycle progression and lower SASP. **A.** UMAP projection of cells color-coded by transcriptional cell cycle score. **B.** Stacked bar graph representing ratio of cells in G2M, G1 and S stages according to cell cycle score and population of origin. **C.** Heatmap representing expression of SASP genes in all populations. **D-E.** Ridge plots representing cell distribution of all populations and their respective calculated module scores for Senescent Associated Secretory Phenotype factors (SASPs) and growth factors.



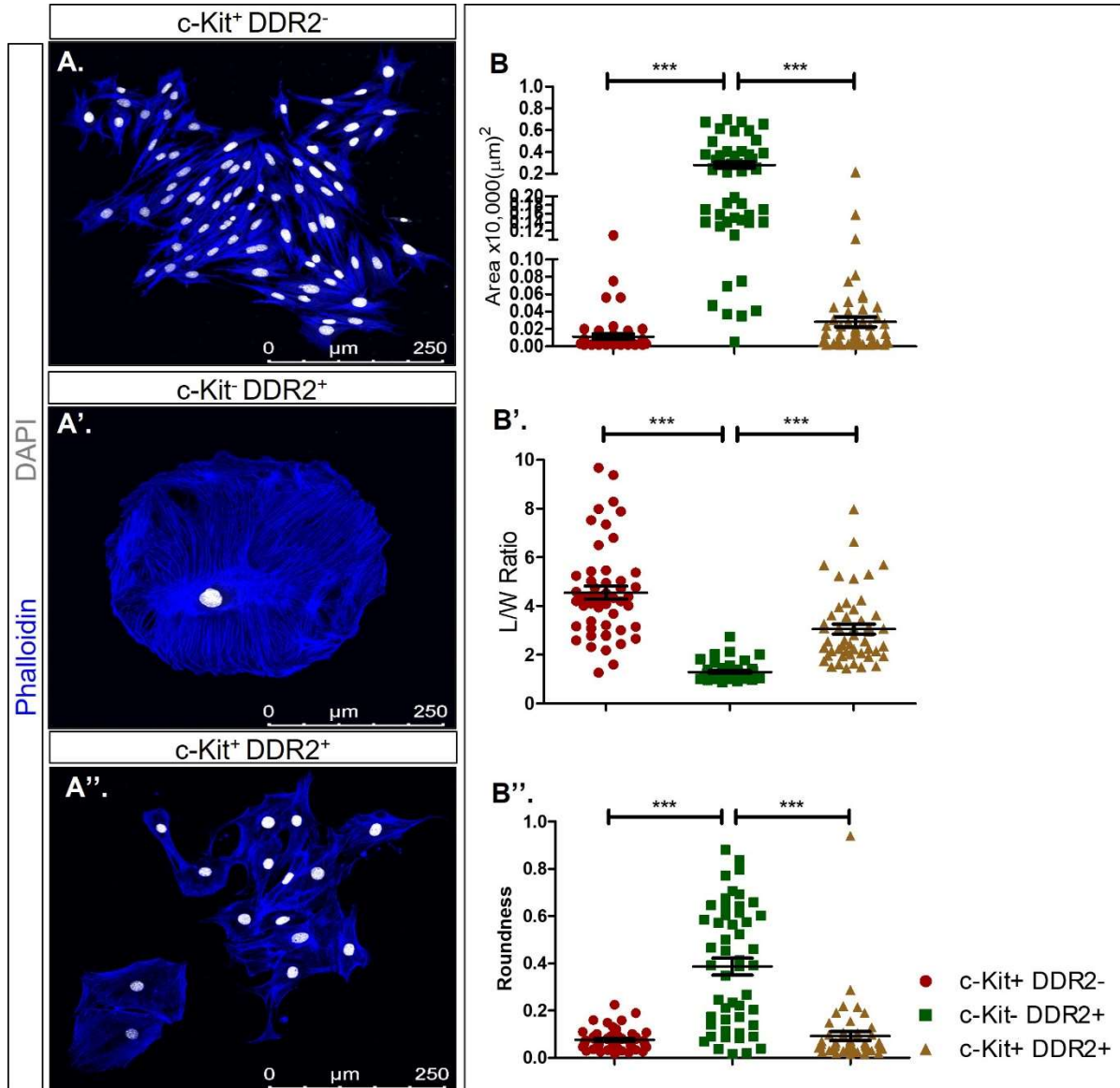


Figure 4.13. c-Kit expressing cardiac fibroblasts exhibit lower level of cellular senescence. **A-A''**. Representative images of phalloidin staining for p3 c-Kit⁺ DDR2⁻, c-Kit⁻ DDR2⁺ and c-Kit⁺ DDR2⁺ CICs with quantification of mononucleated (solid) and binucleated (shaded) cells shown below. Numbers represent percentage of binucleated cells in each group. Error bars represent \pm SEM. *** $p < 0.001$ as measured by one-way ANOVA followed by the Tukey post hoc test. DAPI (gray) was used to visualize nuclei. Green arrows show binucleated cells. **B-B''**. Representative images of SA- β -Gal staining for p3 c-Kit⁺ DDR2⁻, c-Kit⁻ DDR2⁺ and c-Kit⁺ DDR2⁺ CICs with quantification of cells negative (solid) and positive (shaded) for SA- β -Gal shown on top. Numbers represent percentage of SA- β -Gal⁺ cells in each group. Error bars represent \pm SEM. *** $p < 0.001$ and ** $p < 0.01$ as measured by one-way ANOVA followed by the Tukey post hoc test. Dashed line delineates boundary of a SA- β -Gal⁺ cell. **C-C'**. Immunoblot analysis showing expression of p53 in cell culture lysates from p3 c-Kit⁺ DDR2⁻, c-Kit⁻ DDR2⁺ and c-Kit⁺ DDR2⁺ CICs with quantification on the right. GAPDH is the loading control. Dashed line represents c-Kit⁺ DDR2⁻. Error bars represent \pm SEM. * $p < 0.05$ as measured by one-way ANOVA followed by the Tukey post hoc test. P3: passage 3.

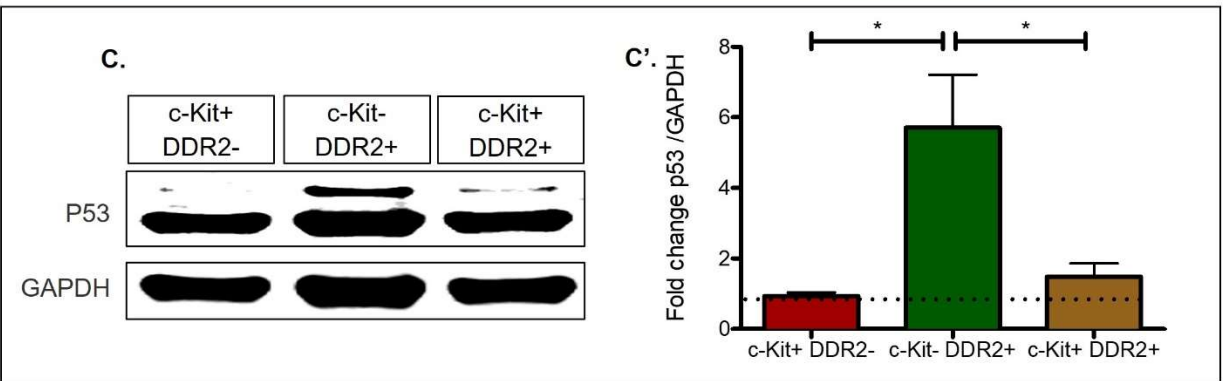
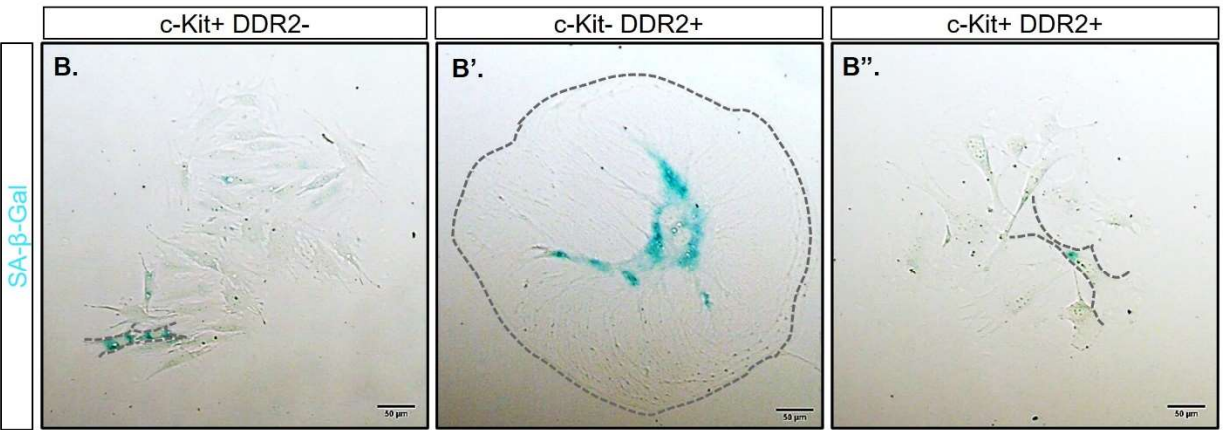
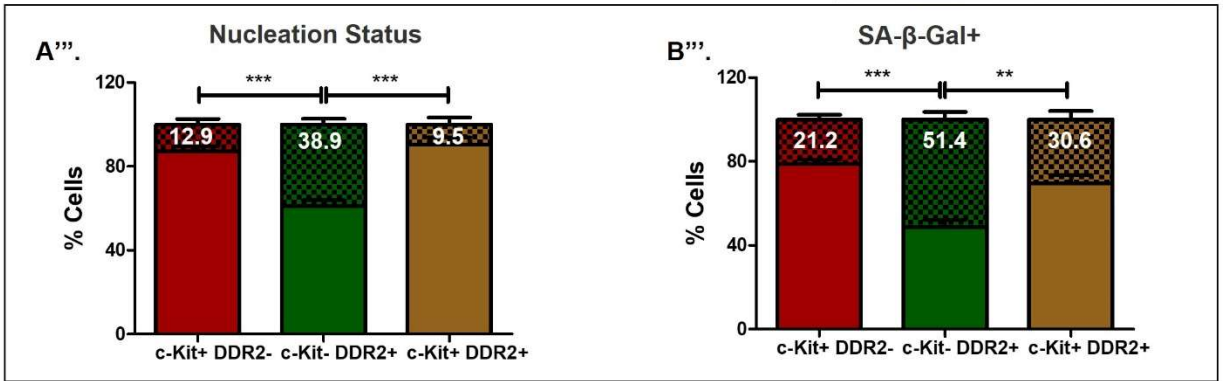
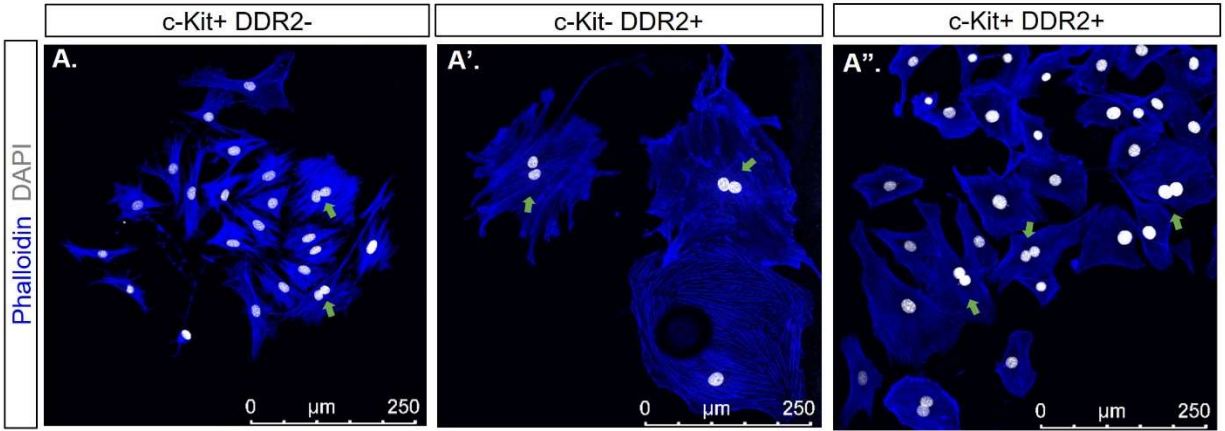
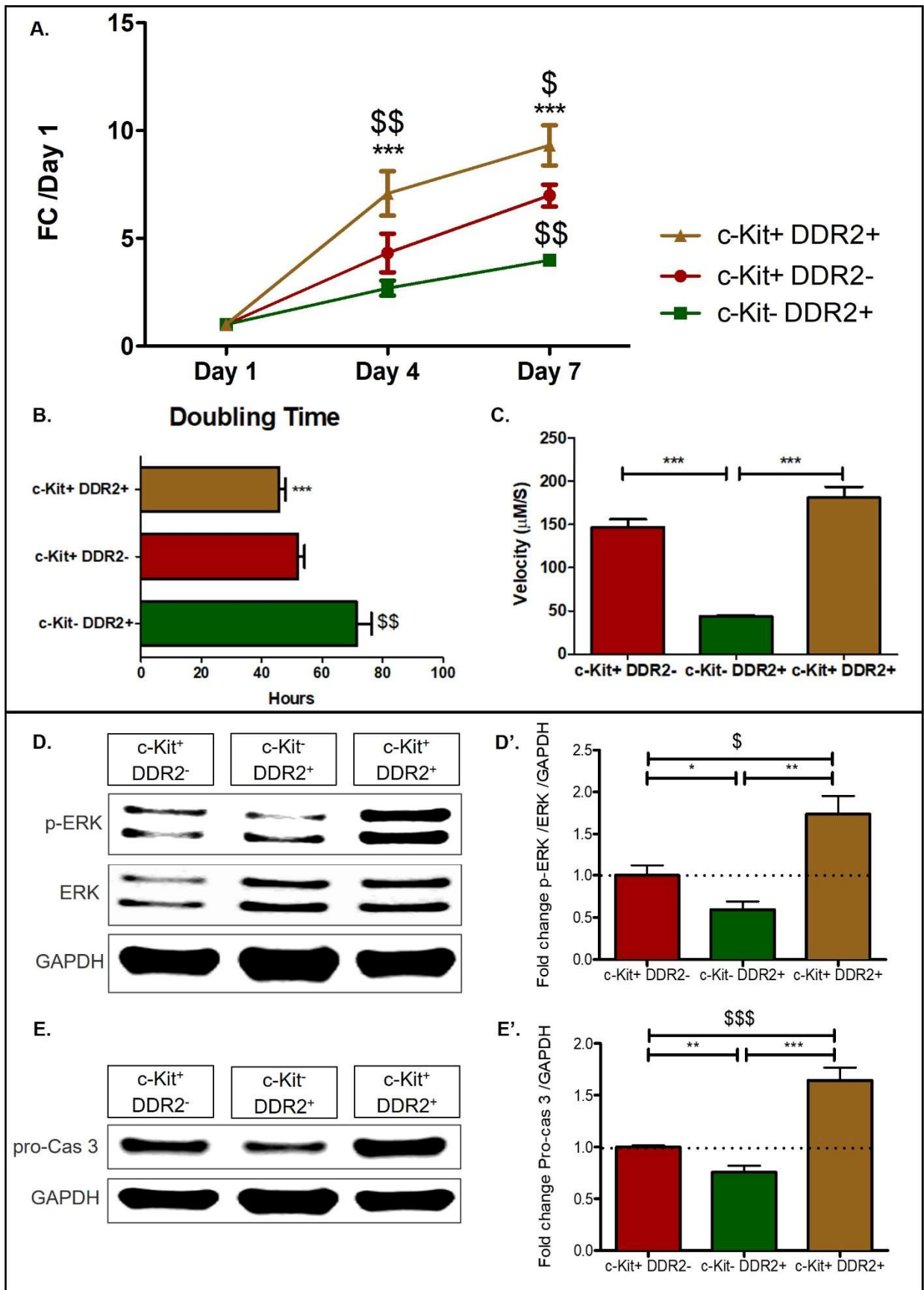


Figure 4.14. Self-renewal and cellular motility are enhanced in c-Kit expressing cardiac fibroblasts. **A.** Proliferation rate of p3 c-Kit⁺ DDR2⁻, c-Kit⁻ DDR2⁺ and c-Kit⁺ DDR2⁺ CICs represented as fold change over day 1. Error bars represent \pm SEM. \$ p < 0.05 and \$\$ p < 0.01 vs c-Kit⁺ DDR2⁻, *** p < 0.001 vs c-Kit⁻ DDR2⁺ as measured by two-way ANOVA followed by the Bonferroni post hoc test. **B.** cell doubling time represented in hours. Error bars represent \pm SEM. \$\$ p < 0.01 vs c-Kit⁺ DDR2⁻, *** p < 0.001 vs c-Kit⁻ DDR2⁺ as measured by one-way ANOVA followed by the Tukey post hoc test. **C.** Measurement of cell motility for n of 4 cells from p3 c-Kit⁺ DDR2⁻, c-Kit⁻ DDR2⁺ and c-Kit⁺ DDR2⁺ CICs. Error bars represent \pm SEM. *** p < 0.001 as measured by one-way ANOVA followed by the Tukey post hoc test. **D-D'.** Immunoblot analysis showing expression of p-ERK and ERK in cell culture lysates from p3 c-Kit⁺ DDR2⁻, c-Kit⁻ DDR2⁺ and c-Kit⁺ DDR2⁺ CICs with quantification on the right. **E-E'.** Immunoblot analysis showing expression of pro-Cas-3 in cell culture lysates from p3 c-Kit⁺ DDR2⁻, c-Kit⁻ DDR2⁺ and c-Kit⁺ DDR2⁺ CICs with quantification on the right. Error bars represent \pm SEM. Dashed line represents c-Kit⁺ DDR2⁻. \$ p < 0.05 and \$\$\$ p < 0.0001 vs c-Kit⁺ DDR2⁻, * p < 0.05, ** p < 0.01 and *** p < 0.001 vs c-Kit⁻ DDR2⁺ as measured by one-way ANOVA followed by the Tukey post hoc test. P3: passage 3.



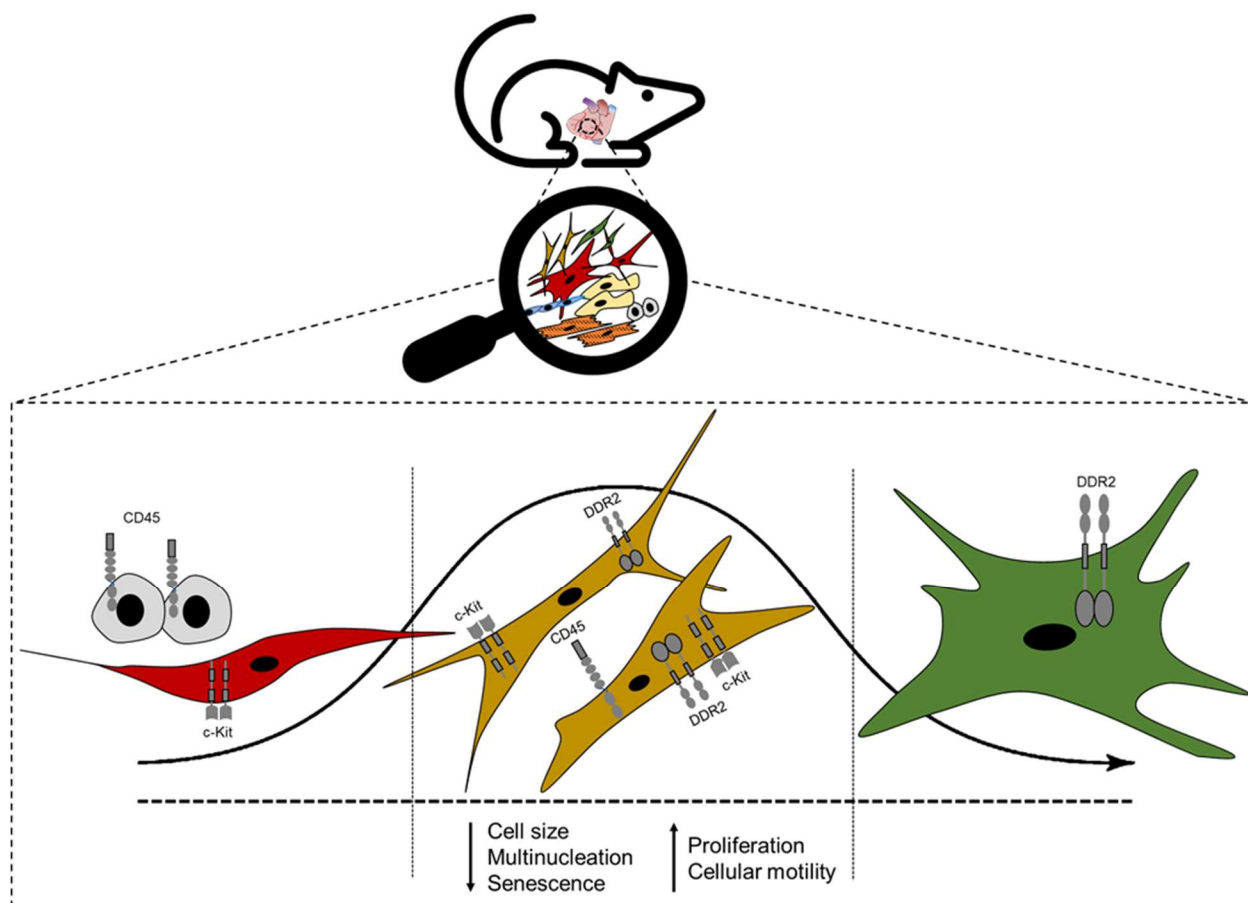


Figure 4.15. c-Kit protein is present in a subset of CFs. A fraction of c-Kit expressing DDR2⁺ cells also express CD45. Regardless of CD45 expression, c-Kit expressing DDR2⁺ CFs exhibit a transcriptionally transitional phenotype and progress toward DDR2⁺ CFs. In vitro characterization confirmed CFs with c-Kit expression are morphologically and functionally distinct revealing a youthful and pre-committed phenotype.

REFERENCES

1. Banerjee I, Fuseler JW, Price L, Borg TK, Baudino TA. Determination of cell types and numbers during cardiac development in the neonatal and adult rat and mouse. *Am J Physiol Heart Circ Physiol*. 2007;293:H1883–H1891.
2. Porter KE, Turner NA. Cardiac fibroblasts: At the heart of myocardial remodeling. *Pharmacol Ther*. 2009;123:255–278.
3. Deb, A. & Ubil E. Cardiac fibroblast in development and wound healing. *J Mol Cell Cardiol*. 2014;70:47–55.
4. Krenning G, Zeisberg EM, Kalluri R. The Origin of Fibroblasts and Mechanism of Cardiac Fibrosis. *J Cell Physiol*. 2010;225:631–637.
5. Plikus MV, Wang X, Sinha S, Forte E, Thompson SM, Herzog EL, Driskell RR, Rosenthal N, Biernaskie J, Horsley V. Fibroblasts: Origins, definitions, and functions in health and disease. *Cell*. 2021;184:3852–3872.
6. Morrison-Graham K, Takahashi Y. Steel factor and c-kit receptor: from mutants to a growth factor system. *Bioessays*. 1993;15:77–83.
7. Rönstrand L. Signal transduction via the stem cell factor receptor/c-Kit. *Cell Mol Life Sci*. 2004;61:2535–2548.
8. Lennartsson J, Rönstrand L. Stem Cell Factor Receptor/c-Kit: From Basic Science to Clinical Implications. *Physiol Rev*. 2012;92:1619–1649.
9. Gambini E, Pompilio G, Biondi A, Alamanni F, Capogrossi MC, Agrifoglio M, Pesce M. C-kit⁺ cardiac progenitors exhibit mesenchymal markers and preferential cardiovascular commitment. *Cardiovasc Res*. 2011;89:362–373.
10. Liu Q, Yang R, Huang X, Zhang H, He L, Zhang L, Tian X, Nie Y, Hu S, Yan Y, Zhang L, Qiao Z, Wang QD, Lui KO ZB. Genetic lineage tracing identifies in situ Kit-expressing cardiomyocytes. *Cell Res*. 2016;26:119–130.
11. Sultana N, Zhang L, Yan J, Chen J, Cai W, Razzaque S, Jeong D, Sheng W, Bu L, Xu M, Huang GY, Hajjar RJ, Zhou B, Moon A, Cai CL. Resident c-kit(+) cells in the heart are not cardiac stem cells. *Nat Commun*. 2015;6:1–10.
12. Gude NA, Firouzi F, Broughton KM, Ilves K, Nguyen KP, Payne CR, Sacchi V, Monsanto MM, Casillas AR, Khalafalla FG, Wang BJ, Ebeid DE, Alvarez R, Dembitsky WP, Bailey BA, van Berlo J, Sussman MA. Cardiac c-Kit Biology Revealed by Inducible Transgenesis. *Circ Res*. 2018;123:57–72.
13. Martinez-Anton A, Gras D, Bourdin A, Dubreuil P, Chanez P. KIT as a therapeutic target for non-oncological diseases. *Pharmacol Ther*. 2019;197:11–37.

14. Di Siena S, Gimmelli R, Nori SL, Barbagallo F, Campolo F, Dolci S, Rossi P, Venneri MA, Giannetta E, Gianfrilli D, Feigenbaum L, Lenzi A, Naro F, Cianflone E, Mancuso T, Torella D, Isidori AM, Pellegrini M. Activated c-Kit receptor in the heart promotes cardiac repair and regeneration after injury. *Cell Death Dis.* 2016;7:e2317–e2317.
15. Zani BC, Sanches BDA, Maldarine JS, Biancardi MF, Santos FCA, Barquilha CN, Zucão MI, Baraldi CMB, Felisbino SL, Góes RM, Vilamaior PSL, Taboga SR. Telocytes role during the postnatal development of the Mongolian gerbil jejunum. *Exp Mol Pathol.* 2018;105:130–138.
16. Ding L, Dolgachev V, Wu Z, Liu T, Nakashima T, Wu Z, Ullenbruch M, Lukacs NW, Chen Z, Phan SH. Essential role of stem cell factor-c-Kit signalling pathway in bleomycin-induced pulmonary fibrosis. *J Pathol.* 2013;230:205–214.
17. Guo Z, Li H, Chang Y, Guo K, Li Q, Li C. Multiple Directional Differentiation Difference of Neonatal Rat Fibroblasts from Six Organs. *Cell Physiol Biochem.* 2016;39:157–171.
18. Ni Z, Deng J, Potter CMF, Nowak WN, Gu W, Zhang Z, Chen T, Chen Q, Hu Y, Zhou B, Xu Q, Zhang L. Recipient c-Kit Lineage Cells Repopulate Smooth Muscle Cells of Transplant Arteriosclerosis in Mouse Models. *Circ Res.* 2019;125:223–241.
19. Caruana G, Cambareri AC, Gonda TJ AL. Transformation of NIH3T3 fibroblasts by the c-Kit receptor tyrosine kinase: effect of receptor density and ligand-requirement. *Oncogene.* 1998;16:179–190.
20. Firouzi F, Sinha Choudhury S, Broughton K, Salazar A, Bailey B, Sussman MA. Human CardioChimeras: Creation of a Novel “Next-Generation” Cardiac Cell. *J Am Heart Assoc.* 2020;9:e013452.
21. Konstandin MH, Toko H, Gastelum GM, Quijada P, Torre AD La, Quintana M, Collins B, Din S, Avitabile D, Völkers M, Gude N, Fässler R, Sussman MA. Fibronectin Is Essential for Reparative Cardiac Progenitor Cell Response After Myocardial Infarction. *Circ Res.* 2013;113:115–125.
22. Ebeid DE, Firouzi F, Esquer CY, Navarrete JM, Wang BJ, Gude NA, Sussman MA. PIM1 Promotes Survival of Cardiomyocytes by Upregulating c-Kit Protein Expression. *Cells.* 2020;9:2001–2015.
23. Fransioli J, Bailey B, Gude NA, Cottage CT, Muraski JA, Emmanuel G, Wu W, Alvarez R, Rubio M, Ottolenghi S, Schaefer E, Sussman MA. Evolution of the c-kit-positive cell response to pathological challenge in the myocardium. *Stem Cells.* 2008;26:1315–1324.
24. Kim T, Echeagaray OH, Wang BJ, Casillas A, Broughton KM, Kim BH, Sussman MA. In situ transcriptome characteristics are lost following culture adaptation of adult cardiac stem cells. *Sci Rep.* 2018;8:1–9.

25. Camelliti P, Borg TK, Kohl P. Structural and functional characterisation of cardiac fibroblasts. *Cardiovasc Res*. 2005;65:40–51.
26. Gao E, Lei YH, Shang X, Huang ZM, Zuo L, Boucher M, Fan Q, Chuprun JK, Ma XL, Koch WJ. A novel and efficient model of coronary artery ligation and myocardial infarction in the mouse. *Circ Res*. 2010;107:1445–1453.
27. Macosko EZ, Basu A, Satija R, Nemesh J, Shekhar K, Goldman M, Tirosh I, Bialas AR, Kamitaki N, Martersteck EM, Trombetta JJ, Weitz DA, Sanes JR, Shalek AK, Regev A, McCarroll SA. Highly Parallel Genome-wide Expression Profiling of Individual Cells Using Nanoliter Droplets. *Cell*. 2015;161:1202–1214.
28. Yu G, Wang LG, Han Y HQ. clusterProfiler: an R package for comparing biological themes among gene clusters. *OMICS*. 2012;16:284–287.
29. Trapnell C, Cacchiarelli D, Grimsby J, Pokharel P, Li S, Morse M, Lennon NJ, Livak KJ, Mikkelsen TS, Rinn JL. The dynamics and regulators of cell fate decisions are revealed by pseudotemporal ordering of single cells. *Nat Biotechnol*. 2014;32:381–386.
30. Tirosh I, Izar B, Prakadan SM, Wadsworth MH 2nd, Treacy D, Trombetta JJ, Rotem A, Rodman C, Lian C, Murphy G, Fallahi-Sichani M, Dutton-Regester K, Lin JR, Cohen O, Shah P, Lu D, Genshaft AS, Hughes TK, Ziegler CG, Kazer SW, Gaillard A, Kolb KE, Villani A. Dissecting the multicellular ecosystem of metastatic melanoma by single-cell RNA-seq. *Science*. 2016;352:189–196.
31. Acharya A, Baek ST, Huang G, Eskiocak B, Goetsch S, Sung CY, Banfi S, Sauer MF, Olsen GS, Duffield JS, Olson EN, Tallquist MD. The bHLH transcription factor Tcf21 is required for lineage-specific EMT of cardiac fibroblast progenitors. *Development*. 2012;139:2139–2149.
32. Conway SJ, Izuhara K, Kudo Y, Litvin J, Markwald R, Ouyang G, Arron JR, Holweg CTJ, Kudo A. The role of periostin in tissue remodeling across health and disease. *Cell Mol Life Sci*. 2014;71:1279–1288.
33. Keith MC, Bolli R. “String theory” of c-kit(pos) cardiac cells: a new paradigm regarding the nature of these cells that may reconcile apparently discrepant results. *Circ Res*. 2015;116:1216–1230.
34. Vajravelu BN, Hong KU, Al-Maqtari T, Cao P, Keith MC, Wysoczynski M, Zhao J, Moore JB, Bolli R. C-Kit Promotes Growth and Migration of Human Cardiac Progenitor Cells via the PI3K-AKT and MEK-ERK Pathways. *PLoS One*. 2015;10:e0140798.
35. Ishii G, Sangai T, Sugiyama K, Ito T, Hasebe T, Endoh Y, Magae J, Ochiai A. In vivo characterization of bone marrow-derived fibroblasts recruited into fibrotic lesions. *Stem Cells*. 2005;23:699–706.
36. McDonald LT, Mehrotra M LA. Hematopoietic Origin of Murine Lung Fibroblasts. *Stem Cells Int*. 2015;2015:159713–159725.

37. Ali SR, Ranjbarvaziri S, Talkhabi M, Zhao P, Subat A, Hojjat A, Kamran P, Müller AM, Volz KS, Tang Z, Red-Horse K, Ardehali R. Developmental heterogeneity of cardiac fibroblasts does not predict pathological proliferation and activation. *Circ Res*. 2014;115:625–635.
38. Kisanuki YY, Hammer RE, Miyazaki J, Williams SC, Richardson JA, Yanagisawa M. Tie2-Cre transgenic mice: a new model for endothelial cell-lineage analysis in vivo. *Dev Biol*. 2001;230:230–242.
39. Coppé JP, Desprez PY, Krtolica A, Campisi J. The senescence-associated secretory phenotype: the dark side of tumor suppression. *Annu Rev Pathol*. 2010;5:99–118.
40. Hernandez-Segura A, Nehme J, Demaria M. Hallmarks of Cellular Senescence. *Trends Cell Biol*. 2018;28:436–453.
41. Puzzon MDS, Gonzalez L, Ascenzi S, Cundari E, Degrossi F. Tetraploid cells produced by absence of substrate adhesion during cytokinesis are limited in their proliferation and enter senescence after DNA replication. *Cell Cycle*. 2016;15:274–282.
42. Roger L, Gadea G, Roux P. Control of cell migration: a tumour suppressor function for p53? *Biol cell*. 2006;98:141–152.
43. Gottlieb TM, Oren M. p53 in growth control and neoplasia. *Biochim Biophys Acta*. 1996;1287:77–102.
44. Brentnall M, Weir DB, Rongvaux A, Marcus AI, Boise LH. Procaspase-3 regulates fibronectin secretion and influences adhesion, migration and survival independently of catalytic function. *J Cell Sci*. 2014;127:2217–2226.
45. Pérez-Garijo A. When dying is not the end: Apoptotic caspases as drivers of proliferation. *Semin Cell Dev Biol*. 2018;82:86–95.
46. Bauersachs J, Galuppo P, Fraccarollo D, Christ M, Ertl G. Improvement of left ventricular remodeling and function by hydroxymethylglutaryl coenzyme a reductase inhibition with cerivastatin in rats with heart failure after myocardial infarction. *Circulation*. 2001;104:982–985.
47. Gourdie RG, Dimmeler S, Kohl P. Novel therapeutic strategies targeting fibroblasts and fibrosis in heart disease. *Nat Rev Drug Discov*. 2016;15:620–638.
48. Hayashidani S, Tsutsui H, Shiomi T, Ikeuchi M, Matsusaka H, Suematsu N, Wen J, Egashira K, Takeshita A. Anti-monocyte chemoattractant protein-1 gene therapy attenuates left ventricular remodeling and failure after experimental myocardial infarction. *Circulation*. 2003;108:2134–2140.
49. De Mello WC, Specht P. Chronic blockade of angiotensin II AT1-receptors increased cell-to-cell communication, reduced fibrosis and improved impulse propagation

in the failing heart. *JRAAS*. 2006;7:201–205.

50. Mughal RS, Warburton P, O'Regan DJ, Ball SG, Turner NA PK. Peroxisome proliferator-activated receptor gamma-independent effects of thiazolidinediones on human cardiac myofibroblast function. *Clin Exp Pharmacol Physiol*. 2009;36:478–486.

51. Siddesha JM, Valente AJ, Sakamuri SS, Gardner JD, Delafontaine P, Noda M, Chandrasekar B. Acetylsalicylic acid inhibits IL-18-induced cardiac fibroblast migration through the induction of RECK. *J Cell Physiol*. 2014;229:845–855.

52. Ahmed Abdi B, Lopez H, Karrar S, Renzoni E, Wells A, Tam A, Etomi O, Hsuan JJ, Martin GR, Shiwen X, Denton CP, Abraham D, Stratton R. Use of Patterned Collagen Coated Slides to Study Normal and Scleroderma Lung Fibroblast Migration. *Sci Rep*. 2017;7:1–11.

53. Rasky A, Habiell DM, Morris S, Schaller M, Moore BB, Phan S, Kunkel SL, Phillips M, Hogaboam C, Lukacs NW. Inhibition of the stem cell factor 248 isoform attenuates the development of pulmonary remodeling disease. *Am J Physiol Lung Cell Mol Physiol*. 2020;318:L200–L211.

54. An N, Cen B, Cai H, Song JH, Kraft A, Kang Y. Pim1 kinase regulates c-Kit gene translation. *Exp Hematol Oncol*. 2016;5:1–8.

55. Foudi A, Hochedlinger K, Van Buren D, Schindler JW, Jaenisch R, Carey V, Hock H. Analysis of histone 2B-GFP retention reveals slowly cycling hematopoietic stem cells. *Nat Biotechnol*. 2009;27:84–90.

56. Busche A, Schmitz S, Fleige H, Robbins SH, Walzer T, Stewart CA, Förster R, Messerle M PI. Genetic labeling reveals altered turnover and stability of innate lymphocytes in latent mouse cytomegalovirus infection. *J Immunol*. 2011;186:2918–2925.

57. Klarmann K, Ortiz M, Davies M, Keller JR. Identification of in vitro growth conditions for c-Kit-negative hematopoietic stem cells. *Blood*. 2003;102:3120–3128.

58. Castaldo C, Di Meglio F, Nurzynska D, Romano G, Maiello C, Bancone C, Müller P, Böhm M, Cotrufo M MS. CD117-positive cells in adult human heart are localized in the subepicardium, and their activation is associated with laminin-1 and alpha6 integrin expression. *Stem Cells*. 2008;26:1723–1731.

59. Di Meglio F, Castaldo C, Nurzynska D, Miraglia R, Romano V, Russolillo V, Giuseppina L, Vosa C, Montagnani S. Localization and origin of cardiac CD117-positive cells: identification of a population of epicardially-derived cells in adult human heart. *Ital J Anat Embryol*. 2010;115:71–78.

60. Di Meglio F, Castaldo C, Nurzynska D, Romano V, Miraglia R, Bancone C, Langella G, Vosa C, Montagnani S. Epithelial-mesenchymal transition of epicardial mesothelium is a source of cardiac CD117-positive stem cells in adult human heart. *J Mol*

Cell Cardiol. 2010;49:719–727.

61. Tallquist MD. Cardiac Fibroblast Diversity. *Annu Rev Physiol.* 2020;82:63–78.

62. Olivey HE, Mundell NA, Austin AF, Barnett JV. Transforming growth factor-beta stimulates epithelial-mesenchymal transformation in the proepicardium. *Dev Dyn.* 2006;235:50–59.

63. Mori L, Bellini A, Stacey MA, Schmidt M, Mattoli S. Fibrocytes contribute to the myofibroblast population in wounded skin and originate from the bone marrow. *Exp Cell Res.* 2005;304:81–90.

64. McDonald LT, Johnson SD, Russell DL, Young MRI, LaRue AC. Role of a novel immune modulating DDR2-expressing population in silica-induced pulmonary fibrosis. *PLoS One.* 2017;12:e0180724.

65. Sidles SJ, Xiong Y, Young MRI, LaRue AC. High-Fat Diet Alters Immunogenic Properties of Circulating and Adipose Tissue-Associated Myeloid-Derived CD45 + DDR2 + Cells. *Mediators Inflamm.* 2019;2019:1648614–1648629.

66. Bucala R, Spiegel LA, Chesney J, Hogan M, Cerami A. Circulating fibrocytes define a new leukocyte subpopulation that mediates tissue repair. *Mol Med.* 1994;1:71–81.

67. Yang D, Liu HQ, Liu FY, Tang N, Guo Z, Ma SQ, An P, Wang MY, Wu HM, Yang Z, Fan D, Tang QZ. The Roles of Noncardiomyocytes in Cardiac Remodeling. *Int J Biol Sci.* 2020;16:2414–2430.

68. Ruiz-Villalba A, Simón AM, Pogontke C, Castillo MI, Abizanda G, Pelacho B, Sánchez-Domínguez R, Segovia JC, Prósper F, Pérez-Pomares JM. Interacting resident epicardium-derived fibroblasts and recruited bone marrow cells form myocardial infarction scar. *J Am Coll Cardiol.* 2015;65:2057–2066.

69. Möllmann H, Nef HM, Kostin S, von Kalle C, Pilz I, Weber M, Schaper J, Hamm CW, Elsässer A. Bone marrow-derived cells contribute to infarct remodelling. *Cardiovasc Res.* 2006;71:661–671.

70. Ravikanth M, Soujanya P, Manjunath K, Saraswathi TR, Ramachandran CR. Heterogeneity of fibroblasts. *J Oral Maxillofac Pathol.* 2011;15:247–250.

71. De Santis Puzzon M, Cozzolino AM, Grassi G, Bisceglia F, Strippoli R, Guarguaglini G, Citarella F, Sacchetti B, Tripodi M, Marchetti A, Amicone L. TGFbeta Induces Binucleation/Polyploidization in Hepatocytes through a Src-Dependent Cytokinesis Failure. *PLoS One.* 2016;11:e0167158.

72. Dubois CM, Ruscetti FW, Stankova J, Keller JR. Transforming Growth Factor- β Regulates c-kit Message Stability and Cell-Surface Protein Expression in Hematopoietic Progenitors. *Blood.* 1994;83:3138–3145.

73. Panopoulos A, Pacios-Bras C, Choi J, Yenjerla M, Sussman MA, Fotedar R, Margolis RL. Failure of cell cleavage induces senescence in tetraploid primary cells. *Mol Biol Cell*. 2014;25:3105–3118.
74. Reichardt IM, Robeson KZ, Regnier M, Davis J. Controlling cardiac fibrosis through fibroblast state space modulation. *Cell Signal*. 2021;79:109888–109899.
75. Zhu F, Li Y, Zhang J, Piao C, Liu T, Li HH, Du J. Senescent cardiac fibroblast is critical for cardiac fibrosis after myocardial infarction. *PLoS One*. 2013;8:e74535.
76. Wang L, Yue Y, Yang X, Fan T, Mei B, Hou J, Liang M, Chen G, Wu Z. Platelet Derived Growth Factor Alpha (PDGFR α) Induces the Activation of Cardiac Fibroblasts by Activating c-Kit. *Med Sci Monit*. 2017;23:3808–3816.
77. Lamkanfi M, Festjens N, Declercq W, Vanden Berghe T, Vandenabeele P. Caspases in cell survival, proliferation and differentiation. *Cell Death Differ*. 2007;14:44–55.
78. Suresh K, Carino K, Johnston L, Servinsky L, Machamer CE, Kolb TM, Lam H, Dudek SM, An SS, Rane MJ, Shimoda LA DM. A nonapoptotic endothelial barrier-protective role for caspase-3. *Am J Physiol Lung Cell Mol Physiol*. 2019;316:L1118–L1126.
79. Cardona M, López JA, Serafín A, Rongvaux A, Inserte J, García-Dorado D, Flavell R, Llovera M, Cañas X, Vázquez J, Sanchis D. Executioner Caspase-3 and 7 Deficiency Reduces Myocyte Number in the Developing Mouse Heart. *PLoS One*. 2015;10:e0131411.
80. Yokosawa T, Yamada M, Noguchi T, Suzuki S, Hirata Y MA. Pro-caspase-3 protects cells from polymyxin B-induced cytotoxicity by preventing ROS accumulation. *J Antibiot (Tokyo)*. 2019;72:848–852.
81. Kim JS, Ha JY, Yang SJ, Son JH. A Novel Non-Apoptotic Role of Procaspase-3 in the Regulation of Mitochondrial Biogenesis Activators. *J Cell Biochem*. 2018;119:347–357.
82. McLellan MA, Skelly DA, Dona MSI, Squiers GT, Farrugia GE, Gaynor TL, Cohen CD, Pandey R, Diep H, Vinh A, Rosenthal NA PA. High-Resolution Transcriptomic Profiling of the Heart During Chronic Stress Reveals Cellular Drivers of Cardiac Fibrosis and Hypertrophy. *Circulation*. 2020;142:1448–1463.
83. Farbehi N, Patrick R, Dorison A, Xaymardan M, Janbandhu V, Wystub-Lis K, Ho JW, Nordon RE, Harvey RP. Single-cell expression profiling reveals dynamic flux of cardiac stromal, vascular and immune cells in health and injury. *Elife*. 2019;8:e43882.
84. Lewis-McDougall FC, Ruchaya PJ, Domenjo-Vila E, Shin Teoh T, Prata L, Cottle BJ, Clark JE, Punjabi PP, Awad W, Torella D, Tchkonja T, Kirkland JL E-HG. Aged-senescent cells contribute to impaired heart regeneration. *Aging Cell*. 2019;18:e12931.

85. Ellison-Hughes GM. Senescent cells: targeting and therapeutic potential of senolytics in age-related diseases with a particular focus on the heart. *Expert Opin Ther Targets*. 2020;24:819–823.

Chapter 4, with slight modifications, has been submitted for publication. 'Youthful' Phenotype of c-Kit⁺ Cardiac Fibroblasts. Fareheh Firouzi, Oscar Echeagaray, Carolina Esquer, Natalie A. Gude, Mark A. Sussman. The dissertation author was the primary author and investigator on this manuscript.